UNIVERSITY OF SOUTHAMPTON

FACULTY OF ENGINEERING AND PHYSICAL SCIENCES

SCHOOL OF ENGINEERING

Experimental Evaluation of Railway Switch and Crossing (S&C) Modular Bearer Performance

by

Ali Shahbaz Khan

Thesis for the degree of Doctor of Philosophy

June 2022

University of Southampton

Faculty of Engineering and Physical Sciences

School of Engineering

Thesis for the degree of Doctor of Philosophy

Abstract

Experimental Evaluation of Railway Switch and Crossing (S&C) Modular Bearer Performance

By Ali Shahbaz Khan

Railway switch and crossing (S&C) are an essential part of the railway track as they enable trains to change paths. Traditionally, S&C comprises continuous long bearers, up to over 6 m in length, which help to maintain gauge and prevent lateral movement between the rails. However, to decrease the cost and time associated with maintenance works, modular S&C have been introduced. These use jointed bearers which enables pre-assembled sections of S&C to be transported to and fitted on site. The joints used to tie the bearers can vary in stiffness and their location can change. This poses some questions, as the inclusion of a joint within the bearers may affect track behaviour.

This research investigated the performance implications of introducing a joint in the bearers, the relative merit of various joint types and their locations with respect to the loaded rails. It also explored mitigation options, such as the lateral confinement of the ballast shoulder. This was done using full-scale laboratory testing on a single bearer bay of track, three-point bending tests and finite element modelling.

It was found that eccentric loading of bearers resulted in significant variation in permanent settlement and resilient deflections along the length of the bearers. This effect was mitigated with the lateral confinement of the ballast shoulder, which offered lateral stability to the shoulder ballast. Whilst the use of a joint between the loaded rails exacerbated the variation in permanent settlement along the length of the bearers, it drastically reduced the rate of change in resilient deflections over the course of loading cycles. Joining symmetrically loaded segments of bearers can mitigate the tilting of the bearers and reduce differential settlement along the bearer length. Results from this work will enrich current S&C models and provide insights to benefit the development of new modular bearer joints.

Table of Contents

List of Figures

List of Tables

Declaration of Authorship

I, Ali Shahbaz Khan, declare that the thesis entitled “Experimental Evaluation of Railway Switch and Crossing (S&C) Modular Bearer Performance” and the work presented in the thesis are both my own, and have been generated by me as the result of my own original research.
I confirm that:

- This work was done wholly or mainly while in candidature for a research degree at this University;
- Where any part of this thesis has previously been submitted for a degree or any other qualification at this University or any other institution, this has been clearly stated;
- Where I have consulted the published work of others, this is always clearly attributed;
- Where I have quoted from the work of others, the source is always given. With the exception of such quotations, this thesis is entirely my own work;
- I have acknowledged all main sources of help;
- Where the thesis is based on work done by myself jointly with others, I have made clear exactly what was done by others and what I have contributed myself;
- Parts of this work have been published as:
  Khan A.S., Ferro E., Le Pen L., Powrie W. (2022) Performance of Jointed S&C Bearers. In: Tutumluer E., Nazarian S., Al-Qadi I., Qamhia I.I. (eds) Advances in Transportation Geotechnics IV. Lecture Notes in Civil Engineering, vol 165. Springer, Cham. https://doi.org/10.1007/978-3-030-77234-5_5

Signed: ……..
Date:……..

Acknowledgements

This research project is part of TRACK TO THE FUTURE, funded by the Engineering and Physical Sciences Research Council (EPSRC). I am grateful to Network Rail and Progress Rail for providing the bearers and joints, and to Getzner for supplying the under ballast mats.

I would like to express my utmost gratitude to Professor William Powrie and Dr Louis Le Pen, for giving me the opportunity to work on this project and continuously supporting and encouraging me at every stage. Their valuable knowledge, timely feedback and patience has made this possible.

I would also like to especially thank Dr Edgar Ferro and Dr Taufan Abadi for training me in the lab, and for their practical advice and encouragement.

I am very grateful to the laboratory staff who helped me with the day-to-day laboratory related work - Andy Morgan, Harvey Skinner, Dr Andrew Robinson, Dr Duncan Crump.

Finally, I would like to thank my family for their full support.

In the name of Allah, the Entirely Merciful, the Especially Merciful.

Abbreviations

NR	Network Rail
SRTF	Southampton Railway Testing Facility
S&C	Switch and Crossing
CWR	Continuous Welded Rail
RDD	Rolling Radii Difference
RCF	Rolling Contact Fatigue
RP	Rail Pad
UBM	Under Ballast Mat
FEA	Finite Element Analysis

1 Introduction

This introductory chapter describes the motivation for the research and lays out the aim, objectives and knowledge gap being addressed.

Most of the existing UK railway infrastructure was built in Victorian times using materials and methods that have changed little since. Yet performance requirements are much greater now as demand has almost doubled just in the past two decades. Rail journeys reached a record high of 1.75bn in the year 2018/19, with an increase of 2.8% on the previous year (ORR, 2021). Prior to the Covid-19 pandemic, the rail sector was a promising contributor to the economy and is expected to help the economy as the world recovers (Loughran, 2021).

Increased usage of the rail network together with stringent safety protocols necessitates more frequent and reliable engineering works. Maintenance and renewal together accounted for over half of Network Rail's total expenditure (excluding financing costs) in the year 2019/20 (ORR, 2020). A quarter of the total of £953M spent on track renewals in the UK was attributed to switches and crossings (S&C) (Network Rail, 2021), which make up only 5% of the mainline rail network in the UK. Of the 21,000 S&C units, 340 are renewed annually, making S&C an expensive asset of the rail network (Coleman & Cornish, 2010).

Unlike the unforeseen disruptions, such as those caused by the recent Covid-19 pandemic, planned disruptions such as engineering works are necessary to maintain the rail network. Nonetheless, the prospect of reducing costs and increasing output has driven the rail industry to minimise disruptions to both freight and passenger travel caused when a track is closed for maintenance. One of the ways in which this is done is by utilising the modular S&C concept. In the UK, Network Rail (NR) aims to reduce possession times, the period in which the track is used for maintenance, from 54 hours to 8 hours using this concept (Network Rail, 2012).

S&C are an important element of railway infrastructure, guiding trains from one track to another and enabling lines to cross each other. They allow for a multi-lined, multi-routed rail network. Each S&C consists of three sections: the switch panel, the closure panel, and the crossing panel (Figure 1).

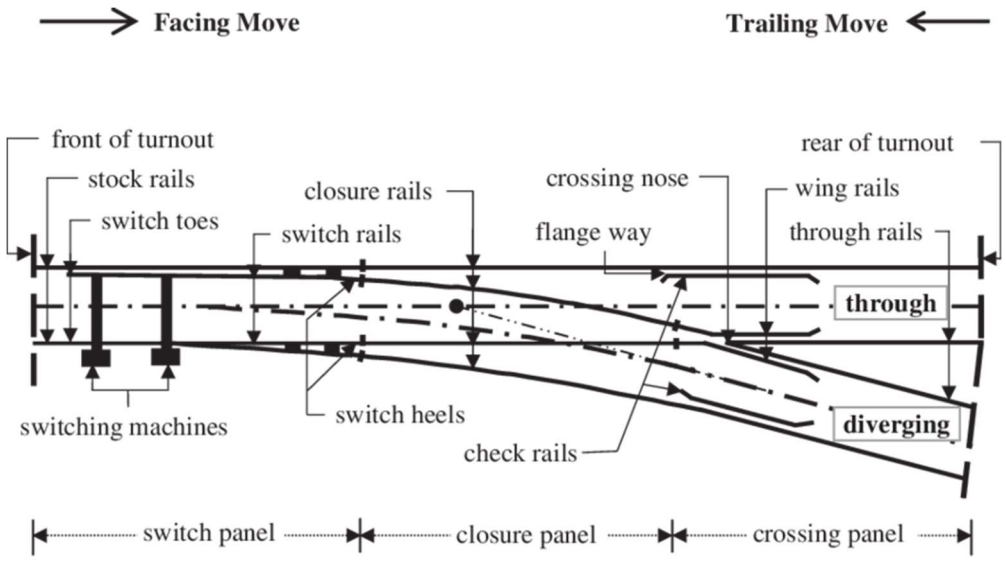

Figure 1 Schematic of a typical S&C and its components (Pålsson & Nielsen, 2012)

Whilst S&C layout complexity can range greatly depending on the number of lines it engages, even the simplest form has several inherent features that differentiate it from a plain line. These features include: the variation in layout geometry as the track converges/diverges, accompanied by increasing length/mass of the bearers; discontinuities in rails such as in the crossing nose, to enable track to cross paths; variation in mass distribution of the rails such as the gradual widening of the switch rails, large cross-sectional area and stiffness of the crossing nose and added stiffness of the wing rails. These features cause variation in system stiffness and impact loads that ultimately lead to differential settlement and damage to the superstructure components like mechanical fasteners and concrete bearers. These issues are amongst the leading drivers for maintenance and renewals of S&C.

The modular concept, developed in 2006, allows an S&C unit to be assembled in smaller segments. These segments are then transported in their assembled state from the manufacturing yard to the site. A mechanical joint or 'bearer tie' is used to join the different modules on or near the site. This results in a potential discontinuity in what would traditionally have been a continuous long bearer (Figure 2). Such an alteration to the conventional S&C design could have an unintended impact on the overall S&C performance.

The introduction of a mechanical fastener within the bearer will alter its local bending stiffness, which will interact with the trackbed support conditions. It will also alter the distribution of loading by the train, as well as other factors relating to the geometry and design of the crossing; thus, fundamentally altering the overall behaviour of the S&C, possibly in unexpected ways.

This could lead to complications such as differential settlement along the length and potentially twist faults. Such faults are thought to have contributed to the derailment of a freight train at Lewisham in 2017 (Figure 3), which had been recently renewed with a modular S&C (RAIB, 2018).

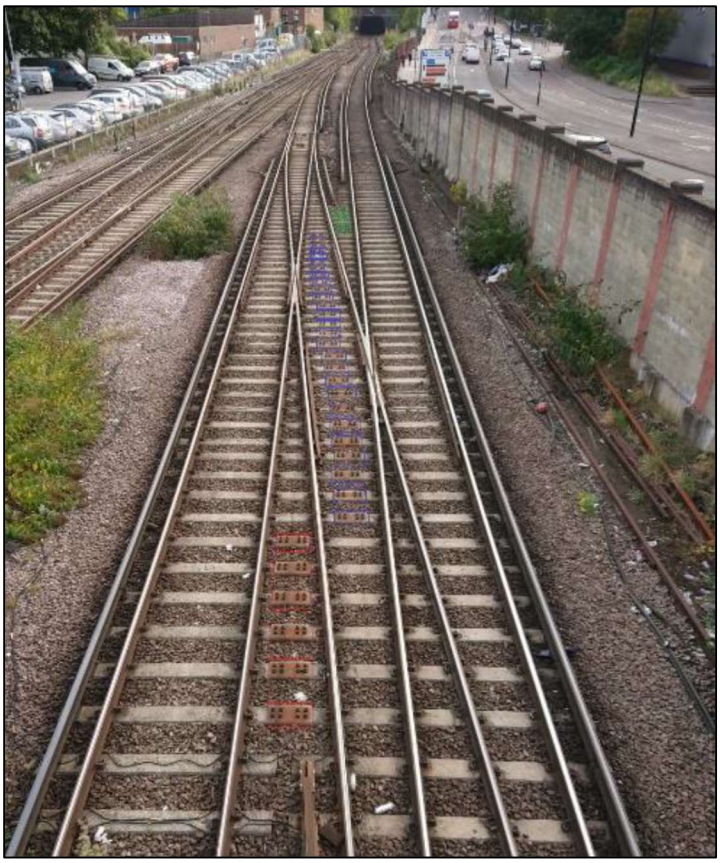

Figure 2 S&C at Southampton Central Railway Station utilising NR joint with changing locations relative to the rails

Figure 3 Image of derailed wagon at Courthill Loop South Junction, Lewisham (RAIB, 2018)

1.1 Knowledge gap

Due to the recentness of the modular concept, there are varying designs of bearer joints with different mechanisms in use by rail operators across various countries. Some examples are shown in Figure 4; these vary from almost rigid joints to joints that allow rotational freedom of movement. The lack of a single joint design creates further uncertainty and the need for research into the new modular concept because little is known on how any of these joints really perform, or their relative merits.

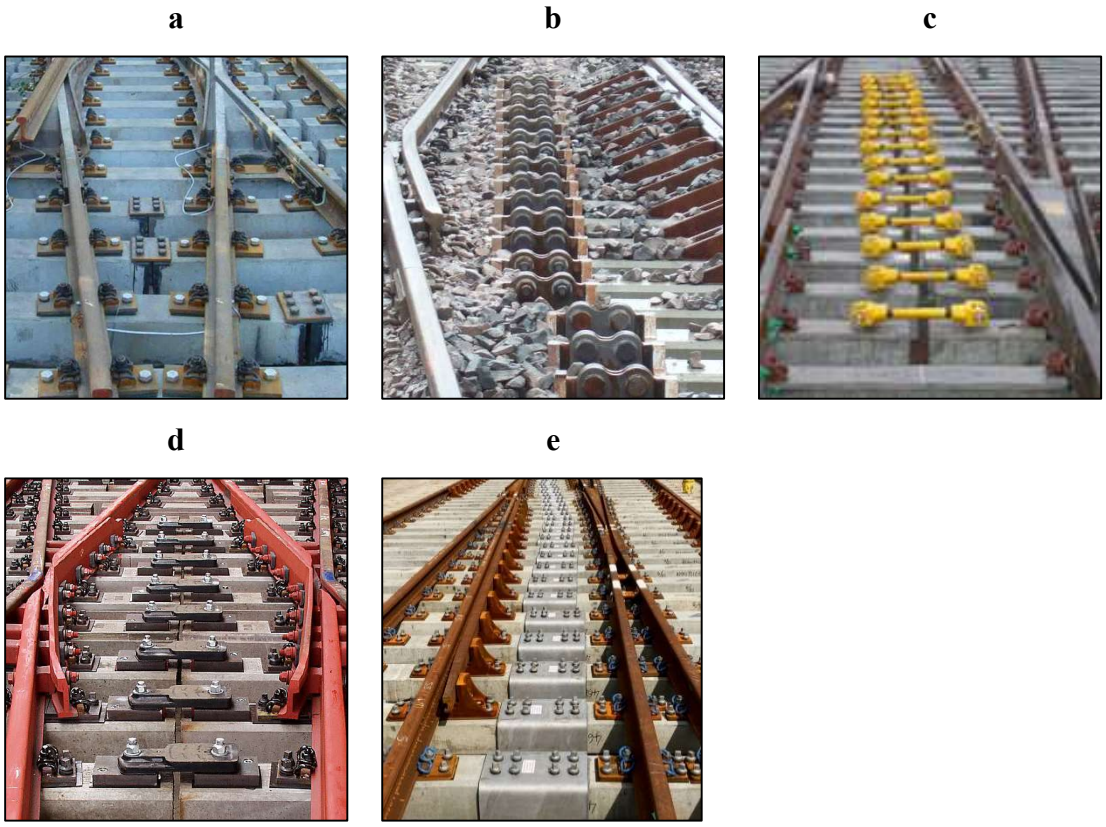

Figure 4 Bearer ties on S&C: a - Chinese rigid joint; b - German hinged joint (Mid) (railone, n.d.); c - Progress Rail Pin-Pin joint used in the USA (courtesy of Calvin Lamb – PR); d – Voestalpine Elastic Couplings (Voestalpine, 2020); e - Network Rail Metal Shrouded Joint (RailEngineer, 2021).

Although research has been conducted on track settlement in railway turnouts (Li, et al., 2014) (Grossoni, et al., 2020) (Six, et al., 2021), there remains a gap in knowledge regarding the implications of introducing the modular bearer in S&C. While there has been limited research on the transient performance, and the influence of the development of permanent settlements has not been assessed. By considering ballast as an elastic support, studies do not capture all of the essential feature of ballast being an elastoplastic material. While some studies have endeavoured to formulate settlement models, these are often based on limited data and generalisations (Alabbasi & Hussein, 2021).

Prior to the start of this research there has only been one study (Zhu & Thompson, 2009) dedicated to the performance of jointed bearers in S&C, which was exclusively numerical and did not address the behaviour of the jointed bearer with accumulating loading cycles and evolving ballast support. The study by Zhu & Thompson (2009) only focused on a single bearer with a joint beside the loaded rails under the crossing nose.

Zhu & Thompson (2009) presented a numerical model for a flexible jointed bearer on an S&C and suggested that joints in bearers reduce bearer rigidity, improve fatigue strength, reduce impact loads, and improve dynamic performance by lowering bearer end accelerations from 8.3 g to 0.07 g. They also reported that introducing a joint in the bearer mitigates the tilting behaviour on continuous bearers in S&C as reported by (Le Pen, et al., 2017). The static finite element model presented by Zhu and Thompson (2009) neglects plasticity of the ground support (i.e., the ballast is not a purely elastic material, and its performance is highly influenced by its complex plastic behaviour), lacks resilient and permanent cyclic deflections of ballast with accumulation of loading cycles and the effect of varying joint location is not considered.

Ballast support conditions determine the distribution and intensity of bearer deflections. Also, the location and mechanical characteristics of the bearer joint will influence the ballast track support along the length of the bearer. Minimising variation in the resilient deflections and ballast settlement underneath the length of S&C bearers will make the track more resistant to twist faults, thereby reducing the risk of derailment and frequency of maintenance.

1.2 Aims and objectives

The research described in this dissertation was initiated in wake of a train derailment at Lewisham in 2017 (RAIB, 2018) and concern over broken joint bolts found on sites as shown in Figure 5.

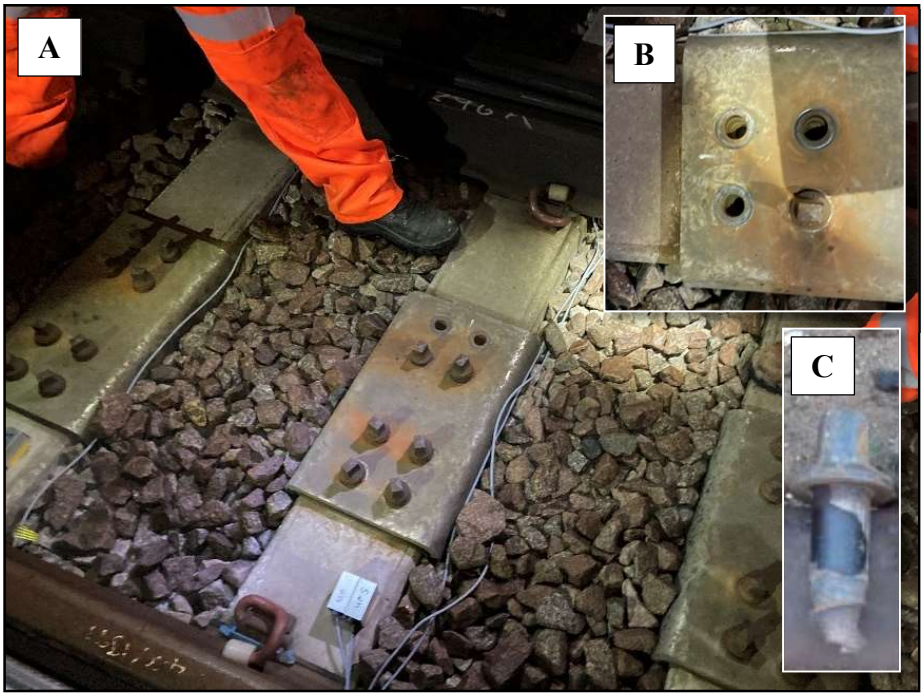

Figure 5 Photograph A and B showing missing bolts on the jointed bearer found during field works (Courtesy of Dr Louis Le Pen) and Photograph C showing broken bolts (Courtesy of Sin-Sin Hsu - NR)

This research aims to:

1. assess the influence of the bearer length, the presence of a joint, joint type/mechanism, and joint location on performance;
2. identify optimum design features for minimising variation in ballast permanent settlement and resilient response along their length.

The research aims are based on bearer-ballast interaction and the resulting ballast settlement and resilient response. This will consider the geometric arrangement of the ballast support. By means of a finite element model and supporting laboratory tests, the design features of the bearer joint were studied, and the bending stiffness of jointed and continuous bearers were quantified. This research will lead to improved jointed bearer designs, and recommendations for ballast placement that will require less maintenance.

The project aims were delivered by a series of objectives, to:

1. understand the current state of knowledge, by carrying out a literature review covering:
    i. S&C designs incorporating modular installations (jointed bearers)
    ii. Features related to S&C
    iii. Track settlement and maintenance at S&C
2. understand the influence of joints on bearer performance, specifically the resilient response and permanent settlements, by carrying out full size laboratory testing on different individual S&C bearer designs, including jointed bearers, in the Southampton Railway Testing Facility (SRTF);
3. from the results of 2, propose and carry out a second series of tests in the SRTF with different ballast arrangements to improve bearer performance. Confined ballast shoulder and under sleeper pads (USPs) were used on jointed bearers and the effects studied;
4. by carrying out further tests in the SRTF, study the effect of a degraded bearer joint on ballast settlement and resilient deflections, with evolving loading cycles. Additionally, assess the impact of differential ballast support on the joint behaviour and the overall bearer performance, specifically in terms of permanent settlements and resilient deflections, with accumulating loading cycles;
5. evaluate the joint rotational stiffness of continuous and rigidly jointed bearers by carrying out full scale three-point bending tests;
6. identify the influence of assembly subparts on the flexural rigidity of the jointed bearer system by developing a finite element model of the rigidly jointed bearer using data from 5 and conducting a parametric study on the jointed bearer assembly assessing the impact of bolt load, washer stiffness and rubber stiffness on the flexural rigidity of the joint.

1.3 Thesis structure

The Introduction is followed by seven further chapters that are grouped into two categories. The first part, Chapter 2 and 3, relates to the background and literature review whilst the second part, Chapter 4 to 7, presents the new information that forms this thesis.

- Chapter 2 gives a brief description of the ballasted rail track structure and load transfer.
- Chapter 3 describes the main components of S&C and highlights the complexity of such systems by reviewing the existing literature on the main issues related to them. It also overviews S&C designs, installation, maintenance procedures and track twist faults.
- Chapter 4 presents a concise description of the modified SRTF. The primary materials and instrumentation used and the procedure of test preparations, loading routine of the apparatus are presented. Through preliminary baseline tests, the justification for data presentation is provided. A summary of the tests carried out is presented.
- Chapter 5 contains the work on the full-scale tests carried out on S&C long bearers using the SRTF apparatus. These tests include baseline tests on bearers in general ballast conditions. These tests are compared with tests carried out where the ballast shoulder was confined and with bearers utilising USPs. The output of these experiments is in terms of resilient deflections and permanent settlement along the bearer lengths, longitudinal and vertical pressures in the ballast, bearer-ballast contact area and ballast shoulder displacement.
- Chapter 6 focuses on the series of tests that mimic differential ballast support under the bearers and evaluates the impact of compromised bolts on the bearer joint, these tests are hereby referred to as interventions.
- Chapter 7 describes the experiments conducted to obtain the essential parameters used within the finite element analysis (FEA) of the jointed bearers. This chapter also presents experimental results and discussion of three-point bending tests carried out on the bearers and compares the results with the FEA results.
- Chapter 8 provides the conclusions to the work carried out to from the thesis, this also lays out scope for future work.

2 Background

This chapter gives an overview of the rail track structure, track loading and stress transfer.

2.1 Rail track structure

Railway track supports and guides the wheels of the passing vehicles, transferring and distributing the loads from the wheels onto the subgrade. There are two main types of track system in use: ballasted track (Figure 6) and slab track. The former is an older, more traditional style of infrastructure that is continuously evolving but its principles remain unchanged. While newer railways may be laid on concrete slabs (slab track), ballasted track is likely to remain the main track form in the UK in the immediate future because of its lower construction cost and time, and its noise reducing properties.

The focus of this project is ballasted S&C. The support structure of S&C can be considered into two sections. The first is the superstructure, which comprises the rails, fastenings, sleepers/bearers, and any intermediate layers such as rail pads and under sleeper pads (USP). The second is the substructure, which comprises the ballast, sub-ballast, subgrade and potentially an under-ballast mat (UBM).

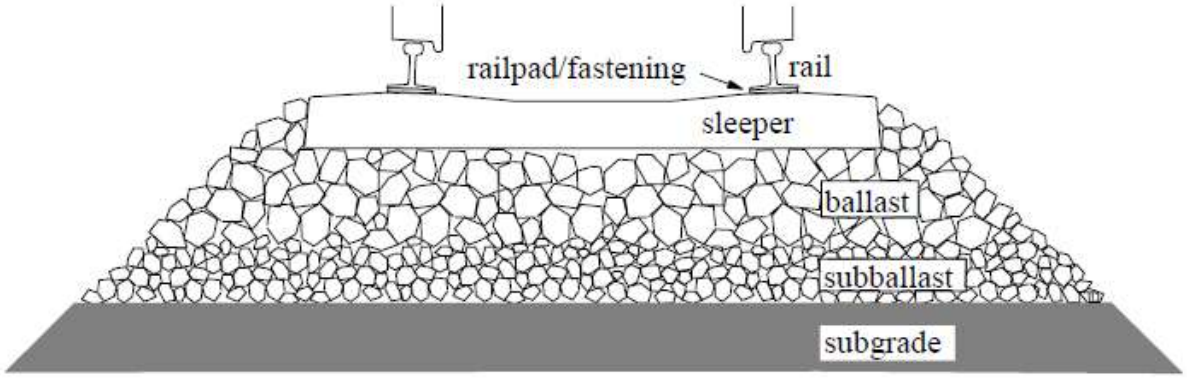

Figure 6 Cross-section of an idealised trackbed (Dahlberg, 2003).

Below is a description of the subcomponents of S&C:

2.1.1 Rails

Made of high strength steel, the rails guide and support the train wheels. Their cross section is approximately that of an I-beam with a rounded head that is in contact with the moving train wheel, and a flat footing that is fastened to the sleeper/bearer. This geometric form is also known as Vignoles. The key features are strength, stiffness, and smoothness.

2.1.2 Fastening systems

Consisting of clips and a pad, the fastening system holds the rail to the sleeper/bearer while allowing for longitudinal movement of the rails after a certain stress threshold, caused by expansion or contraction due to temperature variations.

2.1.3 Sleepers/bearers

Connected to the rail via the fastening system, bearers are laid onto the ballast. They transmit the load onto the ballast as well as prevent lateral movement (rail buckles). Key characteristics include suitable strength, stiffness, and durability. Traditionally made from timber, on higher specification railways they are now commonly manufactured from pre-tensioned steel reinforced concrete.

2.1.4 Ballast

The primary function of the ballast is to transfer loads from the sleepers to the sub-ballast or subgrade. For longitudinal and transverse stability, it is also placed between the sleepers (in the cribs) and may be heaped at the ends (known as the ballast shoulder). It also provides drainage and noise absorption. Important features are particle size distribution, particle shape, surface roughness, parent rock strength and resistance to weathering.

2.1.5 Sub-ballast

When present, a sub-ballast consists of a well-graded sandy gravel or sand in a layer typically 10-15 cm thick, which separates the ballast and the subgrade from the ballast. Sub-ballast helps to distribute the loads onto the subgrade and prevents a weaker fine-grained subgrade from penetrating and fouling the ballast. To achieve its functional qualities, a sub-ballast must be well compacted and of higher stiffness than the subgrade.

2.1.6 Subgrade

This is the layer that receives the reduced loads transferred from the bearers, through the ballast and sub-ballast. It can be natural soil, artificially placed ‘fill material’ or both. Its strength may determine the health of the upper layers of the track structure, therefore adequate consideration is necessary during the design stage. Factors such as moisture content, shear strength, consolidation, and stiffness all affect the performance of the subgrade.

Poor track drainage leads to infiltration of water into the subgrade, softening and deforming the layer directly under the track. Ballast is then added to the affected region and tamped to

restore track geometry. This can eventually create a locally thicker region of ballast called a ballast pocket, which is prone to shear failure.

The condition of the subgrade can influence the degree of ballast fouling, ballast pockets, pumping of soil fines through the ballast and stability failure issues. Loading from vehicles through the track influences subgrade quality. Relevant characteristics include the type of traffic (freight or passenger), train speed (conventional or highspeed trains), axle load, train configuration, wheel condition (e.g., polygonalisaton of wheels), sleeper spacing, and rail condition (Neidhart & Shultz, 2011).

2.2 Track loading and stress transfer

2.2.1 Normal forces

Normal forces acting on the rail head include the weight of the vehicle, any component of centrifugal force from a curving train and influence of wind. The total vertical force has two components: quasi-static $P_{q\text{-}s}$ and dynamic Q_{dyn}:

$$P_{total} = P_{q\text{-}s} + Q_{dyn}$$

The quasi-static component is made up of vehicle weight (P_v), vertical load from wind (P_w) and vertical component of centrifugal force (P_c):

$$P = P_v + P_w + P_c$$

Dynamic forces arise from moving train-track interaction (influenced by wheel/rail profile, presence of discontinuities such as joints or crossing nose in S&C), substructure characteristics such as stiffness of the ballast and how well it is compacted, suspension of the vehicle and damping properties e.g., rail pads.

2.2.2 In-plane forces

Horizontal forces can be in the direction of the rails (i.e., longitudinal) and sideways (i.e., lateral). Longitudinal forces are introduced by dynamic breaking/tractive effort of the vehicle, thermal forces, and expansion. Thermal expansion of rails can lead to rail buckling with or without trains present. Lateral forces from the train arise from trains curving (lateral component of centrifugal force) and wind loading. There may also be lateral forces from dynamic interaction between the moving train and the track.

2.2.3 Load transfer

Vertical load from the wheel is transferred through the base of the rail via the rail pads to the sleeper, the area of the sleeper is either in direct contact with the ballast or through an USP. Force there onwards is transferred to the underlying layers (i.e., ballast/sub-ballast and subgrade).

The load from the sleeper is often assumed to be distributed equally over the area of the sleeper. However, ballast is a coarse aggregate and in practice the load from the sleeper base is distributed over a fraction of ballast grains in contact with the sleeper base. The number of ballast grains in contact with the sleeper can vary depending on the area of the sleeper/bearer as well as ballast grading (Abadi, et al., 2015).

Track stiffness varies along the S&C. Changes in stiffness can occur when the stock rail joins the switch, and when standard-length sleepers become longer S&C bearers. Further change happens along the S&C as bearers become longer towards the crossing region. Together with variation in the rail cross-section, this results in variations in vertical track stiffness as observed by a passing train.

3 Literature Review

This section describes the main elements of S&C and a review of current literature on track settlement in turnouts or S&C. It shows that previous work has focused mainly on computational methods to assess track settlement in S&C with little consideration given to the emerging technique of modular S&C, which utilises a mechanical joint within the bearers.

3.1 Overview of Switch and Crossing (S&C) design

3.1.1 Introduction

This section describes the importance of S&C as a railway asset and highlights the significance of their maintenance and the possible faults that may develop and lead to accidents.

S&C are an integral part of the rail network as they transfer trains from one track to another and allow trains to cross paths. As S&C connect or cross at least two lines, they can have a significant impact on the operation of the network. They are more complex than plain line with high maintenance cost, and more prone to damage caused by dynamic loads because of discontinuities and varying bearer dimensions. They have more components than plain line track and need maintenance more frequently. Their limited lifespan means that they must be renewed or replaced to maintain safety standards. Rail operators benefit from reducing the time renewals take to carry out as tracks can then be available to traffic for longer.

An S&C is made up of three main sections as seen in Figure 7:

1. Switch panel: stock rail, point rail (switch rail) and switch machine
2. Closure panel: straight rail and guide curve rail
3. Crossing panel: guard rail, wing rail, crossing nose (frog)

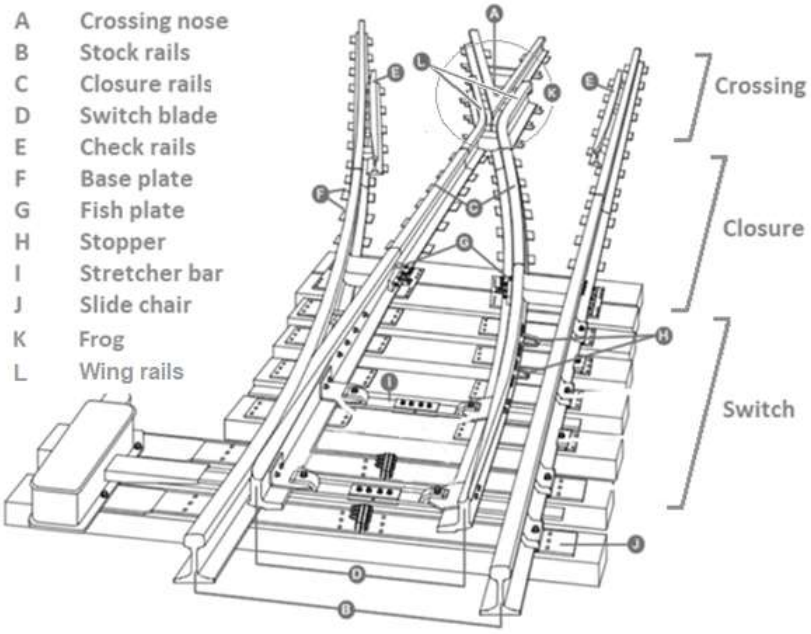

Figure 7 Schematic of an S&C with components labelled, note that fishplates are not used on modern S&C (MI-NE SEISAKUSHO CO., 2014)

3.1.2 Switch panel

A switch panel is made up of two components, as described below:

3.1.2.1 Stock rails

Stock rails are plain line rails with standard rail profiles, inside which the switch rails operate.

3.1.2.2 Switch rails

Switch rails are movable part of the switch panel, tapered to allow a smooth transition of the wheel from the stock rail. The thinnest section is called the toe and the thick end is called the heel.

3.1.3 Closure panel

The closure panel is made up of closure rails (lead rails) and can be straight or curved.

3.1.3.1 Closure rails

Closure rails are straight or curved rails located between the heel of the switch and toe of the frog (see Figure 7), connecting the switch to the crossing panel. The heel of the switch rail is connected to the closure rail via a fishplate joint, although modern designs may not have a fishplate.

3.1.3.2 Fishplate joint (Heel joint)

Fishplate is a metal plate bolted to the web of joining rails on four or six locations. It joins together the heel of the switch rail and closure rail.

3.1.3.3 Heel block

Heel blocks are assemblies placed between the heel of the switch and stock rails to provide a fixed pivoted gap between the stock rails and switch heel, providing a clearance for the wheel flange.

3.1.4 Crossing panel

The crossing panel is the section in the S&C where the track splits. The rail geometry in the crossing panel is discontinuous because there are gaps in the rail sections to allow the wheel flanges of trains on the crossing line to pass through.

The crossing panel consists of the following elements:

3.1.4.1 Crossing nose (Frog)

The crossing nose is a V-section made of manganese steel, formed of two rails joining at an acute angle. It allows the wheel flange to pass through the rail being crossed as shown in Figure 8.

Ideally, the tip of the crossing nose is as thin as possible (Theoretical Nose of Crossing, TNC or Theoretical Crossing Point, TCP) but practically there is a limit, and it is left slightly blunt (Actual Nose of Crossing, ANC) to avoid breakage. On long, high-speed turnouts that require smaller crossing angles, the conventional crossing nose is replaced by a movable crossing nose referred to as a swing nose, operating in the same way as switch blades.

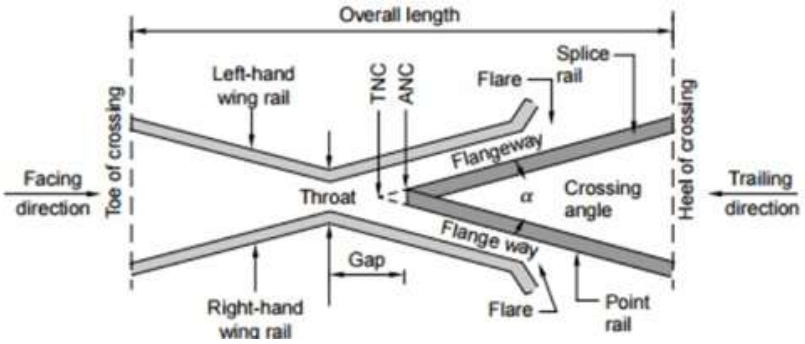

Figure 8 Diagram showing components of crossing nose or 'frog' (Diesel Locomotives, 2019)

3.1.4.2 Check rails

Check rails are a short length of rail fixed close to the stock rail to ensure that the wheels pass through the right flangeway.

3.1.4.3 Wing rails

Wing rails are short sections of rail close to the crossing nose that function in the same way as check rails, i.e., to avoid derailment by ensuring that the wheel goes through the appropriate flangeway (see Figure 8).

3.1.5 Types of S&C

Types of S&C include (Parsons Brinckerhoff, 2012) (see Table 1):

- Single crossover: usually but not always connecting two parallel tracks, consist of two turnouts.
- Double crossover: also called scissor crossover consists of four turnouts and is an improvement to its single counterpart because it allows trains to switch in either direction.
- Track crossing: also known as diamonds, allow two tracks to simply cross each other.
- Slip switch- a single slip switch allows trains to divert to another track or continue the through route (continue the same route). Double slip switch allows the train to transfer from all entry points.
- Lapped turnouts: used in limited space, they provide a compact solution by offering an additional route with the addition of a third crossing (frog).

Table 1 Different types of S&C

Turnout	Diamond crossing	Crossover	Junction
		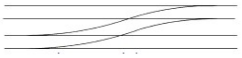	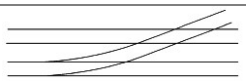
Right-hand	Standard	Single	Single
		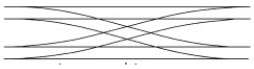	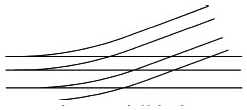
Equal split	Inside single slip	Scissors	Double
		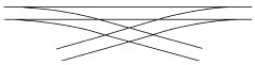	
	Outside single slip	Half-scissors	
			
	Inside double slip		
			
	Outside double slip		

3.1.6 Installation of S&C

Installation of S&C can be carried out by assembling on site, preassembling near the site, or using modular sections. In the UK, NR renews 340 switches annually, the majority of which are assembled on the manufacturing site for quality inspection. Traditionally, these units are then disassembled and transported to the site where they are re-assembled either on site or in its vicinity. This traditional approach is inefficient both in terms of time and cost. Thus, in the past decade or so, NR has introduced modular assembly methods.

S&C require more time for replacement than plain line track, and it is important to minimise the possession times needed to carry out these replacements. The modular technique has the potential for significant reduction in possession times. Typical installation times are ~36 hours for a conventional turnout and ~54 hours for a crossover; NR aims to reduce this to 8 hours for conventional turnouts and to no more than 14 hours for crossovers (Network Rail, 2012). In 2014, 75% of S&C replacements were carried out using the modular concept (MAINLINE,

2014), in which the bearer sections are connected using a metal shroud through eight shanked bolts, with a polymer base elastomeric (rubber) layer sandwiched between them.

The loading gauge defines the maximum height and width of an artefact that is allowed to be transported along the railway; in the UK, a maximum width of 3.7 m is permitted. This puts a restriction on the size of an S&C that can be transported. One way to overcome this is by splitting the longer bearers into two or three segments creating smaller modules that can be transported separately. To aid this, special tilting trains (see Figure 9) are used to make the process of transportation and loading/unloading easer, quicker and safer.

Figure 9 Network Rail's tilting wagon lowering new track panels (Network Rail, 2009)

3.1.7 Maintenance

Maintenance is needed to correct defects (faults) caused by railway structure degradation. The issue of degradation has become a significant challenge to rail transport service providers owing to high traffic demand. While in the past the strategy was to expand existing networks to meet these demands, this is no longer viable owing to commercial reasons and land restrictions. Therefore, the current focus is on how to efficiently manage and maintain the current network. This makes minimising track degradation a crucial step in reducing the costs and improving management of the railway assets via optimising maintenance needs, reducing costs, and improving track conditions.

3.1.7.1 Tamping

The most common maintenance operation employed to correct geometric defects such as longitudinal level, crosslevel, horizontal alignment, and twist is tamping. The process involves the use of hydraulic jacks to lift the track to the required level while correcting its lateral

position, proceeded by rearrangement of the ballast layer under the sleepers to achieve the desired geometry (Selig & Waters, 1994). The operation involves vibrations, which may adversely affect the ballast by rearranging its structure (reduced density) and causing grain attrition and breakage. This can also lead to a phenomenon known as ballast fouling, where fine grains arising from ballast attrition accumulate within the ballast voids (Tennakoon, et al., 2014).

Whilst some modern tamping units can operate on S&C, traditionally these are more likely to be hand packed with the plain line ramped into the ends of the S&C with a tamper.

Tamping can also make the ballast less stiff, and less well damped (Grassie & Cox, 1985). Shi, et al., (2020) carried out DEM modelling of tamping operation and found tamping to decrease the compactness of the ballast immediately under the sleeper by 35%, while lifting the sleeper reduces the support stiffness by over 50%. Such a decrease in support rigidity could be harmful to the mechanical joints, with higher resilient deflections causing excessive strains on the joint assembly.

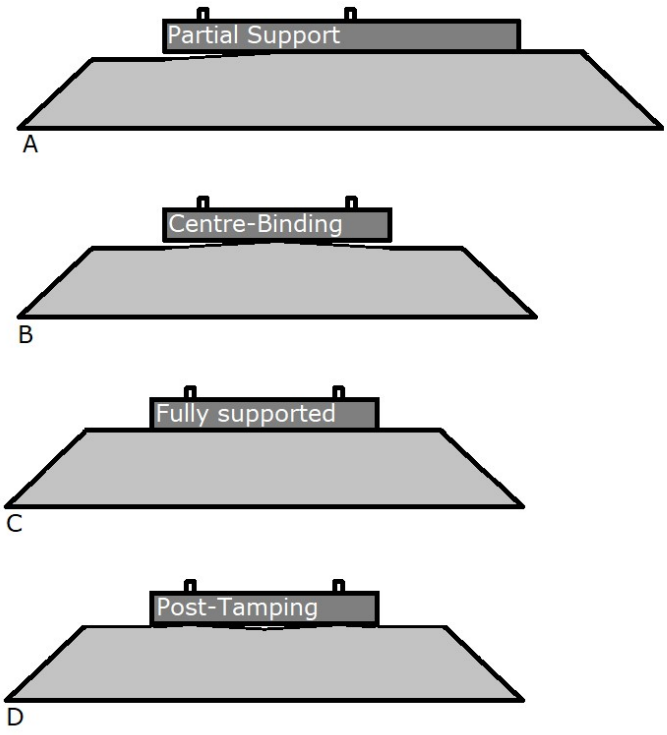

Figure 10 Various ballast support conditions showing; A: Partial support on a long bearer with ballast support shifted away from the rail closest to the ballast shoulder, B: Centre-Binding of a sleeper with ballast support at the middle of the sleeper, C: Fully supported ideal case and D: Post-Tamping ballast support with maximum support under the rails.

Centre-binding is the process in which ballast support, with loading cycles, shifts inwards from immediately under the rails (Figure 10C) to the centre of the sleeper (Figure 10B). This can

lead to a gap below the sleeper ends and, in the case of a long bearer with eccentric loading, partial support as shown in Figure 10A.

3.1.7.2 Possession

Track possession is a formal procedure during which trains are blocked for a defined period from using a certain length of track. This allows safe access for carrying out inspection, maintenance, or renewal activities. Longer and disruptive possession times reduce the revenue earned by rail operators and increase infrastructure costs. Key causal factors are the timing of engineering work, investment in maintainability, contracting policy, possession timetabling, and possession management processes.

3.1.8 Track twist faults

Crosslevel or cant is the difference in vertical height of the two rails over which the wheelset rolls. Twist faults take place on a track with differences between the heights of rails i.e., crosslevel or cant, potentially leading to train derailment irrespective of train speed (ORR, n.d.). Twist is measured over five sleepers or 3 m. It most commonly occurs at regions where the cant changes in the transition of a curve, at track faults, or during renewal where ballast has been poorly compacted or areas that receive high impact loads (CEC, 2002). The absolute limit for twist gradient is 1:90 which requires traffic to be stopped whilst gradients between 1:91 and 1:199 require immediate attention (GCRT5021) (RSSB, 2011). Derailment due to twist faults happen as one or more wheels lose contact on the rail and the flange climbs the rail. Older vehicles with rigid suspension are more susceptible; nevertheless, this type of fault remains a serious risk even on newer vehicles with more independent and softer suspension.

On S&C, causal factors for twist faults include wear on the crossing nose, locations that are unable to receive mechanical tamping - poorly consolidated ballast, hanging sections of bearers, differential settlement, and regions where tamping starts/ends (CEC, 2002). Track twists are measured when the track is loaded (dynamic twist) and unloaded (static twist); the latter does not account for unsupported sleepers. Voiding (gaps) are important in determining dynamic twists.

In 2017, a two-wagon train carrying aggregate on a newly laid modular S&C unit derailed, causing major service disruption (Lewisham train derailment). It has been suggested that the cause was poor ballast support to the bearers, and the flexible nature of the bearer joint that led to a comparatively more compacted ballast on one side of the rails, leaving the other side poorly supported resulting in a significant twist fault (RAIB, 2017).

3.2 Issues related to S&C

The main elements of S&C described in previous section constitute complex and safety-critical assets that are subjected to high operational loads, resulting in the need for regular, costly, and time-consuming maintenance.

S&C design has developed in several ways. Traditionally, the switch blade was joined by a fishplate to the closure rail and on plain track to jointed sections of rail. In areas where it is economically feasible and there is enough ballast to prevent the rails from buckling under thermal stress, continuous welded rail (CWR) has replaced jointed rail because it is more durable, quiet and improves ride quality. However, the occasional physical joint is still important to allow for the thermal expansion and contraction of the rail. This mechanical joint is prone to damage, dipping, creates noise and requires more maintenance.

The stiffness of the track, and how it varies along the length, affects track quality. While an ideal track has a uniform track stiffness, deviations in track stiffness are common, especially in S&C. This is owing to distinct design features of S&C such as changing rail profile, discontinuities in rails and changing soffit areas of the long bearers.

Consequently, S&C are more vulnerable to differential track settlement, which is the main driver for vertical track irregularities and in turn the precursor to maintenance in the form of tamping.

3.2.1 Discontinuities

Discontinuities in rails affect the smooth rolling of the train wheels and induce impact forces. An important feature of an S&C, the frog, is also a region of running surface discontinuity due to the gap between the wing rail and the crossing nose.

3.2.2 Variable geometry

In contrast to plain line where the rail cross-sectional geometry remains uniform, in S&C the rail cross section varies on elements such as the switch blades, to allow the wheels to transfer from the stock rail to the switch rail.

The flexural rigidity EI, where E is the elastic modulus and I is the moment of inertia, of the track varies along the length of the S&C, e.g., in the crossing region where additional rails (the check rails) are fixed to the bearers. Figure 11 shows changing track properties on S&C such as the lower flexibility of crossing nose (dotted line in Figure 11). Track flexibility is the track

deflection per unit load. Sudden, large changes in track flexibility such as that from switch stock rail to crossing nose region can lead to impact loads (Andersson & Dahlberg, 1998).

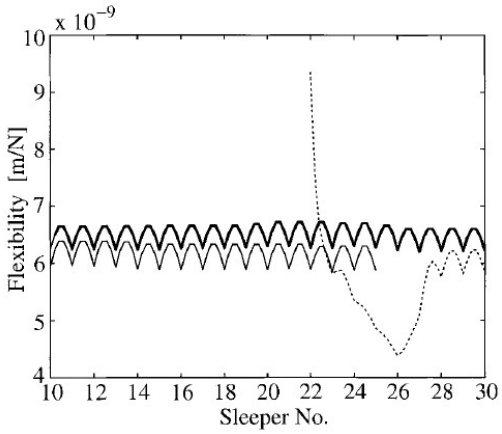

Figure 11 Comparison of track flexibility on S&C, bold line shows flexibility of switch stock rail (cess rail), thin line shows flexibility of switch rail and wing rail and dotted line shows flexibility of nose and nose rail (Andersson & Dahlberg, 1998)

3.2.3 Changing lengths of bearers

On an S&C the length of the bearers increases incrementally to support rails splitting into separate tracks and help with the stability of the rails by allowing spread of the rail loads over a longer span. At some locations, adjacent tracks can be connected by bearers >6 m long (with joints present in the case of modular S&C) and passing trains can be "felt" on the adjacent track.

This has the following implications:

- A train passing on one track can cause long bearers to rotate towards the loaded track. On loading the adjacent track, the rotation reverses and there may be complex dynamic train-track interaction with any partly lifted bearer end deflecting downward through a void before meeting the underlying ballast.
- Different lengths of bearers have different mass; this has implications on the dynamics of the S&C.
- Variation in stress along the length of the bearer-ballast interface may lead to differential settlement along the bearer length as well as along the track between consecutive bearers.

3.2.4 Impact forces

Impact forces create the highest loads in the track structure, and are created by track and vehicle irregularities, producing potentially damaging high frequency short-duration forces. S&C are one of the few places on modern railway where impact loads are a concern. In the past impact

loads were a concern at every joint (fishplates) but on modern tracks it is relevant only at expansion joints, electrical insulation joints and at S&C.

The magnitude of the impact force is influenced by several parameters including the design and manufacturing tolerances of the crossing; the service condition of wheel; the stiffness of the wing rail, crossing nose and track (which can in turn depend on the presence of voided sleepers, the use of under sleeper pads, etc.); the axle load; the vehicle speed; and the lateral position of the wheel when approaching the crossing nose.

Vehicle-track dynamics are influenced by the distribution of forces at wheel-rail contact (Zhang, et al., 2009). These forces are influenced by vehicle speed, wheel-rail geometric parameters and mechanical properties such as track flexibility (Andersson & Dahlberg, 1998) (Kalker, 1991). Wheel-rail interaction influences traffic safety. While dynamic forces caused by wheel-rail interaction contribute to impact loads on plain line at locations such as rail joints, these are more common and severe on S&C owing to the features described earlier.

Impact loads are affected by factors such as changing track stiffness at the crossing, change in mass distribution (the crossing nose has a variable mass distribution and a larger mass than the stock rail), irregularities in wheel-rail contact as it transitions from wing rail to nose (and vice versa) and the difference in height between the wing rail and the nose (Anderson & Zeitlinger, 2000).

A dip in a rail is characterised by the dip angle, α, illustrated in Figure 12. Contact impact forces are categorised as P_1 and P_2; these are illustrated in Figure 13, for a wheel passing over a dipped rail joint (Mandal, et al., 2016). Modern CWR do not have such issues, but it remains relevant to S&C.

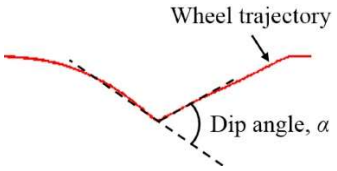

Figure 12 Illustration of dip angle, α (Torstensson, et al., 2019)

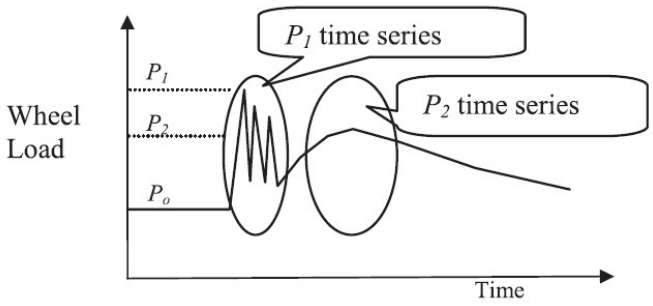

Figure 13 P1 and P2 forces at a dipped joint ((Mandal, et al., 2016))

Torstensson, et al., (2019) used a non-linear vertical dynamic vehicle track interaction model to calculate the vertical wheel-rail contact force over a crossing and the influence of dip angle on contact force. Figure 14 shows the calculated time history was for a facing move, axle load of 20T and speed of 100km/h, passing through crossings with varying dip angles. The sharp peak vertical force can be identified as P_1 force. These forces are created directly after impact and have a characteristic high frequency (~200-1000 Hz) seen on time history of impact force. High in magnitude and short in duration, they result from excitation of vibrational modes between the wheel and rail (Remennikov & Kaewunruen, 2007). Damage from P_1 forces is to the contact points of railhead and wheel thread.

The P_1 forces are followed by P_2 forces which are lower in magnitude with a frequency range of ~50-200 Hz. The P_2 forces occur when the wheel-rail contact vibrates in phase on the ballast (Remennikov & Kaewunruen, 2007). These forces remain for longer time. P_2 forces can cause damage to a broader range of components in the vicinity of the contact zone.

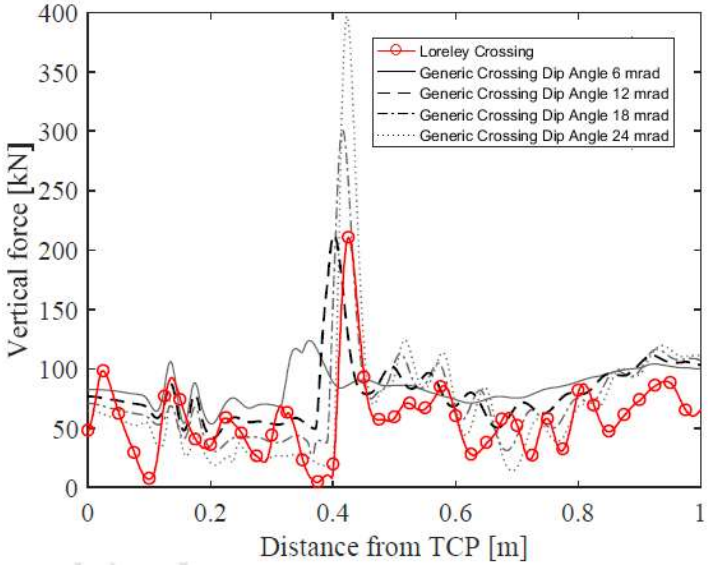

Figure 14 Calculated time history of vertical wheel–rail contact force in the crossing panel, TCP is the Theoretical Crossing Point (Torstensson, et al., 2019)

3.3 Research into S&C performance – global performance

Research on S&C superstructure is often through computer simulation software and field/laboratory work. This can be divided into two main categories: wheel-rail interaction and substructure (railpads, bearers, ballast, foundation). Research carried out on wheel-rail interaction includes optimisation of rail profiles (including rolling radii difference (RDD)) (Wang, et al., 2017), mechanical behaviour of the rail (plastic deformation of rail, rolling contact fatigue (RCF) (Johansson, et al., 2011), impacts at rail joints, flexural behaviour (Sun, et al., 2010) (Askarinejad, et al., 2012) etc. Research focusing on the substructure emphasises the variation in ballast settlement at S&C (Grossoni, et al., 2021), impact loads at prominent locations such as the crossing nose (Torstensson, et al., 2019). It also considers interventions such as under sleeper pads (USP) (Le Pen, et al., 2017) (Loy, 2009) and rail pads (RP) (Markine, et al., 2011) to optimise stiffness profile of S&C to achieve more homogenised track bed stiffness, with the intention that this should reduce differential track settlement. However, the modelling of trackbed as linear elastic support is a drawback and studies generally neglect development of initial differential settlement/geometry imperfections.

Modelling work reported in the literature has used a variety of software, the two main suites used are: specialised railway multibody simulation software emphasising train-track interaction & vehicle dynamics, and Finite Element Analysis. Examples of the former are VAMPIRE (Sun, et al., 2015), GENSYS (Kassa, et al., 2006), VI-RAIL (Jorge, et al., 2020), SIMPACK Rail (Lagos, et al., 2014). Different methodologies for modelling discontinuities at the crossing have been proposed by (Andersson & Dahlberg, 1998) (Coleman, 2014) (Sun, et al., 2010).

Zhu (2006) studied the effect of an elastic slide baseplate on the dynamic performance of a highspeed turnout. The slide plate allows for the movement of the switch blade. Generally, wheel-rail impact loads are caused due to the variation in vertical stiffness when wheels navigate from the stock rail with rail pads (vertical stiffness ~90 kN mm^{-1}) to a switch rail with an ordinary baseplate (vertical stiffness ~270 kN mm^{-1}). By using an elastic rubber between the upper sliding plate and the bottom plate, the vertical stiffness under the switch rail is brought closer to that under the stock rail. This was shown to decrease track accelerations in the region (Zhu & Luo, 2004). The study considered impact loads caused by vertical geometric irregularities due to the change in height from the switch blade to the stock rail. It also considered the variation in stiffness resulting from the presence of elastic rail pads under the

stock rail but not under the switch blade. However, there is no consideration of changes in ballast/foundation behaviour over time.

Alfi & Bruno (2009) carried out a finite element study to investigate train-S&C interaction by considering S&C features such as rail profile variation, track flexibility variation and multiple contact points. It was shown that large impacts occur as the wheel transfers from the wing rail to the crossing nose. Vertical contact forces on the wheel are shown in Figure 15 (Alfi & Bruno, 2009). The study focuses on the rail irregularities but does not consider the effect of accumulating plastic settlement along the length of the bearers. It is important to note that change in track flexibility may affect the behaviour of the track in terms of permanent and resilient deflections. The accumulated effect of these will change the impact loads over the course of the loading cycles.

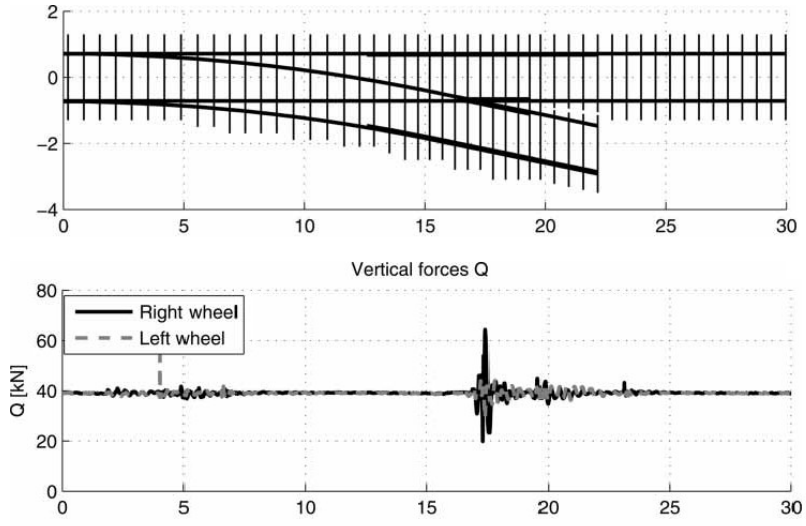

Figure 15 Vertical contact forces on both wheels as the train negotiates (at 54 Km/h) the main line of an S&C with no track irregularity and new wheel-track profile (Alfi & Bruno, 2009)

The switch section of an S&C is a region where the wheel-rail contact changes. As the switch blade is lower than the stock rail, the wheel moves down as it transitions. The wheel elevates when it transfers from switch rail to stock rail as the rolling radius decreases as illustrated in Figure 16. This produces a dynamic impact force in the switch region that is amplified by the difference in basepad stiffness between the stock rail and switch rails (Zhu, 2006).

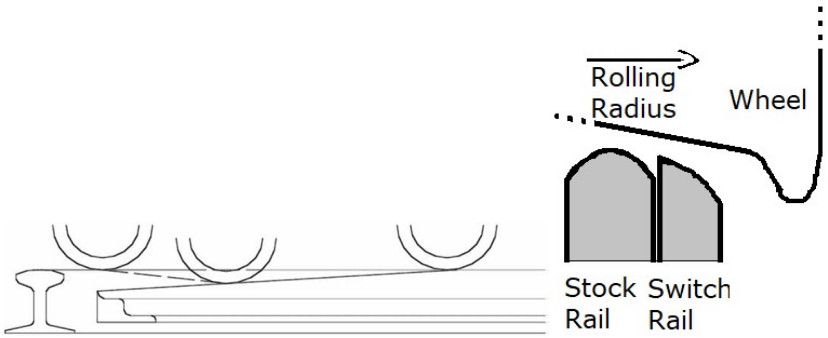

Figure 16 Drawing showing vertical irregularity on switch rail, side view (L) (Zhu, 2006), cross sectional view (R)

Lau and Hoff (2018) performed train-turnout coupled dynamic analysis to show variations in vertical and lateral normal force of the wheels on the leading wheelsets as the train navigates through the diverging route, these force variations are prominent in the switch and the crossing region (Figure 17).

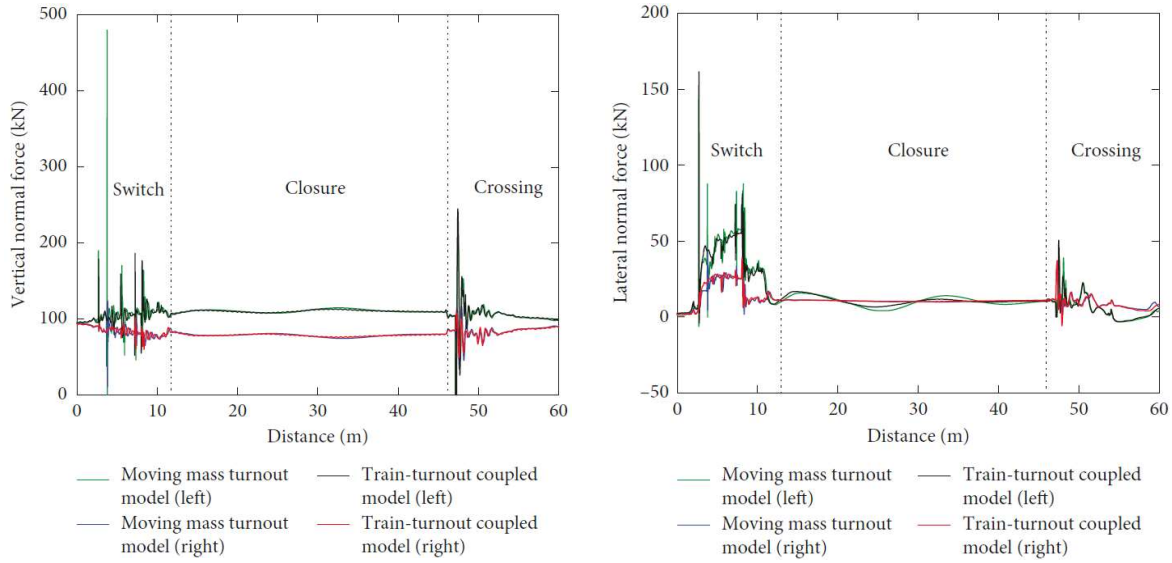

Figure 17 Vertical (L) and Horizontal (R) forces on leading wheelset (Lau & Hoff, 2018)

3.4 Research into the performance of S&C components – long bearers

The role of S&C bearers, like that of plain line sleepers, is to distribute loads from the rails to the underlying ballast bed and to retain the gauge of rails and crossings under running traffic. However, they differ from sleepers in their length (which varies from 2.2 m to 7.5 m), position relative to the rails, the complex geometry of rails they support and the dynamic loads they receive. The operational life of S&C bearers is half that of main line sleepers (Kaewunruen, et al., 2018).

Recent studies indicate that the possibility of intense impact loads can jeopardise structural integrity and durability of S&C bearers (Siew, et al., 2017). These impact loads are evident at transfer zones where the wheel passes over gaps in the rails, notably at the bearer supporting the crossing nose but also at other locations such as where a mechanical joint is used, e.g., heel-block joints. Historic findings suggest that failure of just a single bearer at a critical location such as at crossing panel can result in crossing nose damage, broken rails/joint/bolts and have adverse effects on train operation (Kaewunruen, et al., 2018).

Studies have shown that the bearer under the crossing nose is subject to the highest impact loads. A 3D FE model studying the forces and reactions in S&C found that bearers under the crossing nose underwent the largest deflections as well as greatest bending moment and shear force (Siew, et al., 2017).

A study by Lau & Hoff (2018), however, suggests that regions receiving high dynamic impacts do not necessarily have the highest forces on the corresponding bearers. This is because regions such as the crossing panel do receive high dynamic impacts. Figure 18 shows that the forces transferred to bearers in the crossing panel (sleeper number 70-90) are reduced due to the high bending stiffness of the rails whilst highest forces are seen in the switch panel (sleeper number 1-20) (Lau & Hoff, 2018).

Siew, et al., 2017 presented a 3D finite element model to simulate a turnout with moving load of a coupled locomotive which had a single 360 kN axle, 2 m ahead of four 300 kN axle loads. Deflections of the ballast layer under the critical bearer at the crossing nose revealed that the directions of calculated translations were not vertical and indicate rotation or twisting of the bearer as shown in Figure 19 (Siew, et al., 2017). This was confirmed in S&C field measurements in which long bearers using soft USPs rotated towards the loaded track with cess to 6 ft end movements at ratios of between 1.1 to 2.3. The higher ratios are thought to be due to uneven support conditions along the bearer (Le Pen, et al., 2017). Plasek & Hruzikova (2017)

identified a similar uplift effect of bearers in a field trial of S&C utilising USPs (Plasek & Hruzikova, 2017).

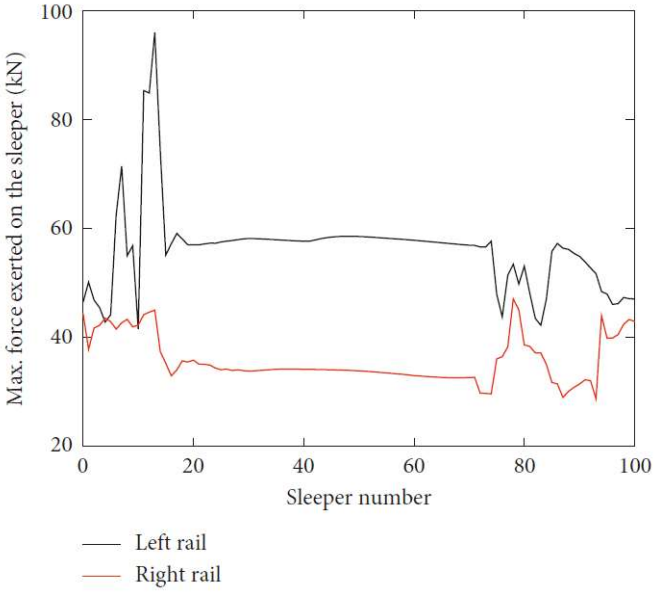

Figure 18 Difference in maximum force exerted on sleeper in S&C due to curving forces (Lau & Hoff, 2018)

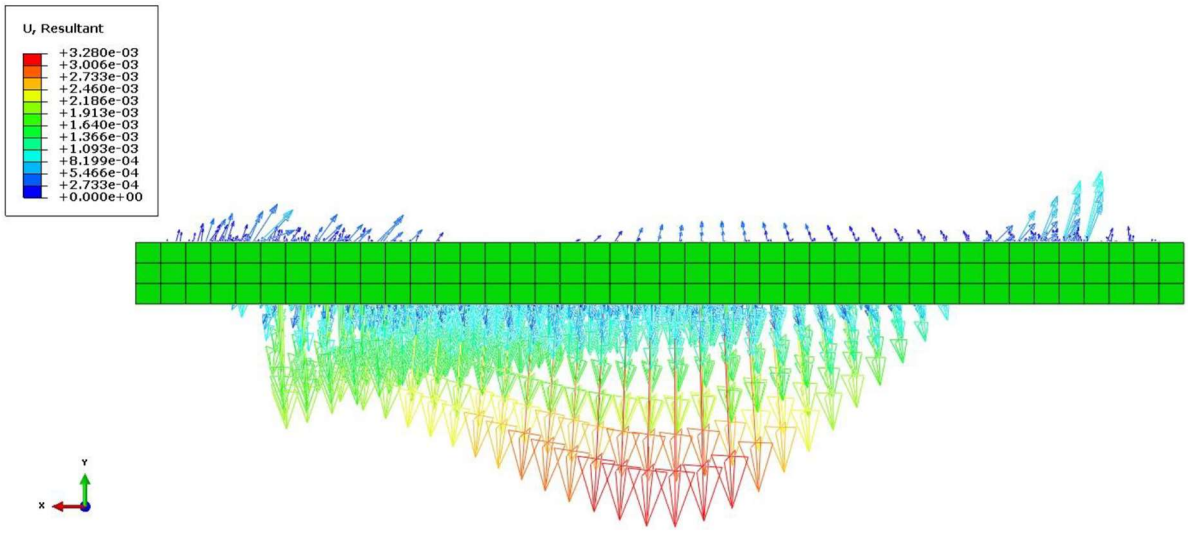

Figure 19 Deflection of ballast layer (unit: meters) under bearer exactly under the crossing nose showing the resultant displacement of the ballast which indicates rotation of the bearer (Siew, et al., 2017)

Curvature of the track causes asymmetric loads on the bearers. For example, on a single switch (right- hand) turnout, where the diverging route is to the right of straight through route. The maximum force exerted on the left rail (when the train is navigating the right-hand diverging route) is greater than that on the right rail (Lau & Hoff, 2018), tending to cause a further rotation of an S&C bearer towards the loaded side S&C. This is due to the curving forces shown in Figure 18 where the force applied on the bearer is higher on the left rail. Priest et al., 2013 performed field measurements and numerical modelling of sections of track with cant

deficiency. This showed that a Class 390 train travelling over a cant of 0.15 m at 180 km/h with a nominal axle load of 13.75 Mg and the distance from the railhead to the centre of mass of the train carriage, H_c of 1.65 m produced normal wheel load on the outer rail to be 63% greater than that on the inner rail. This would yield the maximum normal displacements of the outer rails to be 1.6 times greater than those of the inner rail provided that the sleeper support stiffness is uniform (Priest, et al., 2013).

The position of the rails relative to the ends of the bearers will also lead to asymmetric loads on the bearers. In a finite element study of a right-hand S&C by Lau and Hoff (2018), it was observed that forces under the bearers were higher on the right than on the middle and left. This is because on the diverging route, rails were located increasingly to the right-hand side of the bearers Figure 20.

As mentioned previously, the length of bearers in S&C varies (2.6 – 6.3 m) depending on their location in the crossing and the number of rails they support. Changing bearer length along the length of the S&C will influence the track dynamics and needs to be accounted for when estimating resilient track deflections. Forces along the length of the S&C have been reported to vary owing to changing bearer mass (Lau and Hoff 2018).

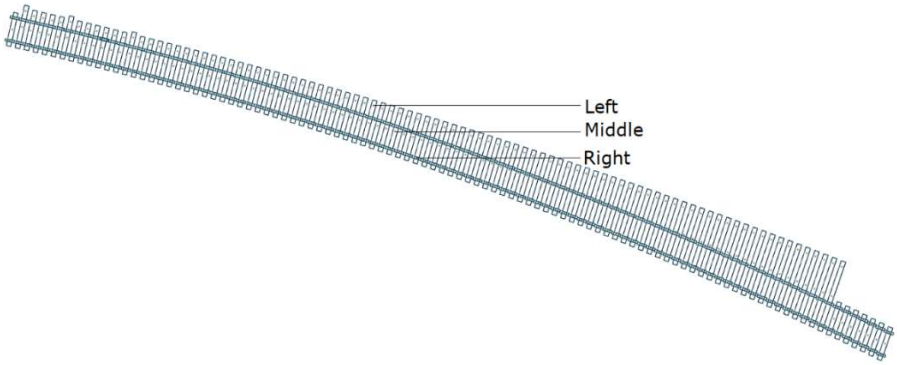

Figure 20 Schematic view of the turnout model used in finite element analysis to evaluate forces on bearers (Lau & Hoff, 2018)

Zhu & Thompson (2009) carried out a finite element study to characterise the forces and dynamic response of a modular S&C bearer. Timoshenko beams were used to simulate the bearers together with a bi-linear approach to account for the tensionless nature of the ballast. The bearer under the crossing nose was the focus of the study; the joint was beside the loaded rails. Maximum loads applied to both rails were derived from load time history through vehicle dynamic calculations, considering rail discontinuities and wheel-rail contact geometry (Zhu & Thompson, 2009).

Increased bending moments can occur on sleepers because of centre-binding, which causes negative bending (hogging), induces cracks in concrete bearers and is detrimental to service life. Zhu & Thompson (2009) showed that flexible joints, of rotational stiffness 5×10^4 Nm rad^{-1}, used in the bearer reduce the maximum sagging and increase the maximum hogging, resulting in a 20% reduction in moment variation compared with a continuous bearer (Figure 21). Stiffer joints tended towards the behaviour of continuous bearers in terms of both vertical displacements and maximum positive bending moment. Track stiffness on the through route is reduced using a flexible joint between bearer parts on the diverging route. This influence weakens as the bearer lengths increase. Joints of lesser stiffness provide an uncoupling effect, resulting in less lifting of the bearer end on the unloaded part of the track. Consequently, reducing the impact on the underlying ballast (Zhu & Thompson, 2009). In this study both the jointed and continuous bearers were loaded using the same values but loads in each case would be expected to vary.

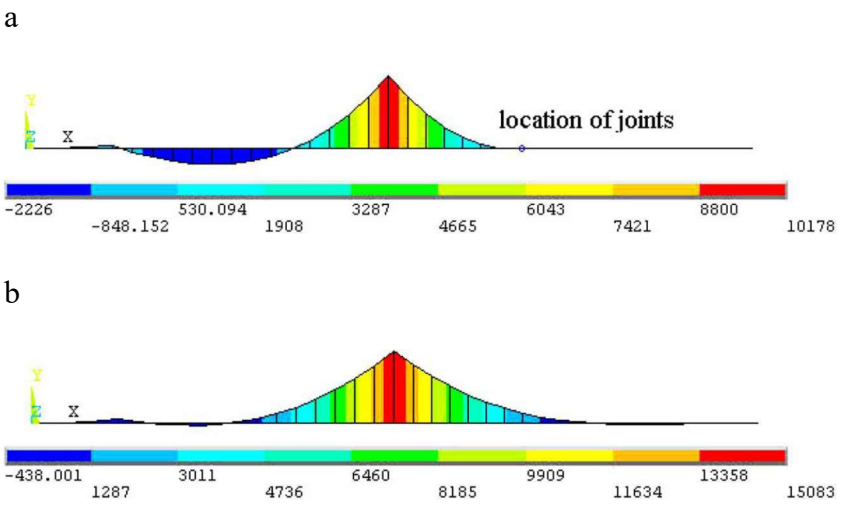

Figure 21 Bending moment diagram of (a) jointed switch sleeper and (b) continuous switch sleeper (unit: Nm, horizontal axis is distance along sleeper under crossing nose (Zhu & Thompson, 2009).

3.5 Research into the performance of S&C components – Rail pads

Rail pads are an important element of ballasted track superstructure. Made from a polymeric compound (e.g., HDPE, TPE, EVA), rubber or composite materials, they are located between the rail seat and sleeper where they transfer stresses to the sleeper from the rail toe. The additional compliance introduced into the system from the railpads helps to distribute wheel load along the track between adjacent sleepers. This also limits peak stresses from wheel-rail impact forces. Softer rail pads, by offering greater isolation between the rail and sleeper, reduce the forces and consequently the strains acting on the sleepers (Grassie & Cox, 1984).

It is also worth noting that the elastic modulus of the railpads does not remain constant and effects of pre-stress (bolt loads) and train loading and ageing should be considered when determining its response. Likewise, the use of a resilient layer within a bearer joint could influence its rotational stiffness properties, and the bolt loads used within the joint could influence the stiffness of the resilient pads therefore influencing the overall behaviour of the joint.

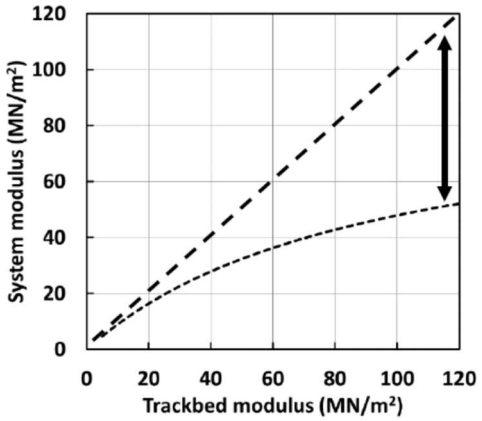

Figure 22 Effect of railpad compliance on the overall support system modulus (railpad stiffness = 60 MN m^{-2}) (Le Pen, et al., 2016).

Support system modulus is defined as the load per unit length causing a unit displacement at the rail. The inclusion of railpad stiffness in system modulus is important, as they are utilised over most of the UK's railway network. Neglecting its contribution introduces an error which increases with the trackbed modulus as shown in Figure 22 (Le Pen, et al., 2016).

Nicklisch, et al., (2010) performed numerical simulations on S&C that used soft under sleeper pads and showed that increase in train speed improved the effect of softer rail pads in reducing the normal contact forces on the rails. Soft rail pads are used in S&C to reduce the support stiffness of the switch, notably in the crossing nose. Markine, et al., 2011 showed using vehicle track interaction model that reducing the stiffness of the rail pads by a factor of 6 has shown the potential to decrease the impact load at the crossing by 21% of the original load, forces on sleepers and ballast by 67% and 28%, respectively (Markine, et al., 2011). In the study it was also indicated that soft rail pads were more effective than under sleeper pads in reducing impact loads. The track structure was modelled in 2D using linear material properties, so the trackbed/ballast response was linear elastic.

Track stiffness variation along a switch was reduced by an INNOTRACK project by using soft rail pads with a range of stiffnesses and placing them strategically. Such that stiffer rail pads

are located towards the front of the S&C and softer rail pads in proximity to the switch heel (from toe to nose). As a result, track stiffness variation was brought down to only 8% (MAINLINE, 2014). Similar observations have been reported by (Nicklisch, et al., 2010). These studied are however based on modelling the ballast as linear elastic, and whilst variation in stiffness of the ballast is incorporated into the model, the effect of initial geometry is neglected, and perfect support is assumed. The effect of ballast material as a nonlinear elastoplastic is not covered. The use of a joint within the bearers (at varying distances relative to the rails) could influence track stiffness and is therefore important to explore in such studies. These studies neglect the effect of pre-existing differential settlement of the track, which is affected by the loading of the track, and track superstructure. Experiments show that track superstructure properties affect the rate and amount of settlement (In2Rail, 2017).

3.6 Research into the performance of S&C components – Under Sleeper Pads (USP)

Under Sleeper Pads (USP) are polymeric elements placed between the sleeper and ballast to increase the compliance of the superstructure, increase the ballast-sleeper contact area, and increase ballast tamping intervals by decreasing the rate of ballast deterioration and track settlement.

USPs are effective in providing softer contact points by acting as a cushion between the hard grain edges and sleeper base, thus facilitating a more uniform track support and potentially reducing the likelihood of gapping between the sleeper and the ballast (Ngamkhanong & Kaewunruen, 2020).

Sleepers contact with the ballast in a more uniform manner as the hard contact points between the sleeper base and ballast grains are lessened. This helps reduce the damage to the immediate layer of ballast underneath the sleeper that is otherwise subject to high stresses and susceptible to damage in the form of abrasion and breakage (Abadi, et al., 2015) (Cui, et al., 2021). Ballast migration or the movement of ballast grains across the track due to dynamic forces, is reduced at the top surface of the ballast layer by providing stable contacts (IN2TRACK, 2020).

Le pen, et al., (2017) measured the performance of a renewed S&C with and without the use of soft UPSs. Measurements from track site fitted with a USP for two years indicated that the use of USPs gave a more uniform range of movements in bearers than bearers without any USP. Data also indicated that the bearers rotated in the direction of the loaded track with train passage, leaving the bearer position rotated towards the loaded track even after train passage. The effect was intensified with the use of soft USPs (Le Pen, et al., 2017).

Variation in track stiffness along S&C units can be reduced by USPs of different stiffnesses. Loy (2009) reported a finite element model of an S&C with a single type of USP, variation of USPs stiffnesses and no USPs were compared. Figure 23 shows that positioning the different stiffness USPs optimally to improve the load bearing of the track reduced the irregularity in stiffness along the S&C unit and reduced rail seat forces by 10-20% (Loy, 2009). This numerical study however did not account for the development of initial differential settlement/geometric imperfections.

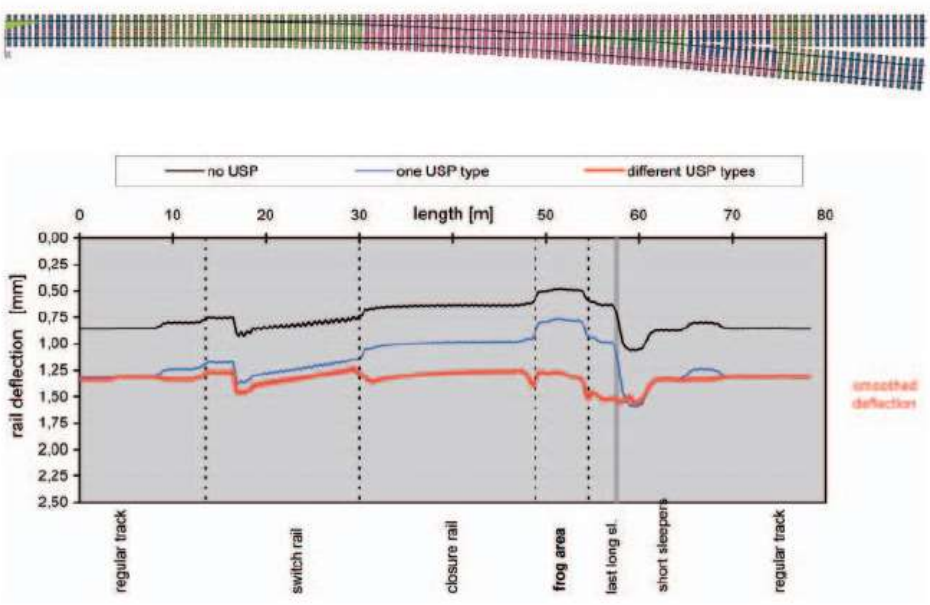

Figure 23 Comparison of rail deflection patterns with optimised track using different USP along the S&C (Loy, 2009)

Mainline (2014) reported that soft rail pads can reduce the impact loads related to rail damage (P_1 forces), while USPs are more effective in reducing the P_2 forces and prolonging sleeper and ballast life. Both dynamic loads on the sleepers and ballast as well as impact loads received by the rails could be further reduced if both softer railpads and USPs are used in conjunction (MAINLINE, 2014). However, such models do not consider that the ballast may settle differentially and increasing the range of movement through softer rail pads and USPs could adversely influence this, therefore more research is needed.

3.7 Conclusion

In this chapter, a standard S&C and its constituting elements have been described, together with some non-standard elements such as fishplates. It has been shown that an S&C is a complex assembly that includes features such as varying geometry e.g., increasing cross-sections of switch rails and crossing nose, changing lengths of bearers, discontinuities in the

rails (such as the gap between the closure rails and the crossing nose), changing flexibility of the rails as in the crossing nose and difference in height of transition points (such as stock rail to switch rail and wing rail to crossing nose and vice versa).

Dynamic impact loads have a detrimental effect on the turnout system, and mechanical joints within the system could be more prone to damage from such heightened loads. As it has been noted that bearers (and sleepers) undergo greater bending because of centre-binding, so a mechanical joint within the bearers would be more susceptible to damage from the increased strains imposed by bending.

Voided sleepers or gaps that form at the sleeper/ballast interface are a common occurrence and the bearer rotating towards the side of the track that is loaded has also been reported in literature. The effectiveness of mitigation options such as ballast shoulder interventions and the use of USPs, on bearer voids and bearer rotation will be useful to explore.

These features of S&C lead to high dynamic impact loads which determine its performance. The crossing nose is the region where the greatest vertical contact forces and impact loads are seen; this is also the region of highest flexural rigidity. Issues related to S&C bearers include partial voiding and tilting of bearers, which exacerbate the impact loads experienced by the underlying ballast.

It is also noted that variation in track stiffness can be reduced by applying appropriate stiffness of rail pads and/or under sleeper pads over the length of the S&C. Studies that were conducted on jointed bearers at modular S&C suggested that changing the stiffness of the joint in the bearers could alter track stiffness. Jointed bearers have also shown the potential to reduce tilting of the bearers on the unloaded side of the track.

The literature review suggests that the limited work on the performance of S&C bearers has focused on its transient structural performance. It does not include the effect of evolving ballast permanent settlement with increasing loading cycles and the accompanied changes in resilient deflections of the bearers.

4 Materials and Methods

This chapter describes the materials and methods employed in carrying out full scale laboratory experiments to understand the behaviour of S&C bearer performance, and full scale three-point bending tests conducted on the continuous/jointed bearers which were used within the finite element analysis (FEA) of the jointed bearer assembly.

4.1 Introduction

Previous chapters have highlighted the rise in railway usage, strict safety regulations and the role of railways in sustaining economic growth. To cater for such demands and expectations, railway operators are dedicated to reducing the costs for maintenance and renewal of the rail network. One way of achieving this is by the recently introduced modular S&C. These are pre-assembled segments of S&C that are joined together on site via a mechanical fastener between the bearer sections.

Changing ballast support with the accumulation of loading cycles can lead to centre-binding which can exert detrimental forces on the bearer hence the joint and impact its structural integrity. The evolution of vertical resilient deflections and permanent settlement of the bearers with increasing loading cycles can indicate such changes in bearer-ballast interaction. These were measured on full scale bearers of various lengths with different joint locations and types. The use of two lengths of bearers with joint location varying from between the loaded rails (loaded rails were towards the ballast shoulder) to joint beside the loaded rails (away from the loaded rails and the ballast shoulder) were used in this research to generalise the three parameters i.e., joint type, location, and bearer length.

The laboratory experiments were carried out in the SRTF apparatus, shown in Figure 24. This is a bespoke sleeper/ballast testing rig that represents a cross-sectional cut of a track in near plane strain conditions. Modifications to the earlier design (Le Pen, 2008) (Abadi, 2015) (Ferro, 2018) allowed accommodation of up to 5.6 m long Switch and Crossing (S&C) bearers and the ability to block the shoulder opening at various distances from the loaded rails. The single bearer rig had the benefit of providing feasible comparative study of the effect of individual bearers with reasonable experimental complexity, but its limitation was that it ignored the loading on the ‘unloaded’ or diverging route and the stiffness of the rail in the longitudinal direction. Although the diverging line is less heavily trafficked than the through line and considering that 33% to 55% of normal load is transferred to the sleeper under the axle, the comparative study reproduced the worst-case scenario.

Data from tests on jointed bearers in general ballast formation (shoulder slope 1H:1V) and standard bearer conditions (without the use of USPs) were obtained and compared with baseline tests (continuous bearers in general conditions) to show how the joint type and its location affected the permanent settlement and resilient deflection both spatially (along the length of the bearers) and with increasing loading cycles. Then in the next phase of laboratory experiments, confined ballast shoulder where the ballast shoulder was restricted to movement using a bespoke steel section forming a wall between the rig walls (see Figure 25) was tested. Moreover, the effect of USPs on jointed bearer and its continuous counterpart was studied.

To understand the mechanics of S&C bearer performance, the modified SRTF was utilised to:

- Study the spatial development of vertical settlement and resilient deflection behaviour of long bearers subjected to off-centre (eccentric) loading (Objective 2-4),
- Quantify bearer-ballast contact characteristics (Objective 2-4),
- Measure lateral spreading of the ballast shoulder (Objective 2-4),
- Measure lateral pressures on the shoulder confinement (Objective 3),
- Characterise the longitudinal confining stresses (Objective 2-4),
- Understand vertical pressures beneath the track superstructure (Objective 2-4).
- Quantify strains on the bearer joint (Objective 4)

In addition, laboratory three-point bending tests were carried out on the continuous and rigid jointed bearers to characterise the rotational stiffness of the joint and use the bearer deflection data to support a finite element model that was created to understand the influence of rubber pad stiffness, spring washer and bolt load of the joint and understand the type of stresses developed within the bolts used in the joint (Objective 5 & 6).

This chapter describes the materials (ballast and bearers) and instruments used in the experiments. A description of the test preparation and methods for measuring ballast shoulder movement, bearer-ballast contact and gap at the end of a test. Finally, it presents the test plan and summary.

Figure 24 Photograph of the SRTF

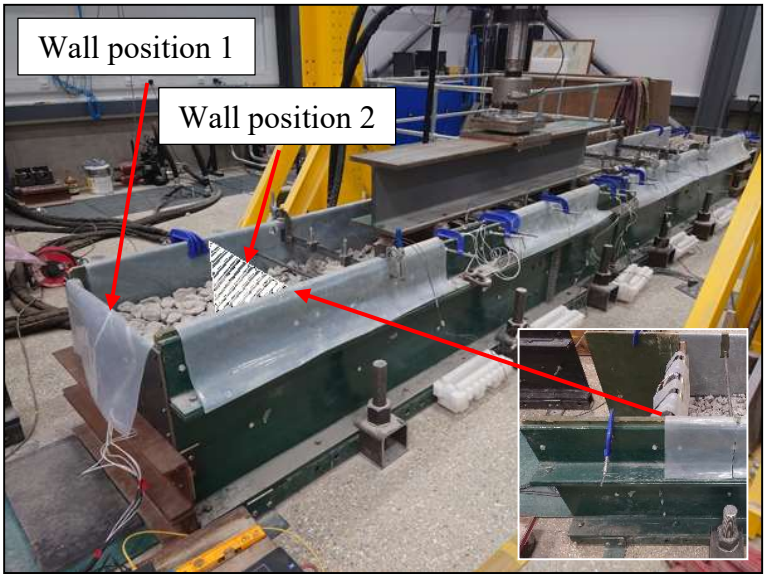

Figure 25 Photograph of SRTF modified to confine ballast shoulder at two different distances from the loaded rails

4.2 Large scale ballast tests

Large scale box tests have been used in the literature to simulate field-like conditions of railway ballast. This method allows the vertical and horizontal settlement behaviour to be studied in reasonably realistic conditions.

A relatively small box test (Figure 26) was built at the University of Massachusetts in the early 1980s from wood reinforced with steel angle iron (Stewart, et al., 1985). It was used to evaluate the development of horizontal stresses in the ballast layer under cyclic loads and to examine the change in behaviour of ballast as it degrades. It was succeeded in the late 1980s by a box apparatus of the same dimensions built from metal sheets with angle iron welded for reinforcement (Han & Selig, 1996). The sides and base were covered by rubber lining between thin sheets of stainless steel. This apparatus was utilised to understand the effect of fouling on ballast behaviour under long term cyclic loading. Ballast box tests showed that horizontal stresses accumulate, up to a limit, with the number of loading cycles as shown in Figure 27 (Selig & Waters, 1994).

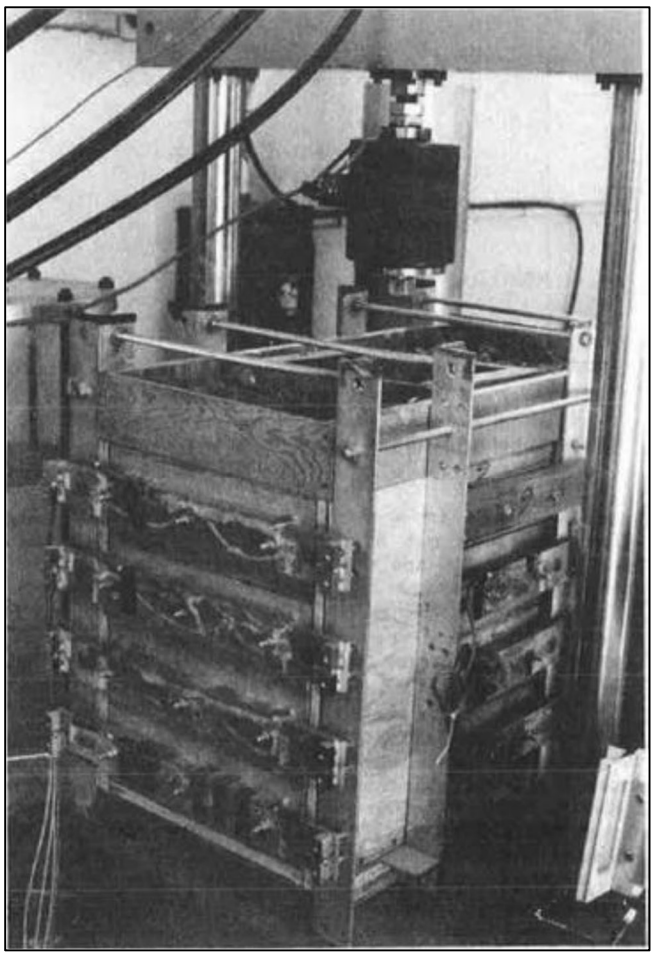

Figure 26 Wooden box apparatus from University of Massachusetts first developed in 1980 (Stewart, et al., 1985)

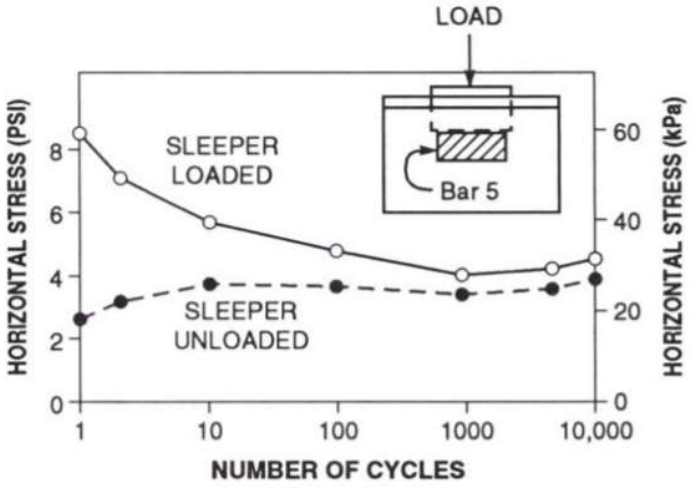

Figure 27 Effect of loading cycles on horizontal stress (Selig & Waters, 1994)

Anderson & Key (2000) reported a box apparatus 1000 mm × 800 mm × 600 mm deep, constructed from steel. Rubber pads 10 mm thick of stiffness 5000 kPa were used on the bottom to replicate the track subgrade. A concrete sleeper of dimensions 600 mm × 100 mm × 100 mm deep was used with full-scale ballast. The objective was to compare the effects of stone blowing and ballast tamping on ballast performance. The ballast box was filled with new ballast at the start of each test and loaded for 1M loading cycles between 2.1 kN and 18.2 kN. A frequency of 0.5 Hz for an initial 50 cycles and 6 Hz for a further 50,000 cycles was applied to achieve a consistent initial ballast state before starting the main 1 million loading cycles. Ballast density was reported to be between 1470 kg/m^3 and 1500kg/m3 when compacted after 1M loading cycles. They state that after compaction only the top 100 mm of the ballast layer was disturbed by particle rearrangement/breakage. Gravel (20 mm) was added to the ballast bed as stone blowing material. It was observed that stone blowing improved ballast performance in comparison with tamping, as shown in Figure 28 (Anderson & Key, 2000).

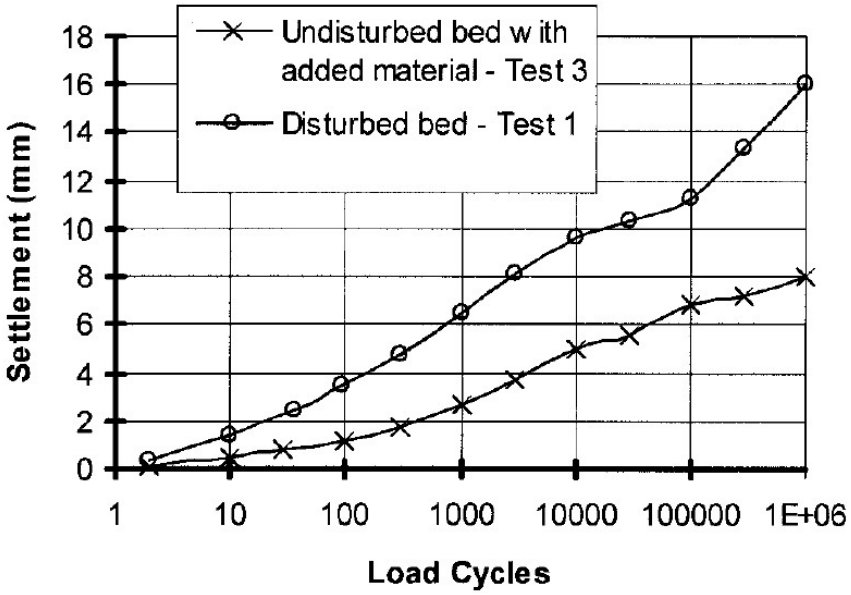

Figure 28 Ballast vertical settlement comparing the effect of stone blowing and tamping as a ballast maintenance method (Anderson & Key, 2000)

The GRAFT facility (Figure 29) at Heriot-Watt University is a larger box apparatus constructed within a steel tank 1.072 m × 3 m × 1.5 m depth. It includes three 250mm × 125 mm × 600 mm long sleepers overlain by a 3 m long I-section steel beam. This facility was succeeded by GRAFT-2, which can accommodate three full size sleepers at 650 mm spacing. Ballast was in a field-like configuration with a ballast shoulder at either end. Tests performed on the earlier GRAFT-1 apparatus were loaded sinusoidally from 5 kN to 90 kN at a frequency of 3 Hz. They reported a maximum ballast dry density of 1540 kg/m^3 (Kennedy, et al., 2012).

Figure 29 GRAFT facility at Heriot-Watt University (Kennedy, et al., 2012)

The SRTF (Figure 30) at the University of Southampton represents a single sleeper bay of track. It is built from heavy steel reinforced sections that form side walls of 5 m length and 0.65 m depth, which are 650 mm apart (i.e., a typical sleeper spacing). Hence a full size G44 sleeper of length 2.5 m can be accommodated in conditions as near to plane strain as possible (Abadi, et al., 2016). In a study to evaluate the effectiveness of ballast interventions, a shallower ballast shoulder slope (1:2) showed the most promising potential of reducing settlement (36% reduction after 3M cycles) thereby increasing the time between maintenance intervals (Abadi, et al., 2018).

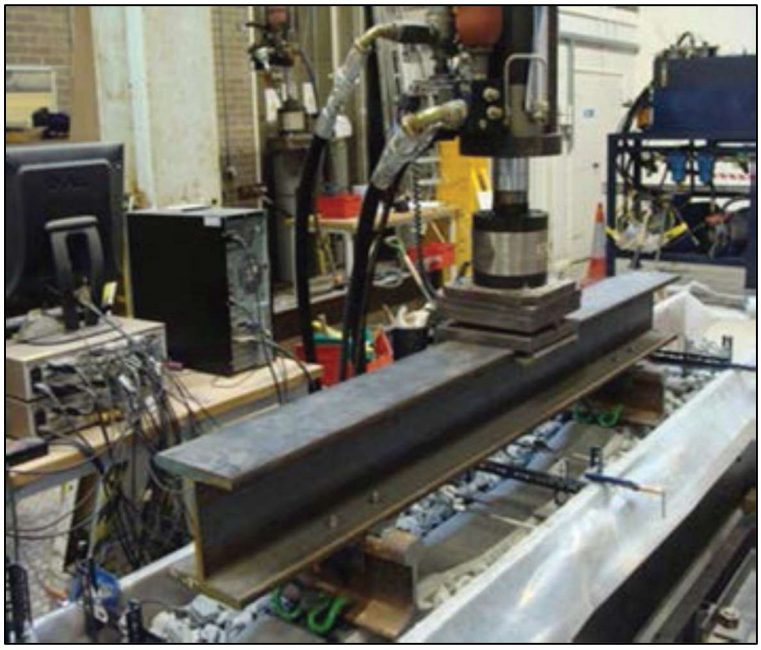

Figure 30 The SRTF (Abadi, et al., 2016)

In the large Prismodial triaxial apparatus (Figure 31) at the University of Wollongong, a hydraulic actuator was used to apply normal stress together with two hydraulic presses for application of lateral stresses. Cyclic loading was applied at 15 Hz, with the axial stress varying from 15 kPa to 385 kPa, over up to 500,000 loading cycles. This apparatus has been used to study the contribution of ballast and capping layer on overall settlement and showed that over half of the total settlement (60%) was attributed to ballast layer deformation (Indraratna & Ionescu, 2000). The same apparatus has been used to evaluate the effectiveness of re-used ballast reinforced with geosynthetics. It was shown that recycled ballast was more prone to particle damage than fresh ballast, but reduced breakage was seen using geosynthetics (Salim, 2004). A biaxial geogrid reduced ballast degradation and deformation more than a geotextile membrane (Indraratna & Nimbalkar, 2013). The apparatus has also been used to evaluate the mechanical behaviour of sub ballast reinforced with geocells under different confining

conditions and loading frequencies; confinement by geocells resulted in a reduction in permanent settlement by 12.5-25% (Indraratna, et al., 2015).

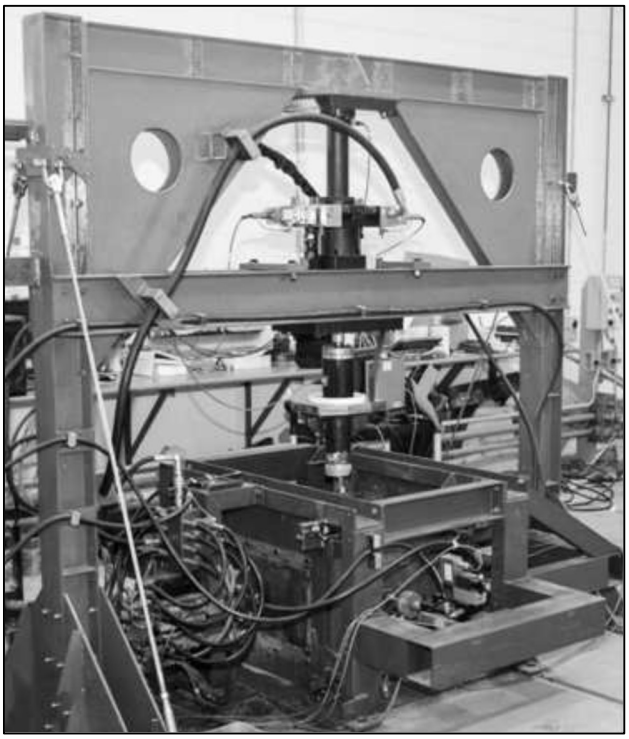

Figure 31 Large 'Prismodial' triaxial apparatus at university of Wollongong (Indraratna & Ionescu, 2000)

The Railway Test Facility (Figure 32) at the University of Nottingham, built from 4.1 m × 2.1 m × 1.9 m deep concrete-lined test pit accommodating three standard sleepers. Hydraulic actuators provided 94 kN vertical loads. It was shown that geogrid reinforcement increased the intervals between maintenance interventions by a factor of about 2.5 (Brown, et al., 2006).

Figure 32 Nottingham railway testing facility (Kwan, 2006)

4.3 Materials

4.3.1 Ballast

The ballast used was a crushed, uniformly graded, angular granite sourced from Mountsorrel quarry (Leicestershire, UK), representative of materials typically used in the UK and Western Europe. Two separate batches of ballast delivered on two different dates (4 years apart) were used in this work. Their Particle Size Distribution (PSD) curves are shown in Figure 33. As the PSD of the two batches of ballast were different and some tests used the newer batch of ballast, baseline tests were repeated for both batches of ballast. The used ballast was replaced with new ballast in each test. The dry bulk density of the ballast (ρ_b) after compaction in the rig was measured to be approximately 1600 kg/m^3 (± 25 kg/m^3). Coefficient of uniformity ($C_u = D_{60}/D_{10}$) was 1.34 for ballast batch 1 and 1.38 for ballast batch 2. Average particle size (D_{50}) was 41 mm and 44 mm for ballast batch 1 and 2, respectively. Coefficient of curvature ($C_c = D_{30}^2/(D_{60}D_{10})$) was 0.96 and 0.99 for ballast batch 1 and 2, respectively

Bulk density of the compacted ballast in the rig was measured as the ratio between the mass of the ballast to the measured volume it occupied in the rig. This is based on the same principle as the method carried out *in-situ* where ballast mass (weighed) is taken out from ballast bed and replaced with water of known volume to achieve the ratio for bulk density (Guo, et al., 2021).

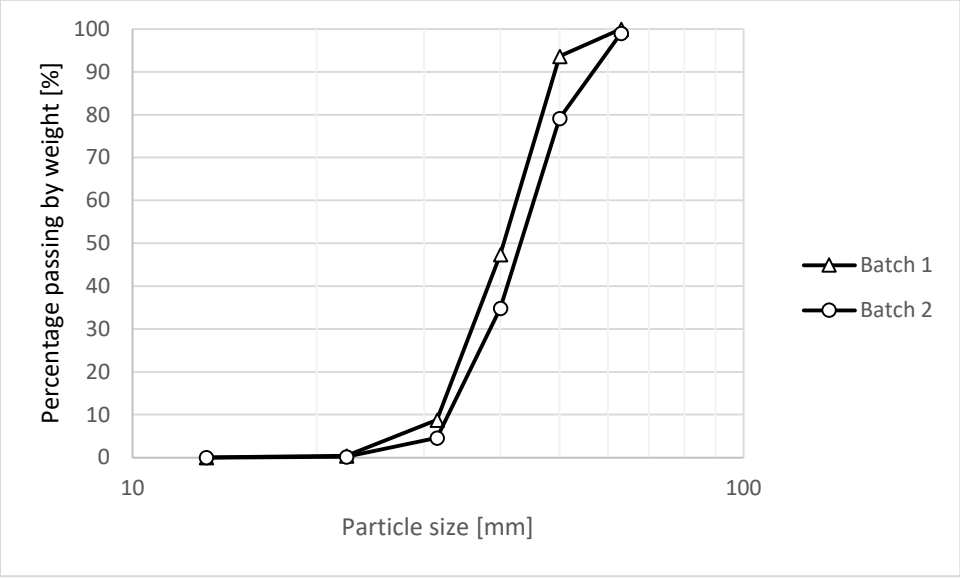

Figure 33 PSD curve for Mountsorrel ballast batch 1 and batch 2 ballast

4.3.2 Bearers

Bearers used in the research were standard Type R section bearers in continuous lengths of 3.8m and 5.6m and in a modular form. In their modular form the short and long bearers were connected via joints of varying stiffness between and beside the running rails, respectively. The mass per unit length (λ_m) was measured to be 135 kg/m.

The USPs of soft type (C_{stat}: 0.120 N/mm³) were bonded to the base of the bearers and used within the tests on ballast batch 1 to investigate the effects of USPs on ballast permanent settlement and resilient deflections along the length of the bearer with number of loading cycles up to 10^6. A USP of harder type (C_{stat}: 0.260 N/mm³) was used in the test on ballast batch 2.

4.4 Instrumentation

4.4.1 LVDTs

Linear Variable Displacement Transducers (LVDTs) were positioned along the bearer to monitor its vertical movements throughout each test. Data were recorded at 100 Hz and subsequently processed to determine permanent settlement and resilient movement. Permanent settlement was taken as the deflection of the bearer at the minimum load (5 kN) and resilient deflection as the difference in vertical position at the maximum (98.1 kN) and minimum loads (5 kN) within each loading cycle. The settlement measurements were zeroed after the first 10 loading cycles to eliminate bedding effects and improve test comparability. As shown in Figure 34, the effects of bedding are vastly reduced by resetting the data after 10 loading cycles.

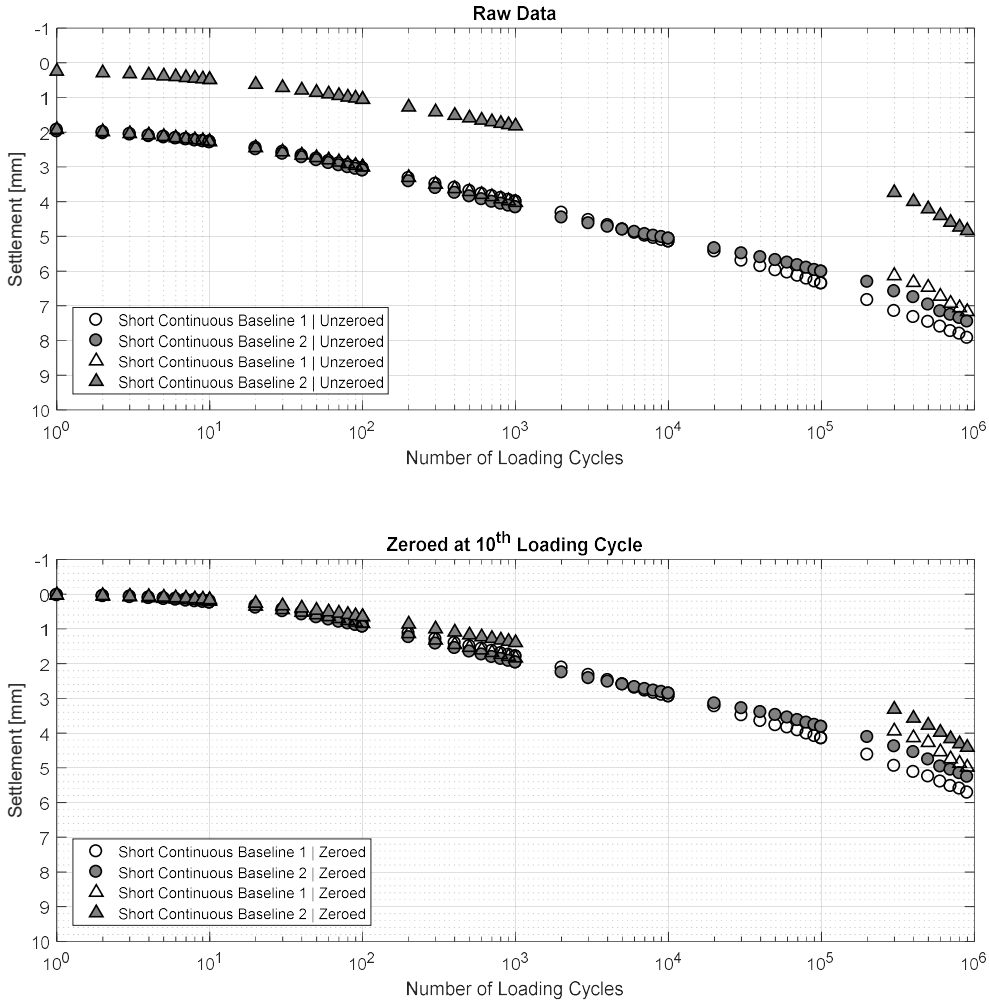

Figure 34 Average settlement of two repeated tests, top: raw data; bottom: data zeroed after 10 loading cycles

4.4.2 Pressure plates

Two 300 mm × 250 mm steel plates (pressure plates), each supported on three Omega LCGD-500 2.2 kN capacity load cells, were incorporated into and flush with the inner panels of the rig walls, to measure longitudinal pressures (Figure 35). The longitudinal pressure was calculated as the summated load on the loadcells divided by the pressure plate area.

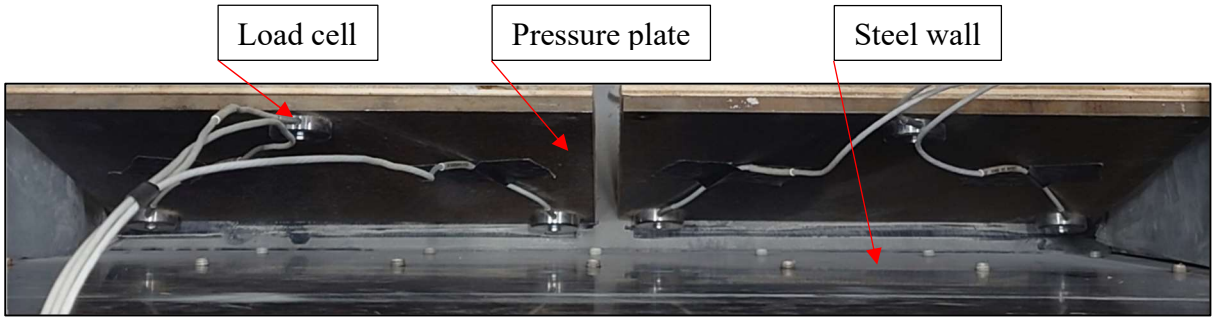

Figure 35 Photograph of the pressure plates with triangular arrangement of the loadcells

4.4.3 Pressure cells

Pressures under the ballast adjacent to the both loaded rails and their midpoint were measured via GeoSense TPC-4000 total earth pressure cells with an active diameter of 305 mm and pressure range of 345 kPa - 20.7 MPa. These pressure cells sat flush with the 12 mm thick steel plates that covered the base area of the test rig.

4.4.4 Strain gauges

Strain gauges were used on the rigid metal shroud 8-bolt joint to measure strains on the surface as shown in Figure 36. This can give an indication of the stress transferred through the metal joint over the cycles of loading.

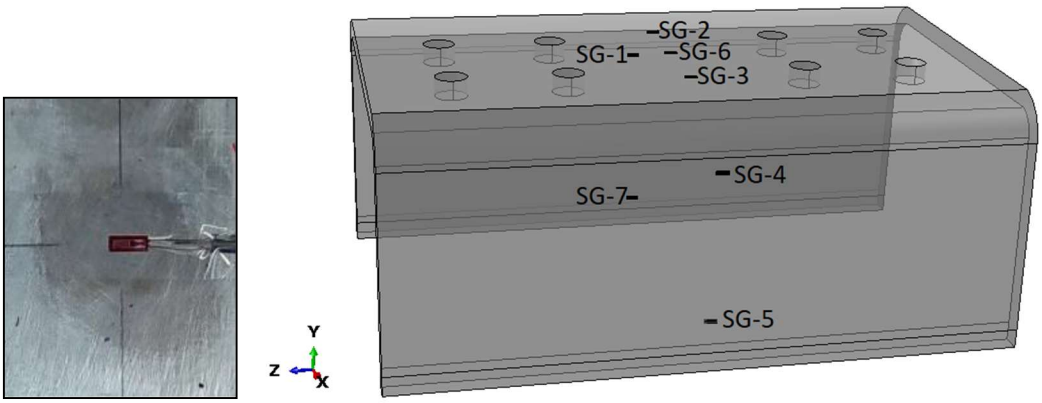

Figure 36 Schematic of the metal shroud with locations of the strain gauges

4.5 Bearer-ballast fatigue apparatus and preparation

The SRTF consists of two steel sides of length 6.5 m and height 0.75 m that are rigidly mounted to the strong floor and spaced at 0.65 m. Figure 37 presents a schematic of the test apparatus showing the instrumentation and test specimen. The steel side walls were made of steel plate that reinforced by bolted steel sections as shown in Figure 38. These walls maintained flexural rigidity of the rig during testing to enforce test conditions as close to plane strain as possible. The walls were linked through tie rods to prevent out-of-plane movements. Friction between the ballast and the walls was minimised by the use of a double layered plastic sheet. A ballast mat (6645 mm × 650 mm ×18 mm depth UBM 1519 Getzner Werkstoffe GmbH, C_{stat} = 0.15 N/mm^3) and two stiffer rubber mats (each 6645 mm × 650 mm × 3 mm thick) were laid to represent the resilient effect of a subgrade as illustrated in Figure 37 and Figure 38. The rubber pads ensured uniform subgrade conditions for the tests and produced realistic deflections (0.5 - 2 mm) (Le Pen, et al., 2017).

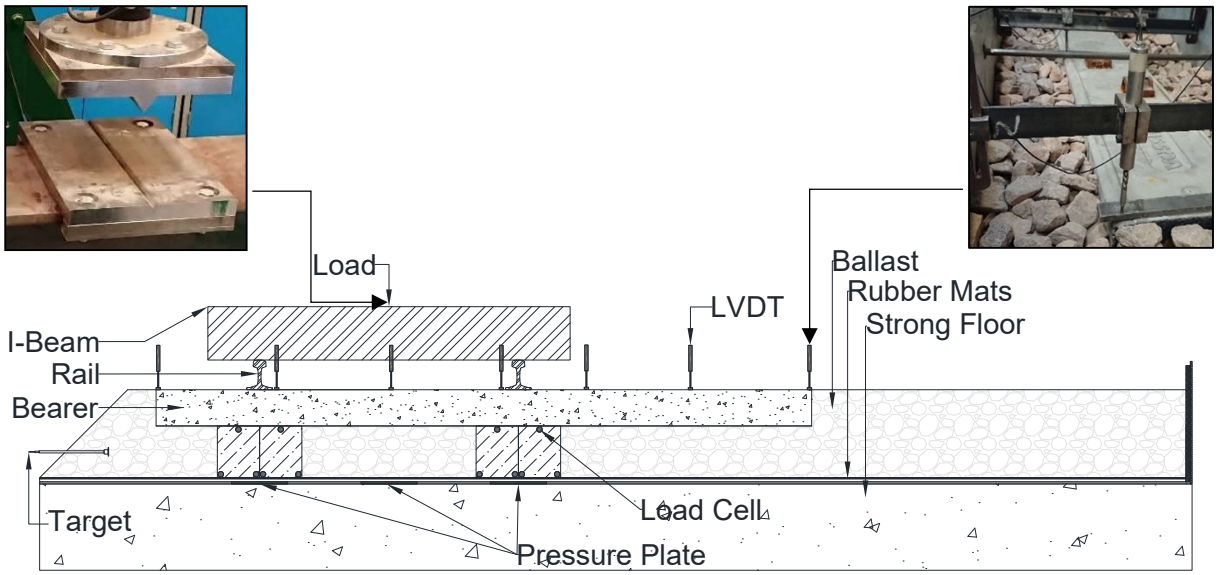

Figure 37 Side view of SRTF showing instrumentation and test specimen

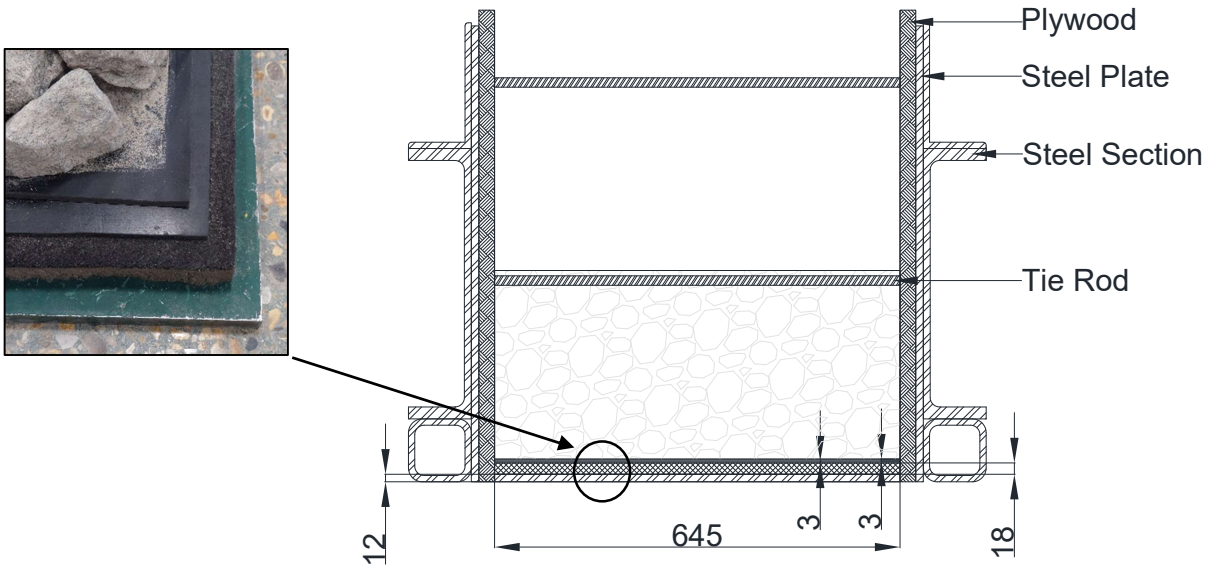

Figure 38 Cross-sectional view of testing apparatus

4.5.1 Preparation of test

Each test was prepared according to a set procedure to ensure repeatability. The following steps were conducted in sequence. Figure 39 shows the testing procedure at different stages:

- The rig wall was covered with a double layered plastic sheet, and two rubber mats and a ballast mat were rolled out between rig walls,
- The rig was filled with dry ballast to 300 mm depth and then compacted with a 22 kg plate vibrator (400 mm × 320 mm) of 5 kN compaction force by seven passes over the whole area of the ballast and levelled simultaneously. Shoulder ballast remained un-compacted and at its natural slope of approximately 1V:1H,
- Upon satisfactory ballast level, pressure papers were attached to the bearer base then the bearer was placed evenly on the ballast bed,
- With the bearer in place, the crib was filled and the mass of ballast that went in was measured,
- The LVDT brackets were clamped onto the rig walls and LVDTs were installed.
- The loading I-beam was placed on the rails,
- Contact was made between the ‘knife edge’ loading point of the loading ram and ‘Vee’ loading socket mounted to the loading I-beam.

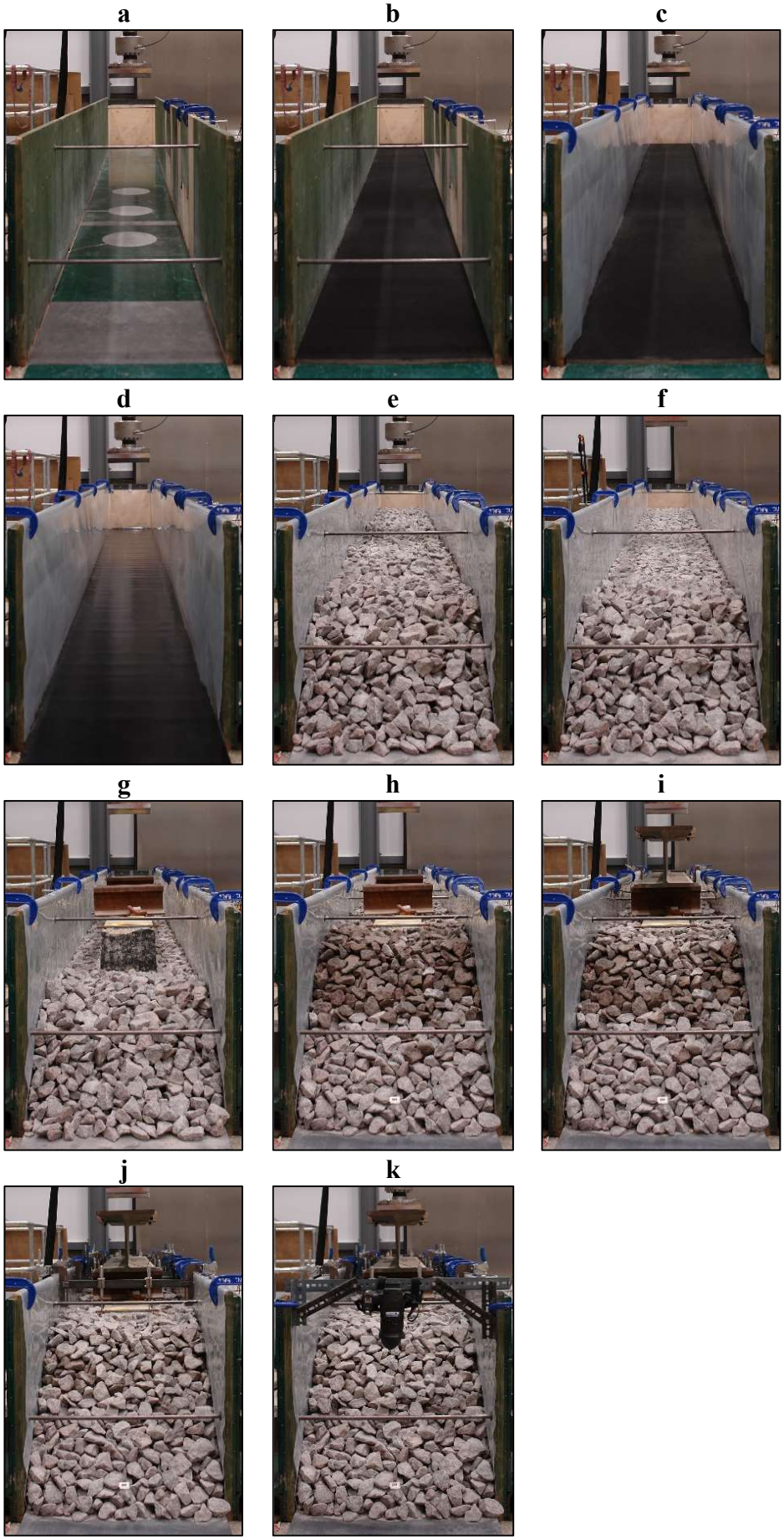

Figure 39 Preparatory stages of test a-d: application of rubber layers and plastic sheet, e-h: addition of ballast; compaction/levelling; placing of bearer; filling of crib, i-k: placing of I-Beam; installation of LVDTs/camera and application of load.

4.5.2 Loading routine and data acquisition

The test was initially loaded statically following a set pattern as shown in Figure 40, followed by a sinusoidal load of 5-98.1 kN. This loading is representative of 20 tonnes axle load, assuming that load distributed by the rails results in the transfer of half of the load to the bearers on either side. The load is applied at a frequency of 4 Hz for up to 1.2 M cycles.

The loading was applied by Instron hydraulic actuator with a maximum capacity of 250kN in tension or compression and a stroke length of ± 125 mm. The hydraulic actuator was attached via a hinge to a portal steel frame with clearance for the loading beam and bearer (Figure 41). Realtime output for load and deflection was provided to the data logger by a type 8400 Instron controller which was automatically tuned to match loading signals with the sample response.

The LVDTs and loadcells data was logged by a Vishay type 5100B data logging system at a frequency of 1 Hz for the first 'static' cycle and then at 100 Hz for the subsequent cycles to provide 25 data points per loading cycle. The pressure plates data was acquired through Campbell CR6 Datalogger which was programmed to record 6 minutes of data at the start followed by 6 minutes of data acquisition every 6 hours. All the data was processed using MATLAB.

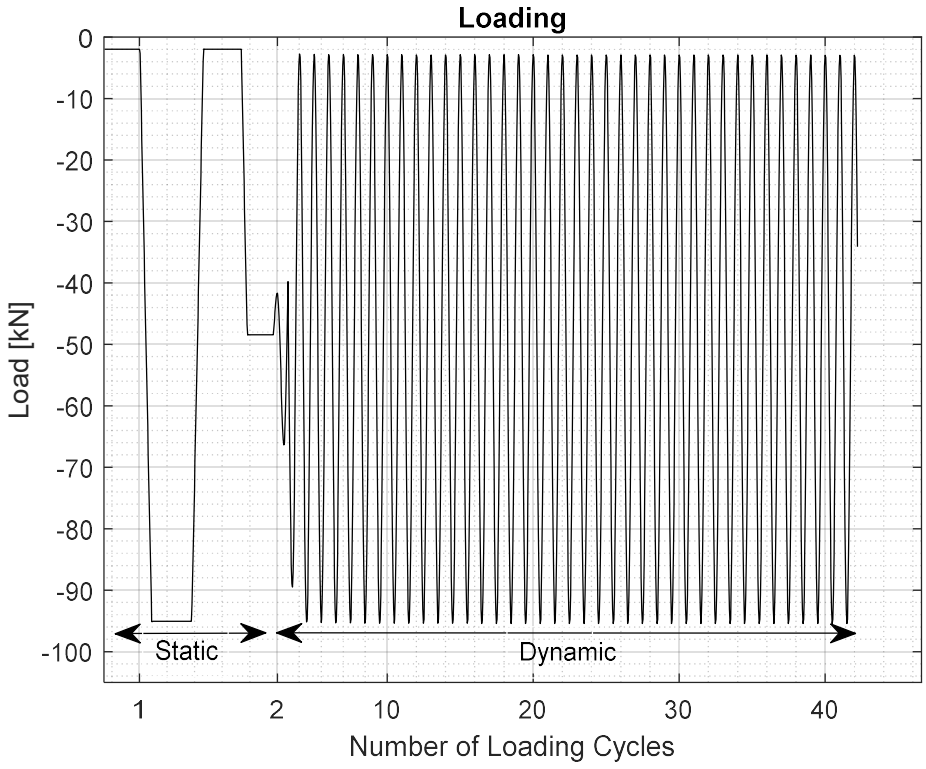

Figure 40 Static load (1st cycle) followed by cyclic loading

Figure 41 Arrangement of loading system

4.6 Bearer-ballast gap

A gap between the bearer and the ballast may arise at a location where the ballast has settled differentially along the length of the bearer. These gaps are generally found under the ends of symmetrically loaded sleepers owing to a tendency for “centre-binding” and are characterised by higher resilient deflections at these locations. In the case of the eccentrically loaded long bearers investigated in this study, higher resilient deflections were measured under the bearer ends closer to the ballast shoulder. The development of these relatively large deflections towards the left end of the bearers (near the ballast shoulder) was attributed to the bearer-ballast gap and verified by measurement at the end of the test at ~1.2 million cycles.

A target was placed in contact with the ballast closest to the bearer end and to the bearer end itself, as shown in Figure 42 and Figure 43. The amplitude of the ballast movement near the bearer end was compared with the movement of bearer end. The difference between the movements of the two targets on unloading was indicative of the gap and was quantified by subtracting the negative deflection (unloading) of the ballast from that of the bearer. This is shown in graphical form in Figure 44.

Figure 42 Targets as seen by camera

Figure 43 Top view of the targets

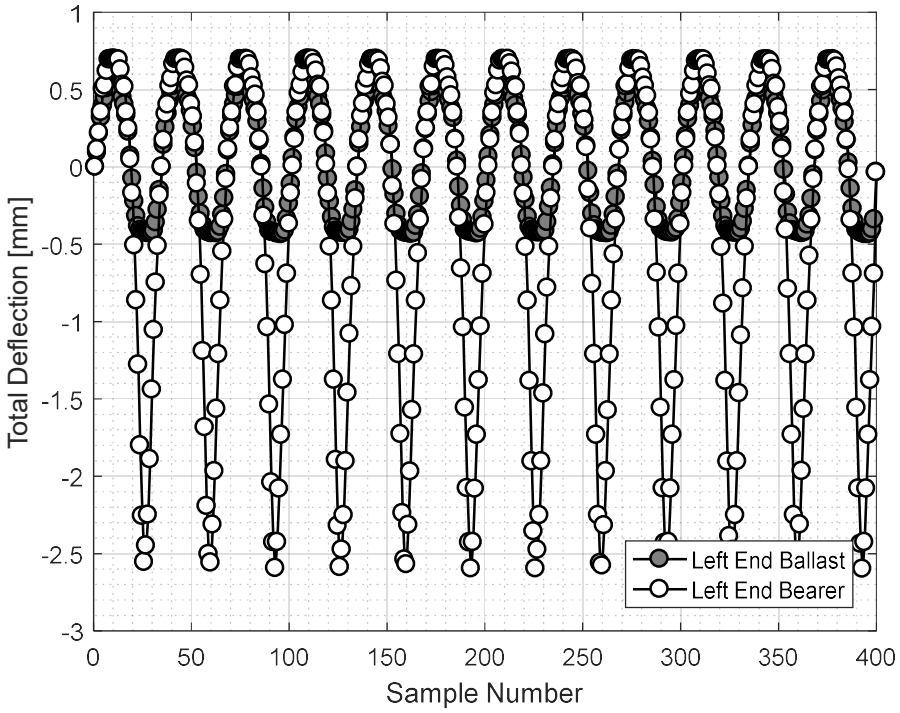

Figure 44 Displacement [mm] seen on bearer and underlying ballast for 12 cycles after ~1.2M loading cycles (end of test)

4.7 Shoulder ballast spreading

Measuring ballast shoulder spreading provides an insight into the mechanical behaviour of the bearer/ballast system. It also allows observation in detail of the differences in the performance of various bearer types. Understanding ballast shoulder spreading can also help to identify a robust mitigation strategy for the variation in settlement along the length of the bearers and gap formation at the bearer/ballast interface on the bearer end.

The measurement was obtained by placing a bespoke device (Figure 45) at the centre of the walls, 150 cm from the base of the shoulder. The device was made up of a steel cylinder enclosing a steel rod that was bolted to a square plate embedded in the ballast. The open end had a target for the camera to monitor. The square plate in contact with the ballast mobilised the target through the steel rod. The movement of the target was thus captured by a camera at the highest (device limited) frequency of twenty pictures/min for 2 min, then one picture/hr for ≈18 hours and then one picture approximately every 18 hr.

Figure 45 Device partially embedded in the ballast shoulder to measure the lateral movement of the shoulder using DIC

The targets were processed in MATLAB 2016b's Image Processing Toolbox. The centroids of each square were calculated, and the top and bottom row centroids were averaged respectively (M_1 and M_2). The distance in pixels (difference between M_1 and M_2) was correlated to the distance in millimetres (10.5 mm) on the actual target to achieve a scaling factor, k. The scaling factor was multiplied by the distance in pixels from the boundary of the image to the centre of the target, C (average of M_1 and M_2). This is illustrated in Figure 46.

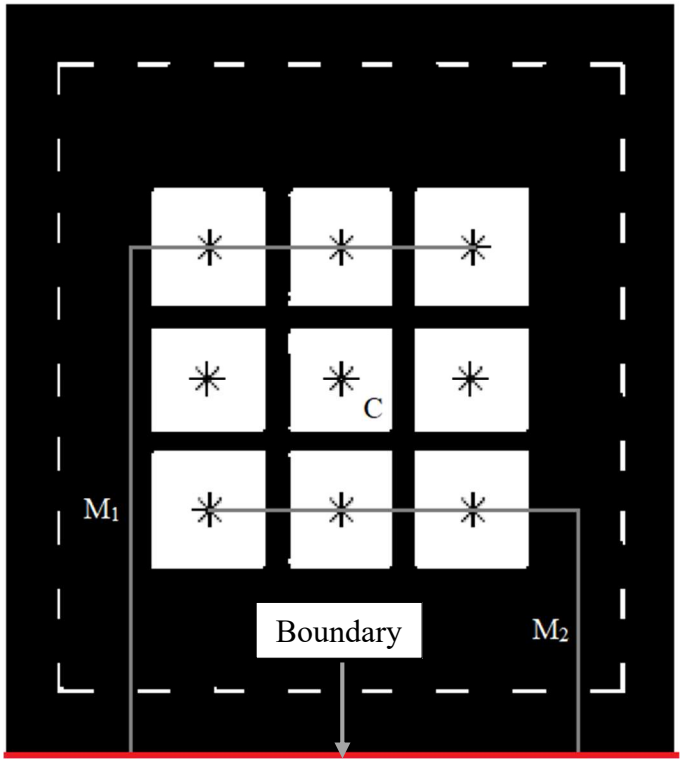

Figure 46 Schematic showing the DIC target where M_1 and M_2 are centroid means of the upper and lower rows of squares respectively, measured from a fixed point on the image.

4.8 Contact characteristics

Bearer-ballast contact characteristics were quantified using Fujifilm pressure sensitive papers that react to pressure by producing red patches. Table 2 specifies the two types of pressure papers used in the experiments. Medium-Pressure and Low-Pressure papers with sensitivity ranges of 10-50 MPa and 2.5-10 MPa respectively were cut to A4 size, and both applied to the base of the bearer at locations between and under the loaded rails and under both ends as shown in Figure 47. Other locations included the joined ends of the bearers. These pressure papers provided adequate pressure sensitivity for capturing the ballast contact with the bearer.

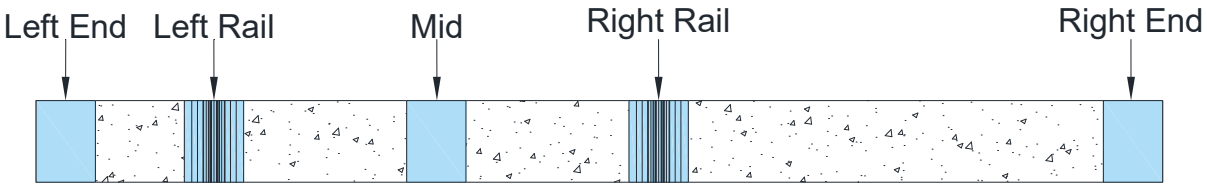

Figure 47 Locations of pressure sensitive papers on bearer, Left End is closest to the Ballast Shoulder, Right End is farthest from the loaded Left and Right Rail and Mid is at the center of the rails.

Table 2 General specifications of the pressure papers used to quantify the bearer/ballast contact area (https://www.fujiprescalefilm.com/)

Product	Product Code	Pressure range [MPa]	Product size	Type
Medium Pressure (MW)	PRESCALE MW R270 10M	2.5-10	270×10	Two-sheet
Low Pressure (LW)	PRESCALE LW R270 10M	10-50	270×10	Two-sheet

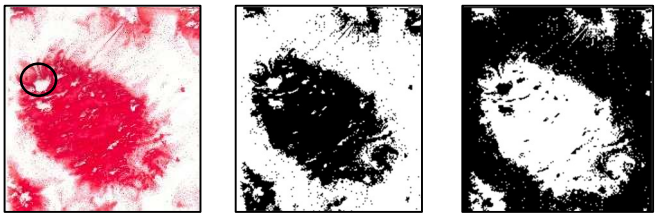

a b c

Figure 48 a - RAW scanned image of a portion of pressure paper; b - B&W image; c - inverted colours image allow measurement of pixels. Circled white spot exemplifies damaged paper - these are counted as contacts.

The papers were scanned at the end of the test to reveal the contact imprints accumulated over 1.2M cycles. Some contact patches had missing spots due to damage caused by high contact pressures and abrasive wear due to cyclic loading as highlighted in Figure 48a. The scanned papers were processed using MATLAB 2016b's Image Processing Toolbox. Images were turned into black and white as in Figure 48b and then inverted as in Figure 48c. Black areas in Figure 48b were added to black areas surrounded by white areas in Figure 48c to measure the imprinted areas including the missing spots.

Contact area as percentage of total area as follows:

$$Contact\ area\ (\%) = \frac{Red\ Patches + Damaged\ Areas\ (White\ enclosed\ by\ re\ )}{Background\ (white\ not\ enclosed)} \times 100$$

4.9 Ballast breakage

Particle loss was measured in the baseline tests on the short continuous bearer by placing 20 particles of size 31.5 mm and 40 mm each at the bearer-ballast interface in specific locations such as under the loaded rails and between the loaded rails. These particles were washed, dried overnight in an oven, and then weighed before and after the test. Results suggested insignificant particle breakage therefore in subsequent tests the ballast was visually inspected for any damage.

4.10 SRTF test plan

Tests were carried out on two lengths of continuous and jointed bearers: a short 3.8m bearer with a joint in the middle of the loaded rails and a long 5.6m bearer with the joint to the side of the loaded rails. The joint type was varied in both cases (Table 3). The three types of joints shown in Figure 49 are (a) Metal shroud joint used in the UK by Network Rail, (b) Vibration damping coupler joint manufactured by Voestalpine VAE GmbH and (c) Pin-Pin joint provided by Progress Rail. These joints together provide a good range of flexural rigidity - from rigid to flexible to fully rotational.

The selection of bearers was on the basis that the common positions of the joints in the field are either between or outside the loaded rails, although the relative distance of the joints from the rails can vary and there may be more than one joint per bearer. Figure 50 shows the location of the short and long jointed bearer in an S&C. There are some small differences in dimensions between the laboratory bearers, due to variations in the sizes provided by different suppliers. The exact locations of joints and bearer dimensions are shown in Figure 51.

Under sleeper pads of soft type were used on the short continuous bearer and pin-pin jointed short bearer. The continuous and pin-pin jointed short bearers were tested with the ballast shoulder laterally confined by a rigid wall.

Further tests were carried out on the short rigid jointed bearers, hereafter termed “interventions”. These interventions included the sequential loosening of the bolts to replicate likely failure of bolts on field, and the differential loosening of ballast where ballast under the joint is looser relative to the rest of the underlying ballast and in another scenario where ballast is refreshed under the jointed segment of the bearers towards the ballast shoulder.

In addition to the bearer-ballast interaction tests, three-point bending tests on bearers alone were carried in the SRTF in a modified configuration to evaluate the rotational stiffness of the rigid joint and the flexural rigidity of the continuous bearer was compared to bearers utilising the rigid joint. These are described in Section 4.11.

Table 3 List of tests carried out. Baseline tests are in general test conditions, interventions evaluate performance of Under Sleeper Pads (USP) and Ballast Shoulder Confinement. Bending tests assess flexural rigidity of the bearers.

Test Type	Joint Type	Bearer Length [m]	Ballast batch	Notes (See Schematic in Figure 51)
Baseline Conditions	None	3.8	1	Continuous Bearer
	None	3.8	1	Continuous Bearer (Repeat)
	None	3.8	2	Continuous Bearer
	Rigid	3.8	1	Metal Shrouded Joint
	Rigid	3.8	1	Metal Shrouded Joint (Repeat)
	Flexible	3.8	1	Vibration Damping Coupler
	Pin-Pin	3.8	1	Fully rotational joint
	None	5.6	1	Joint outside of loaded rails
	Rigid	5.6	1	Joint outside of loaded rails
	Pin-Pin	5.6	1	Joint outside of loaded rails
With USP	None	3.8	1	'Soft' USP C_{stat} = 0.12 N/mm^3
	None	3.8	2	'Hard' USP C_{stat} = 0.26 N/mm^3
	Pin-Pin	3.8	1	'Soft' USP C_{stat} = 0.12 N/mm^3
Shoulder Confinement	None	3.8	1	Confinement 0.87 m from the bearer end
	None	3.8	2	Confinement 0.87 m from the bearer end
	None	3.8	2	Confinement 0.37 m from the bearer end
	Pin-Pin	3.8	1	Shoulder confinement 0.87 m away from the bearer end
Interventions	Rigid	3.8	1	Loosening of bolts differential ballast support under the shorter jointed segment (s5) and under the joint (s6)
Three-Point Bending	None	2.4		Positive bending (sagging)
	None	2.4		Negative bending (hogging)
	Rigid	2.5		Positive bending (sagging)
	Rigid	2.5		Negative bending (hogging)

Figure 49 Photographs of the tested bearer joints

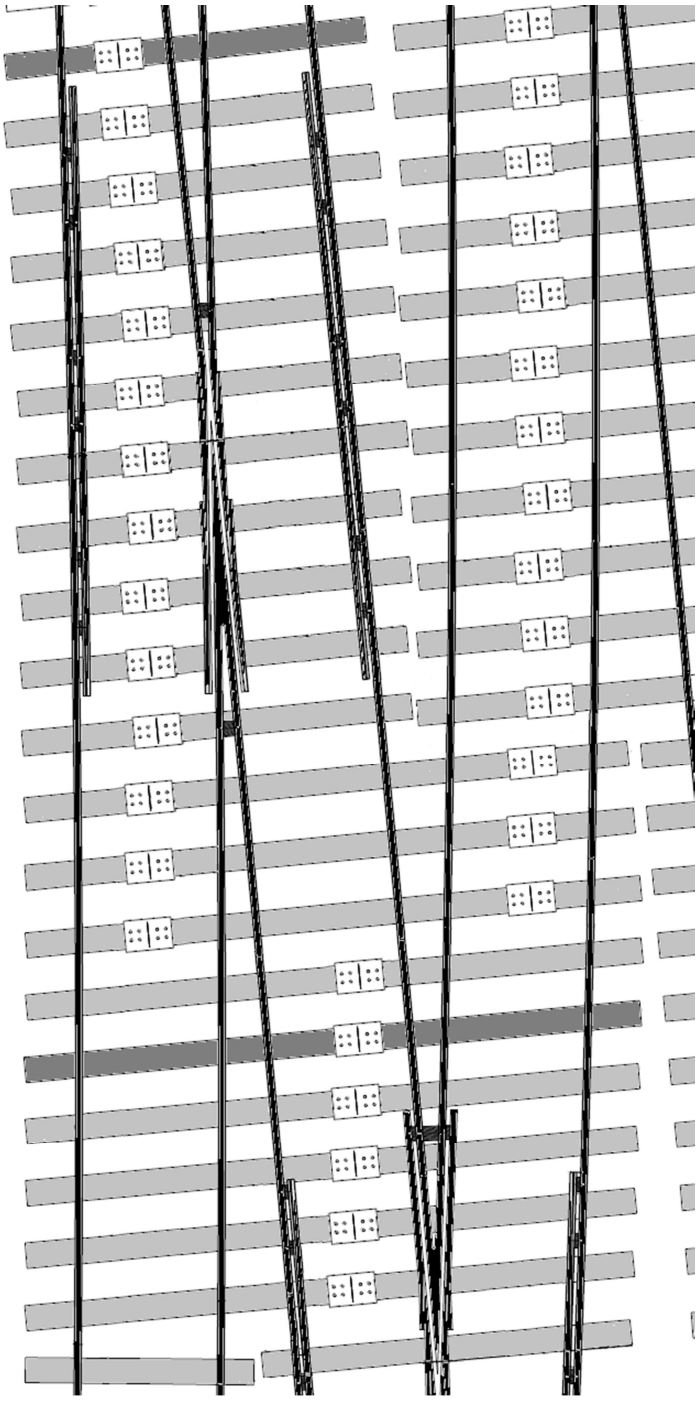

Figure 50 Position along a turnout of the modular bearer utilising the rigid joint

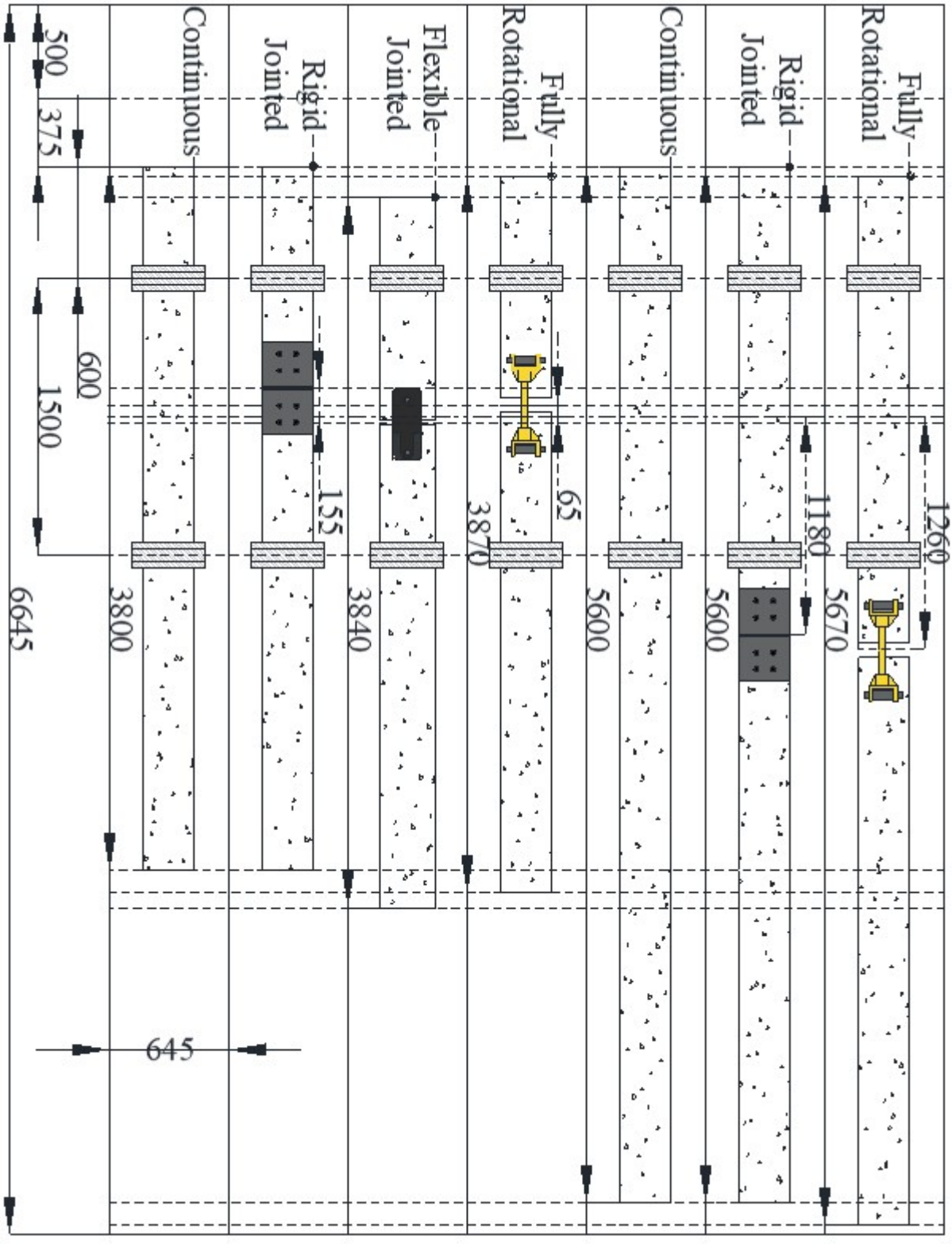

Figure 51 Schematic of the tested bearers showing arrangements and key dimensions [mm].

4.11 Three-point bending tests/FEA

Finite Element Analysis (FEA) was carried out using Abaqus CAE 2019 on models of the continuous and jointed bearers subjected to three-point bending.

Validation of the model was achieved using the modified SRTF apparatus shown in Figure 52. Actuator load was applied through a steel roller at the centre of the bearer that rested on two more rollers, each 0.75 m distant from the point of load. The LVDTs measured vertical deflection of the bearers at two locations vertically aligned with the top and two bottom rollers and mid-way between the top and bottom roller on either side. This is illustrated in Figure 53.

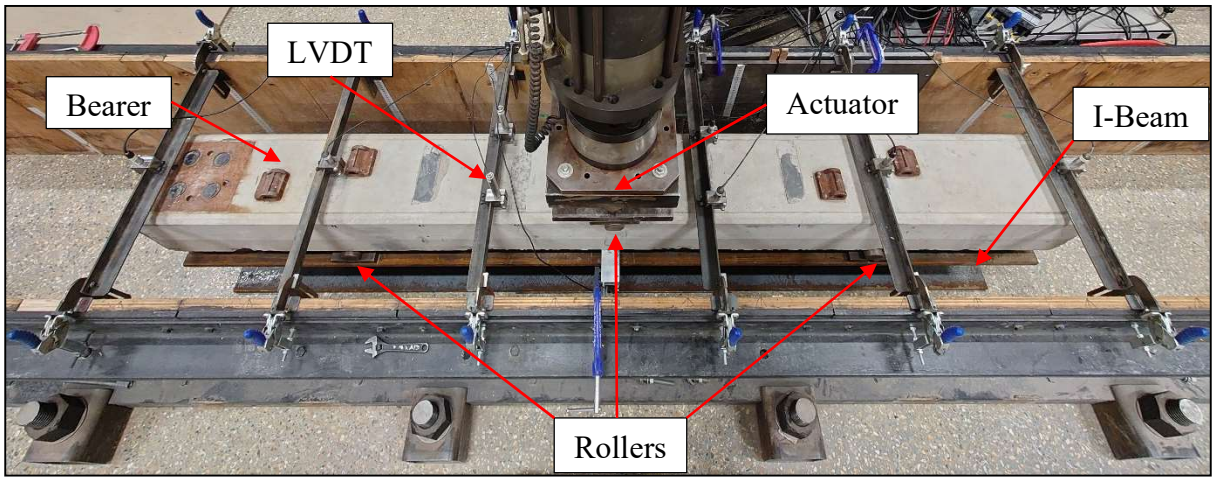

Figure 52 Photograph of experimental setup for the three-point bending test featuring the continuous bearer placed on rollers 750 mm equidistant from the point of load from the actuator (0-35 kN)

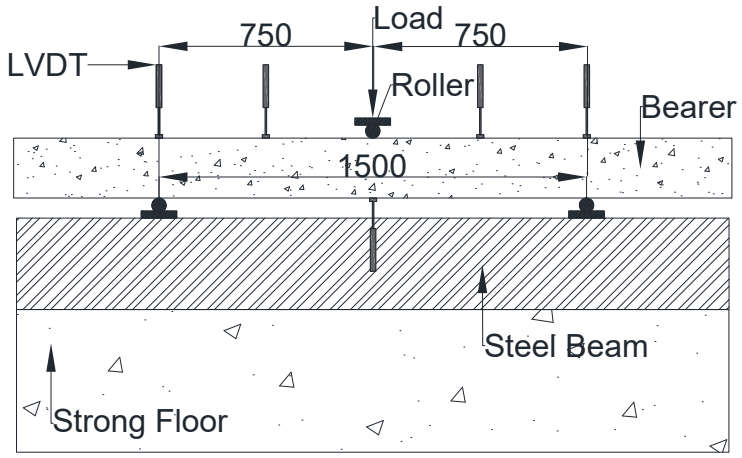

Figure 53 Schematic of three-point test setup [mm] showing roller in the centre on top, with rollers 750 mm equidistant on the bottom supported by an I-Beam (137 kg/m) on strong floor

The jointed bearer consisted of a steel shroud bolted through eight ss8-160 chair screws and double coil spring washers to a housing of four plastic dowels on either end of the joining bearer segments. A shear plate was set flush in the concrete bearer and a rubber bonded cork pad was present between the metal shroud and bearer interface as well as between the joining ends of the bearers. A torque of 340 N m was applied to the bolts. It was prescribed to leave a 1 mm gap in the spring washer. A schematic of the assembly is shown in Figure 54. Drawings of individual parts used within the model are presented in Figure 55 – 60.

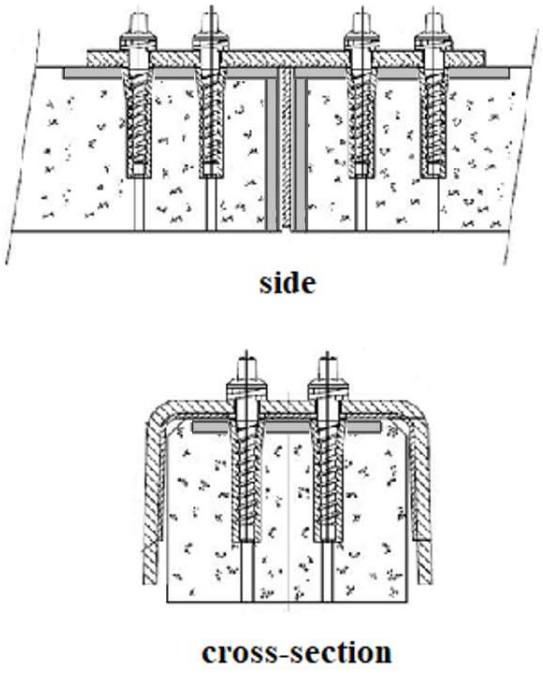

Figure 54 Cross-section of metal shroud joint (RAIB, 2018)

4.12 Summary

This chapter has presented an overview of the materials and methods used in the testing procedures. The SRTF has been described in its modified form and the preparation procedure for the tests presented. The two batches of ballast used showed some variation in terms of their PSDs, and some of the main tests were carried out using the initial ballast batch 1 of ballast and others on ballast batch 2, hence some tests were repeated to form a new baseline for comparison. The different instrumentation utilised in the tests were presented. The methods for shoulder ballast movement, bearer-ballast contact and gap measurement at the end of the tests was also described. The tests carried out were tabulated with notes. This included the three-point bending tests, for which the SRTF was modified. The test arrangement for these tests was presented in Section 4.11.

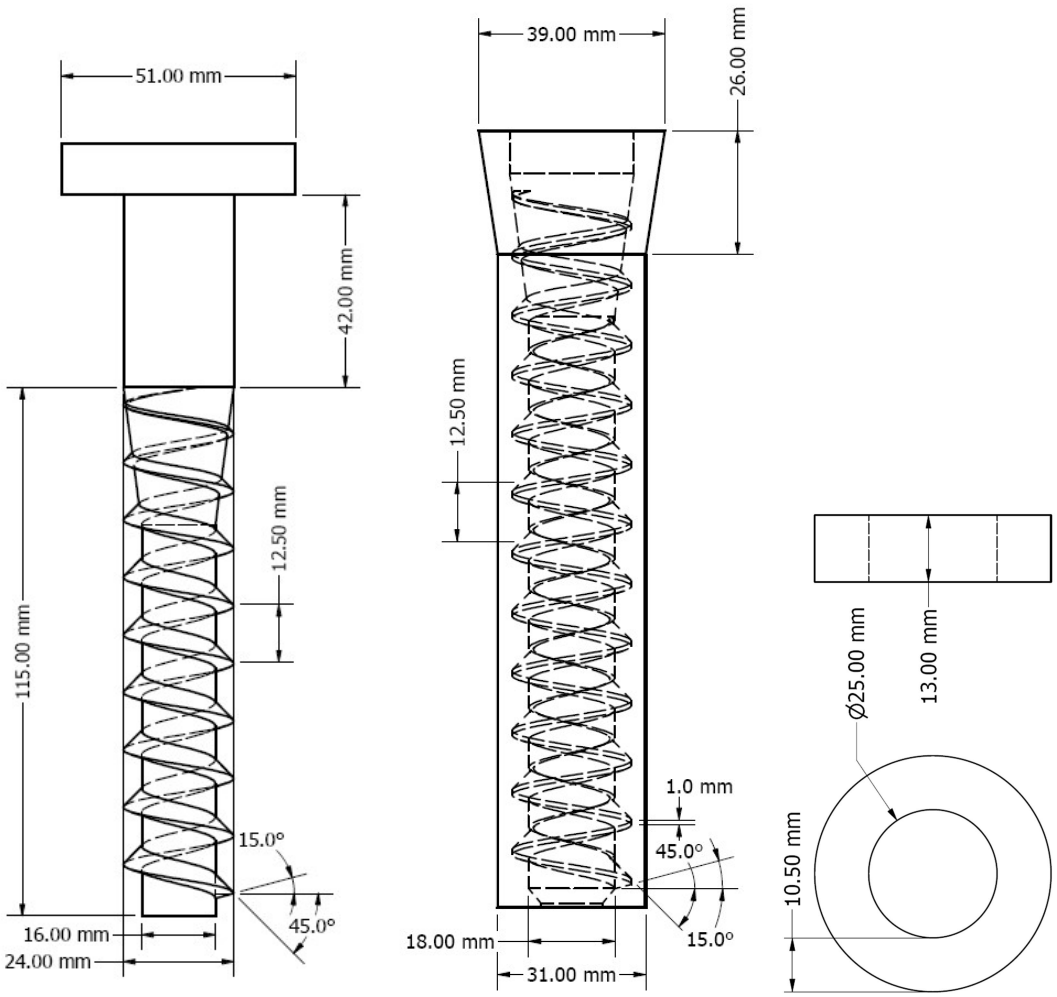

Figure 55 Drawing of spike screw bolt with relevant dimensions (left), polymer threaded dowel (middle) and simplification of double coil spring washer

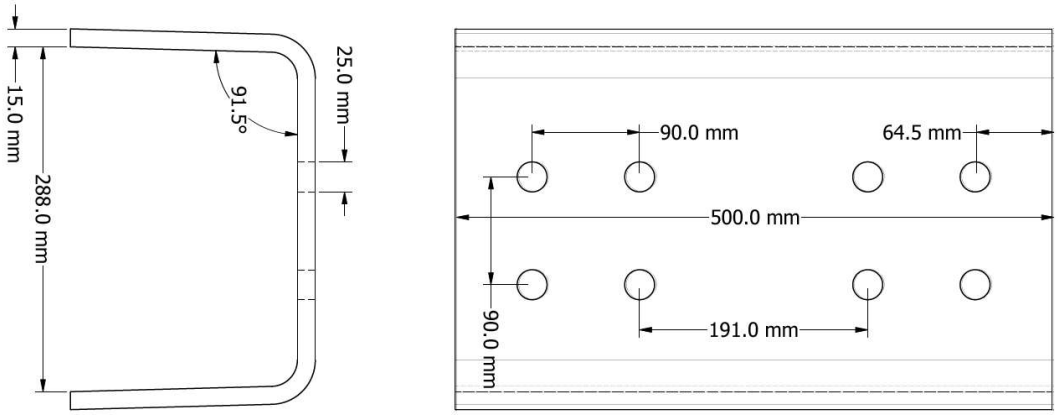

Figure 56 Drawing of the metal shrouded joint

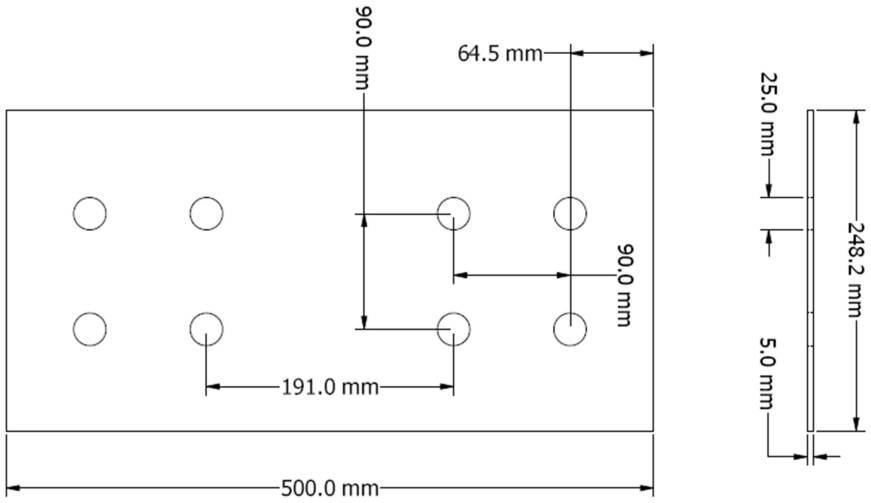

Figure 57 Drawing of the metal shroud rubber gasket present between the metal shroud and the bearer interface

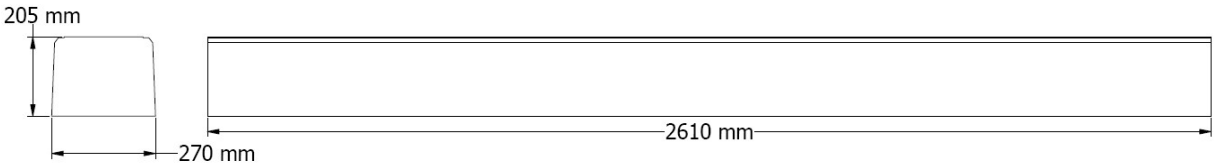

Figure 58 Drawing of the continuous bearer tested

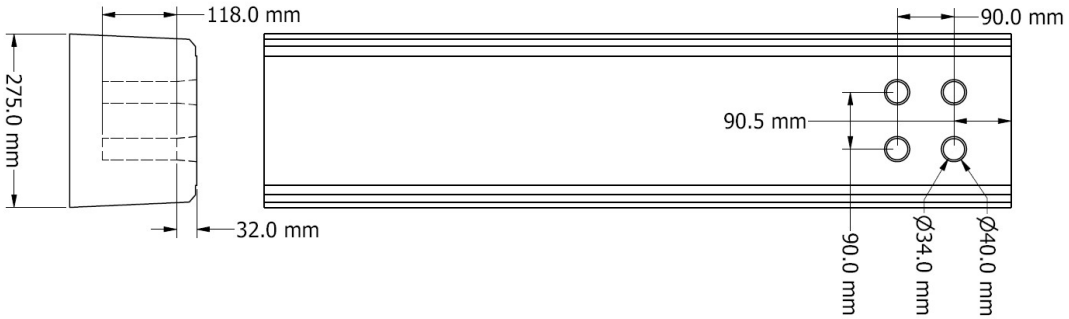

Figure 59 Drawing of Bearer segment with dowel spaces

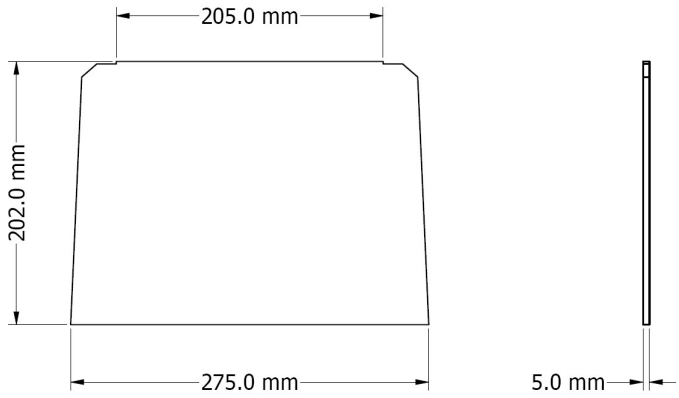

Figure 60 Drawing of the bearer end rubber

5 Fatigue Tests on Continuous and Jointed Bearers - Results & Discussion (Experimental)

This chapter presents results from the test plan in Table 3 for tests on continuous bearers and their jointed counterparts, and tests to evaluate the effect of USPs and ballast shoulder confinement. The objective was to develop an understanding of standard (continuous) and jointed (modular) bearer performance under standard conditions, and to evaluate effectiveness of USPs and changing ballast shoulder confinement.

5.1 Settlement

The settlement behaviour of long bearers was studied by initially observing the general behaviour of a 3.8 m continuous bearer subjected to eccentric loading. Figure 61 presents a diagram of the test set up with the terminology used.

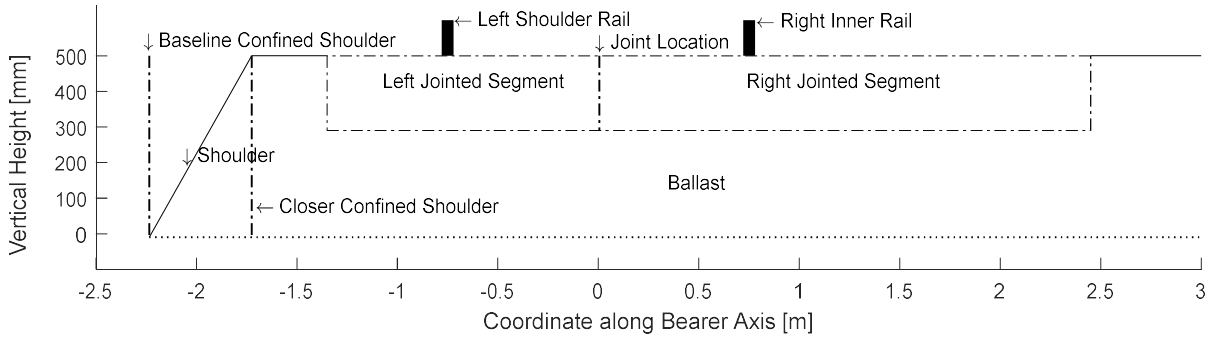

Figure 61 Schematic inlay with the assigned terminology

The baseline characteristic behaviour was then compared with a 3.8 m bearer with rigid, flexible, and fully rotational (pin-pin) joints positioned in the middle of the loaded rails. The location of the rigid and pin-pin joint was then moved to the right-hand side of the loaded rails (long jointed bearers), further away from the ballast shoulder. Interventions such as USPs and ballast shoulder confinement were applied to evaluate their impact on performance in terms of variation in resilient and permanent settlement along the bearer length.

Two baseline tests on the 3.8 m bearer were carried out to confirm repeatability. Settlement data were zeroed after 10 loading cycles to eliminate the effect of variations in ballast bedding between tests. Area weighted average settlements for tests on short continuous and its repeat presented in Figure 62 show good repeatability; the variation in settlement along the length of baseline test (reset after 10^{th} loading cycle) is shown in Figure 63. Figure 64 shows the variation in settlement along the length of long continuous baseline test (reset after 10^{th} loading cycle).

Plastic settlements along the length of the short continuous bearer at selected numbers of loading cycles (Figure 63) show the bearer rotating towards the unconfined ballast shoulder because of the eccentric position of the bearer and the proximity of the loaded rails to the unconfined ballast shoulder.

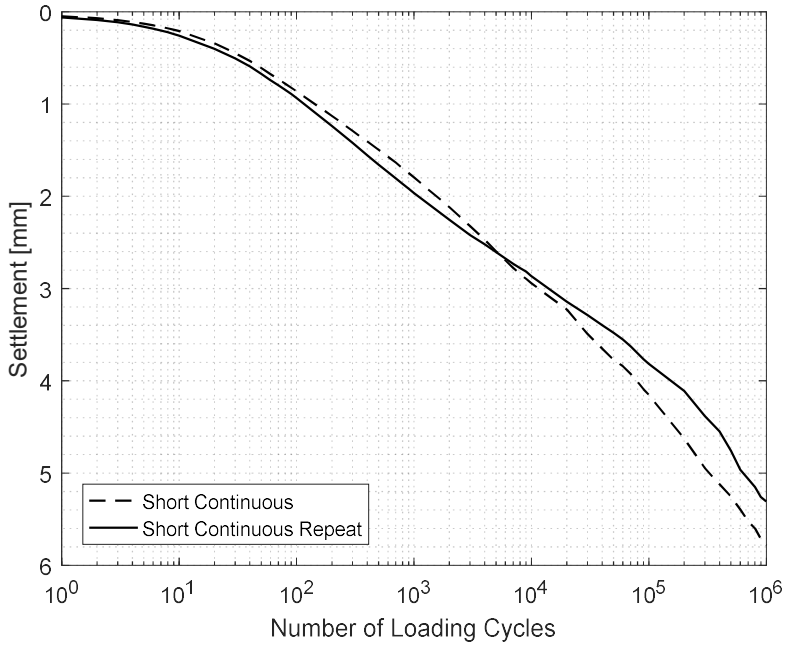

Figure 62 Area weighted average of permanent settlement of a 3.8 m continuous bearer (dashed line) and a repeated test (solid line)

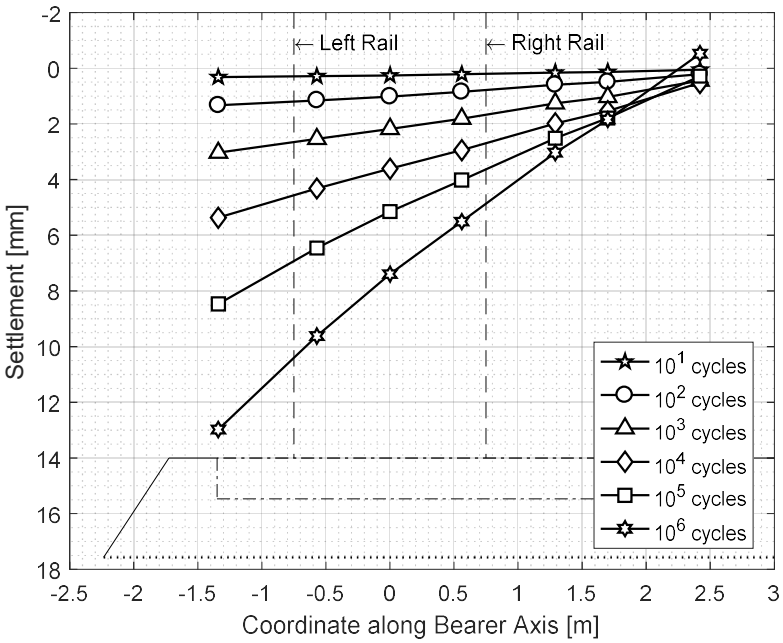

Figure 63 Evolution of permanent settlement along the length of 3.8 m continuous bearer subject to 10^6 cycles with a sinusoidal load equivalent to a 20T axial load. The figure shows rotation of the bearer due to off-centric loading

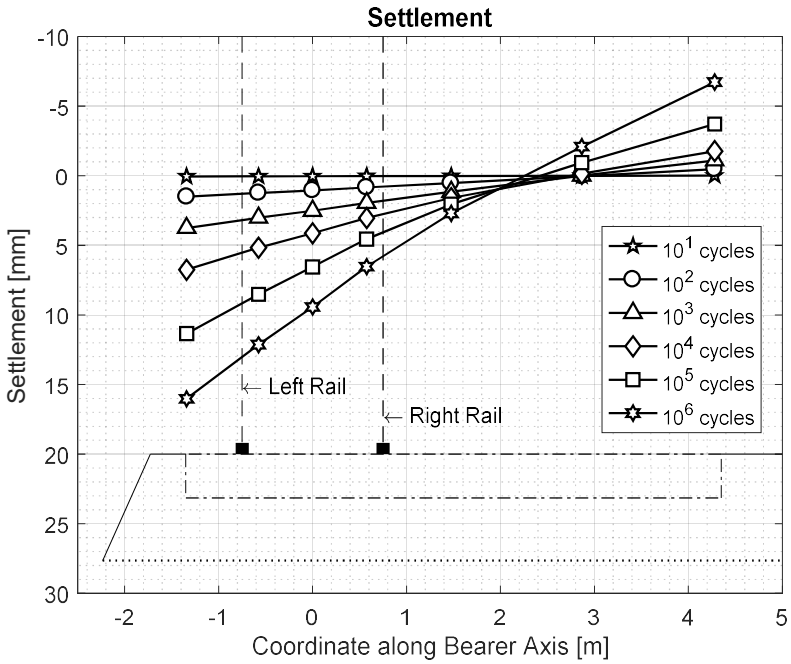

Figure 64 Evolution of permanent settlement along the length of 5.6 m continuous bearer subject to 106 cycles with a sinusoidal load equivalent to a 20T axial load. The figure shows rotation of the bearer due to off-centric loading

Having confirmed test repeatability, the data for the continuous short and long bearers were used as baselines for comparison with subsequent tests. Sections 5.1.1 to 5.1.4 present the settlement data and discuss the results in terms of the effects of the joints, USPs, baseline confined shoulder and closer confined shoulder respectively (refer to Figure 61).

5.1.1 Effect of joints

Figure 65 shows the permanent settlement along the length of the long continuous bearer and its jointed counterparts after selected number of loading cycles. Location of the pin-pin joint adjacent to the loaded rails effectively split the bearer into two individual segments. The loaded rails were more centrally positioned on the left-hand segment, which therefore settled more uniformly over this section than either of the other bearers. Uplift of the unloaded section did not occur at all with the pin-pin jointed bearer. There was, however, some rotation towards the right-hand rail, owing to the proximity of this rail to the right joined end, along with the pin-pin joint practically uncoupling the two joined bearer segments. Below the loaded track, the rigid jointed bearer settled in the same manner as the continuous bearer, with slightly smaller settlements. There was a degree of permanent rotation about the rigid joint, which reduced the permanent uplift on the unloaded end of the bearer by a factor of over two compared with the continuous bearer.

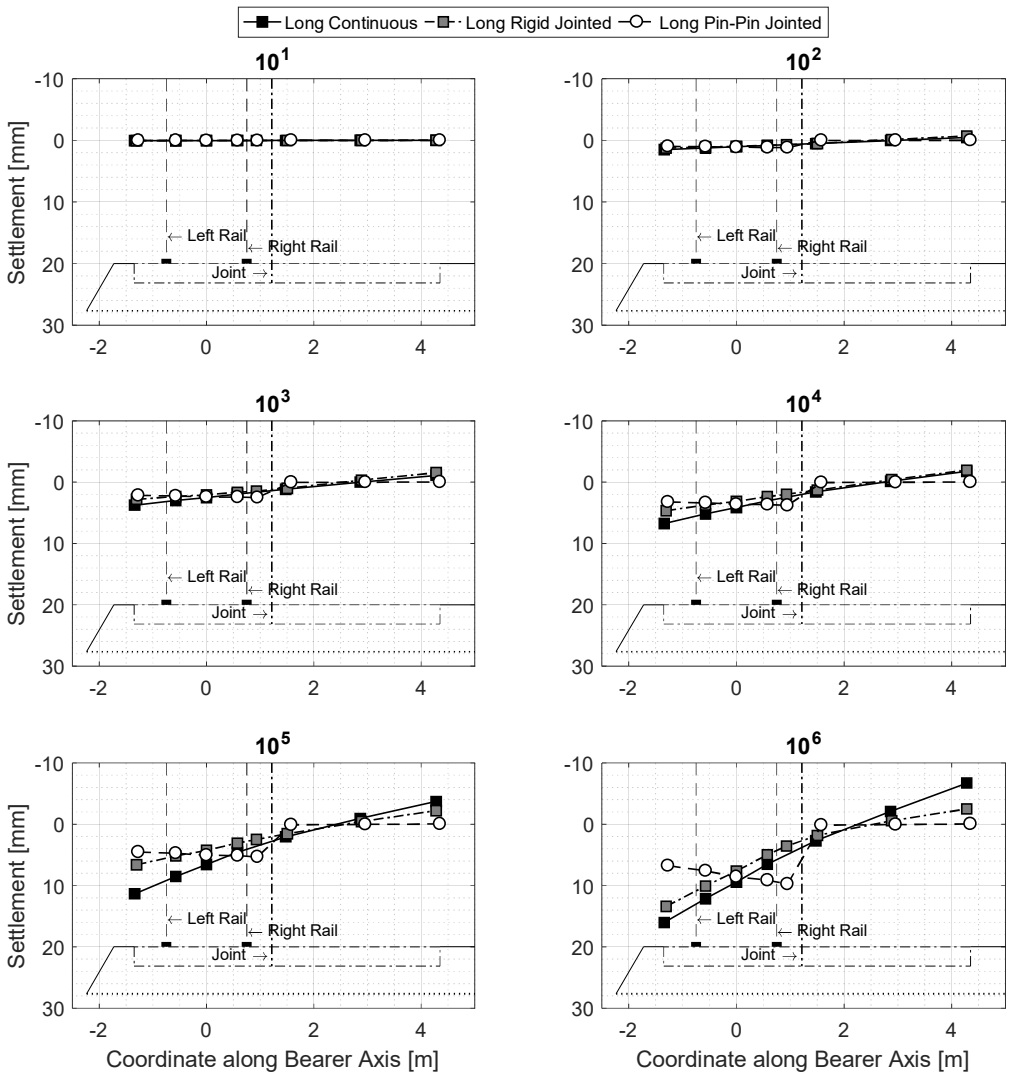

Figure 65 Comparing the permanent settlement along the length of the long 5.6 m continuous, rigidly jointed and pin-pin jointed bearers at key loading cycle

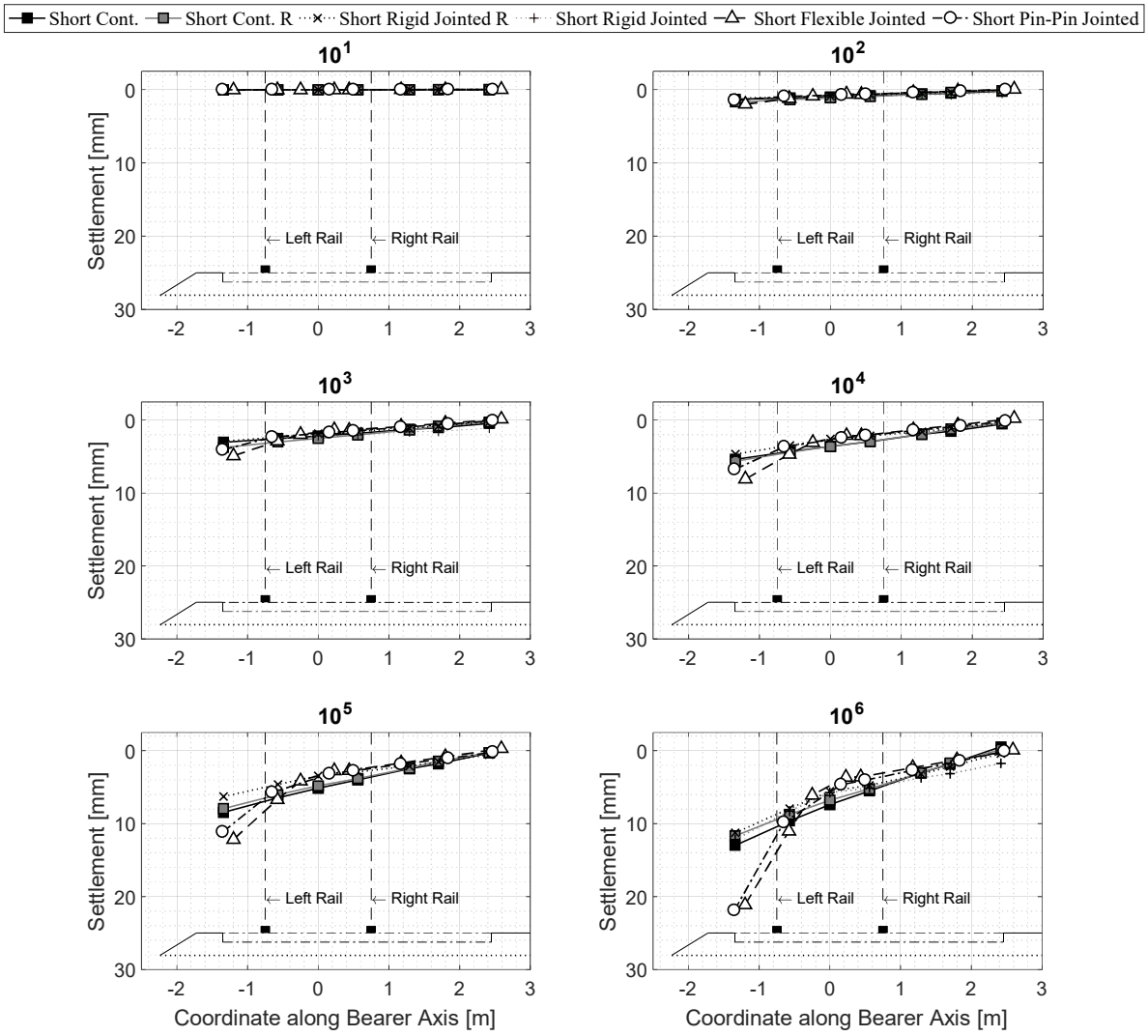

Figure 66 Comparing the permanent settlement along the length of the short (3.8 m) continuous and jointed bearers at key loading cycles

Figure 66 comprises six graphs, each showing the accumulated vertical settlement of the short continuous bearer (and its repeat) in comparison with its jointed counterparts after selected numbers of loading cycles. It shows that the introduction of a joint between the loaded rails on the bearer influenced the permanent settlement along its length. Jointed bearers experienced significant permanent rotations about the joints, which resulted in a greater permanent settlement of the left-hand segment, loaded by the left-hand rail (closer to the ballast shoulder). Settlements under the right-hand segment of jointed bearers were slightly smaller than at corresponding locations on the continuous bearer. The common trend, however, is the large permanent settlement under the loaded rails, that increases towards the unconfined ballast shoulder.

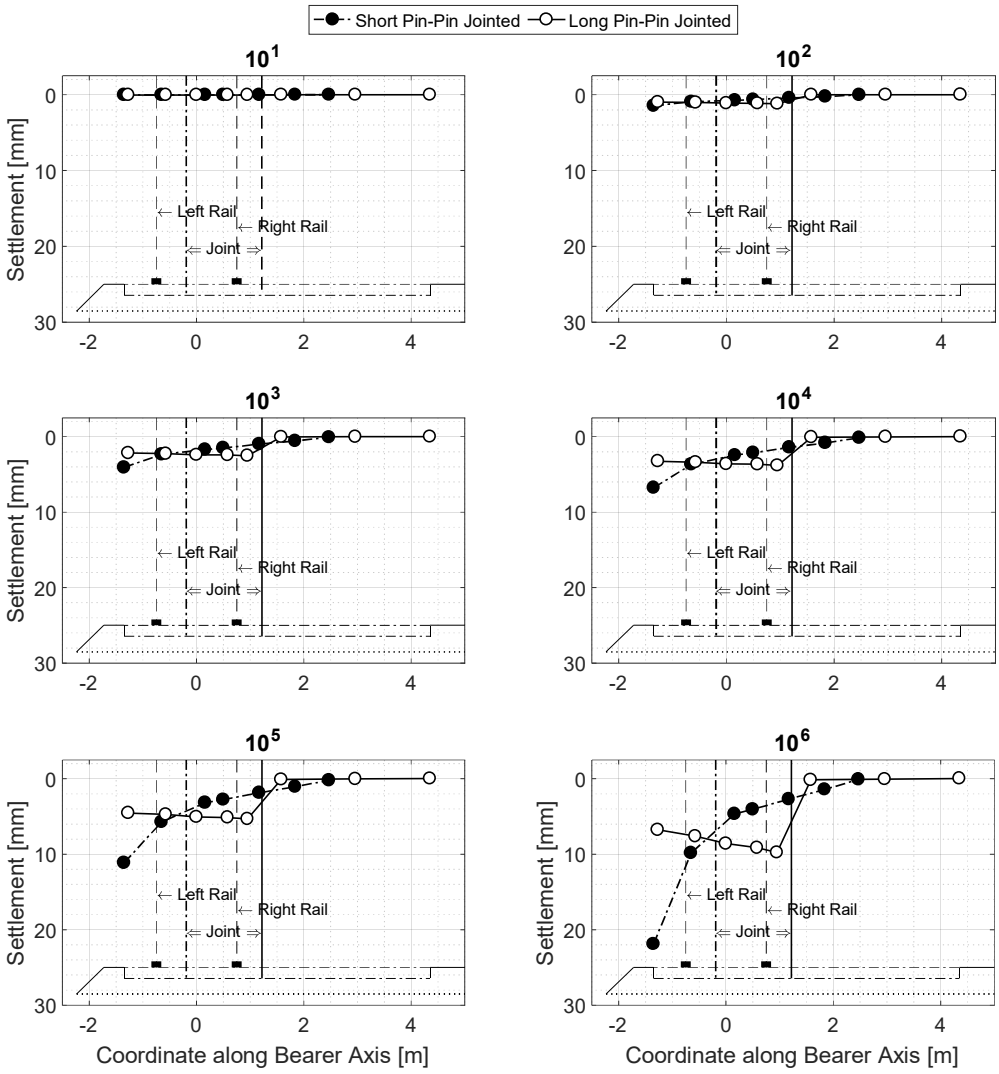

Figure 67 Comparing permanent settlement along the length of short and long pin-pin jointed bearers to show the effect of joint location on vertical settlement – joint location is pointed in the graphs to be between the loaded rails on the shorter bearer and aside the loaded rails away from ballast shoulder on the longer jointed bearer

Figure 67 compares the plastic settlement after selected numbers of loading cycles for short and long bearer with a pin-pin joint between and beside the loaded rails, respectively. It shows a clear change in the trend in settlement along the length of the bearer with changing joint location. Joint located between the loaded rails had significantly higher variation in settlement along its length than the bearer with joint outside the loaded rail.

5.1.2 Effect of USP

Figure 68 compares the plastic settlements of the continuous and pin-pin jointed bearers with and without USP. The data show an insignificant change in plastic settlement for the pin-pin jointed bearer and minimal difference for the continuous bearer utilising the USP. It seems that the USP helped distribute the loads more uniformly on the continuous bearer, as the settlement towards the ballast shoulder (closer to the loaded rails) was reduced by 2 mm (15%). The permanent uplift at the unloaded end of the bearer was also reduced. This is attributed to the loads being more uniformly distributed along the length of the bearer, resulting in less variation in permanent settlement along the length of the bearer.

Figure 69 shows the average rail settlement of the short continuous and pin-pin jointed bearers, plotted against the logarithm of the number of loading cycles. Introduction of the USP made no significant difference to the average settlement of the rails. There was a noticeable improvement in crosslevel for the continuous bearer but little improvement for the jointed bearer with USP as shown in Table 4.

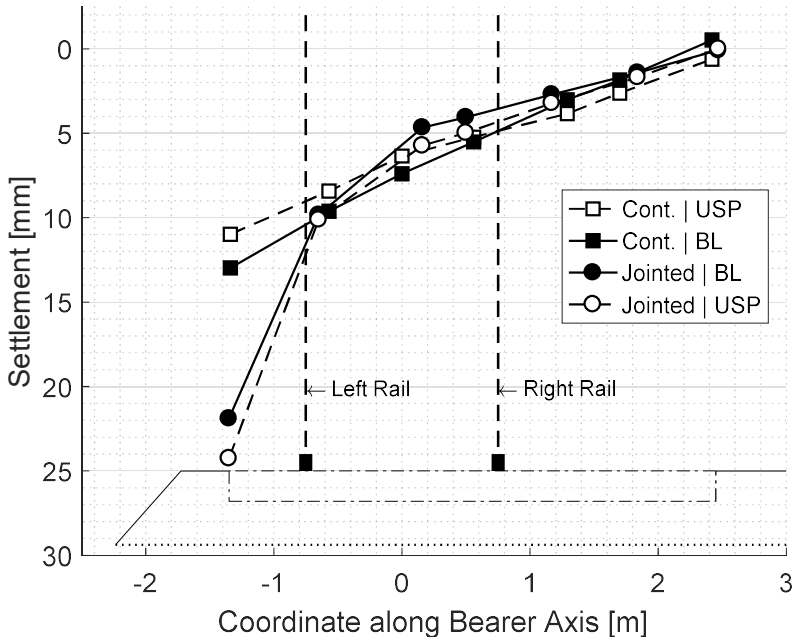

Figure 68 Settlement at 1M loading cycles along the length of the short continuous and pin-pin jointed bearers utilising USP

Table 4 Influence of the use of Under Sleeper Pad (USP) on the average crosslevel (with percentage improvements) of the 3.8 m continuous and jointed bearer in eccentric settings.

Bearer type	Average Crosslevel [mm]	Improvement [%]
Short Continuous (no USP)	3.7049	
Short Continuous (USP)	2.8949	21.86
Short Pin-Pin jointed (no USP)	4.6671	
Short Pin-Pin jointed (USP)	4.3739	6.28

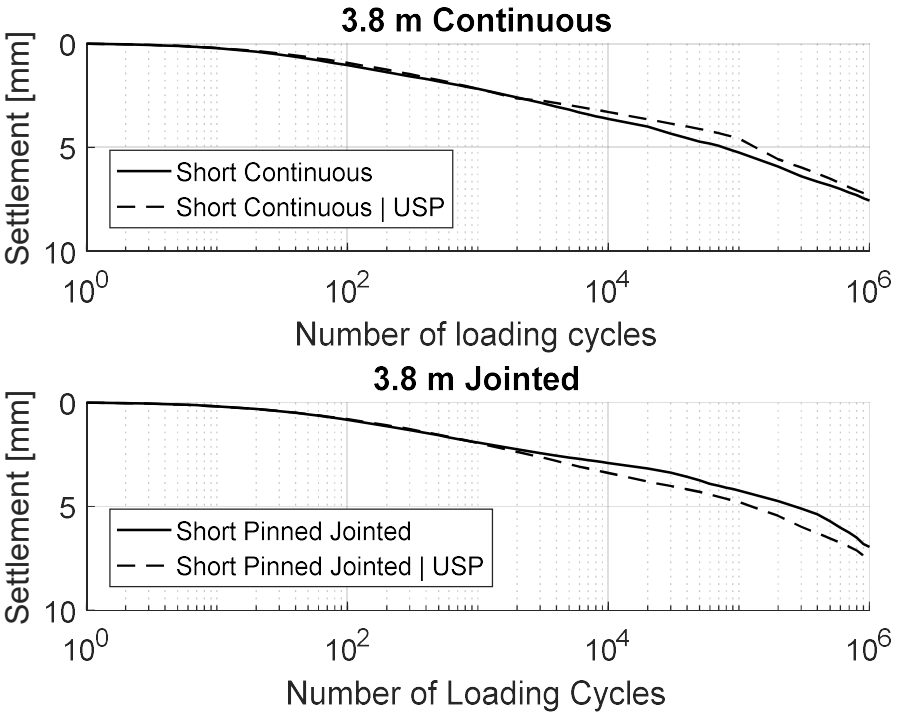

Figure 69 Graph comparing average rail settlement on the short (3.8m) baseline continuous and pinned jointed bearers with those utilising USP

5.1.3 Effects of ballast shoulder confinement

Permanent settlements along the lengths of the continuous bearers with and without shoulder confinement are presented for selected numbers of loading cycles in Figure 70. As the confinement of the shoulder created a more uniform ballast support, permanent rotation towards the shoulder was greatly reduced. This also led to a significant reduction of variation in settlement along the length of the bearer.

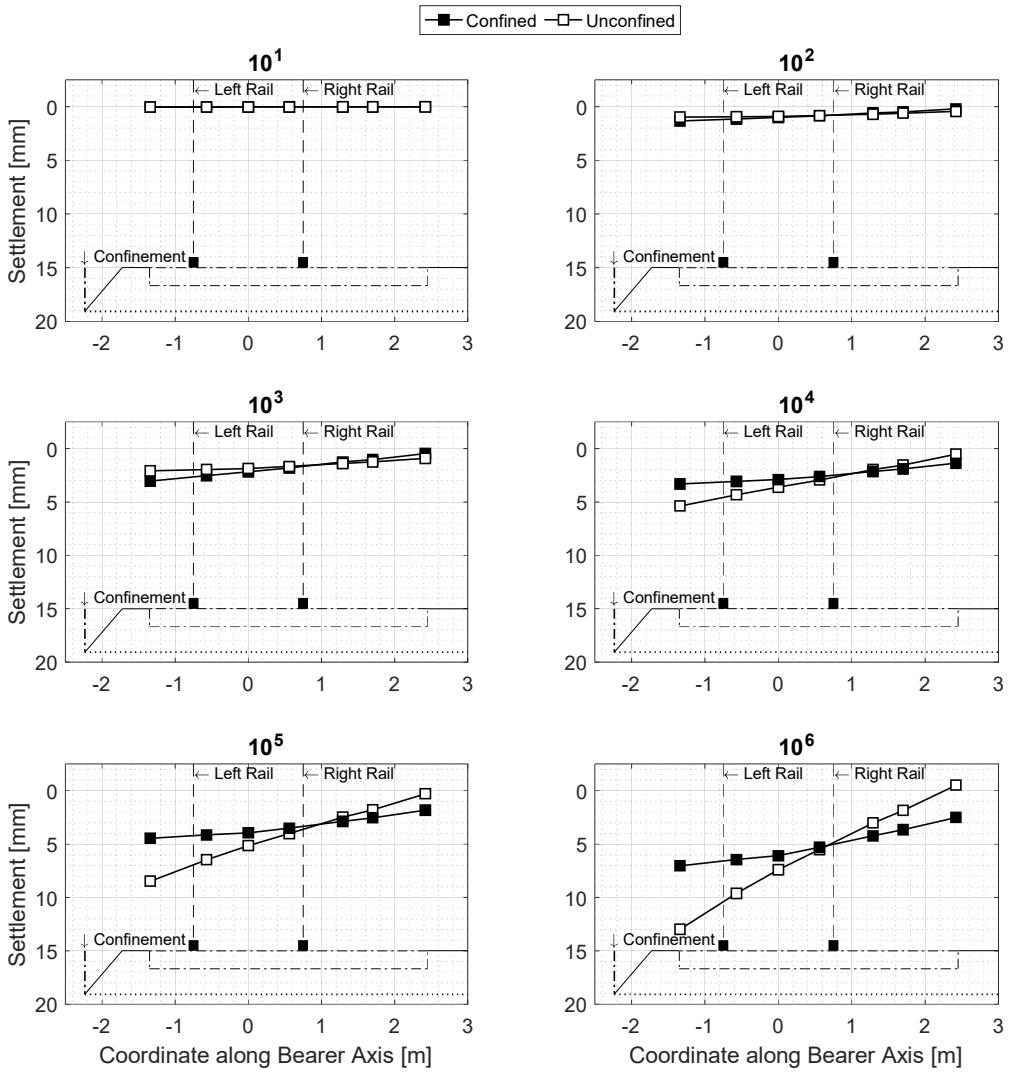

Figure 70 Settlement at key loading stages along the length of continuous bearers in baseline conditions and with the ballast shoulder laterally confined via a rigid wall

The improvement in maintaining the relative level of the rails is further illustrated by Figure 71a, which compares the variation in crosslevel with number of loading cycles for the short continuous bearer tests with confined and unconfined ballast shoulders. While rotation of the bearer towards the shoulder is still present, its magnitude was reduced by confining the shoulder and limiting the ability of the ballast to spread laterally. Ballast shoulder confinement had the same effect on the pin-pin jointed bearer; the crosslevel reduced dramatically as seen in Figure 71b, which shows the crosslevel on the short pin-pin jointed bearer with confined and unconfined ballast shoulder.

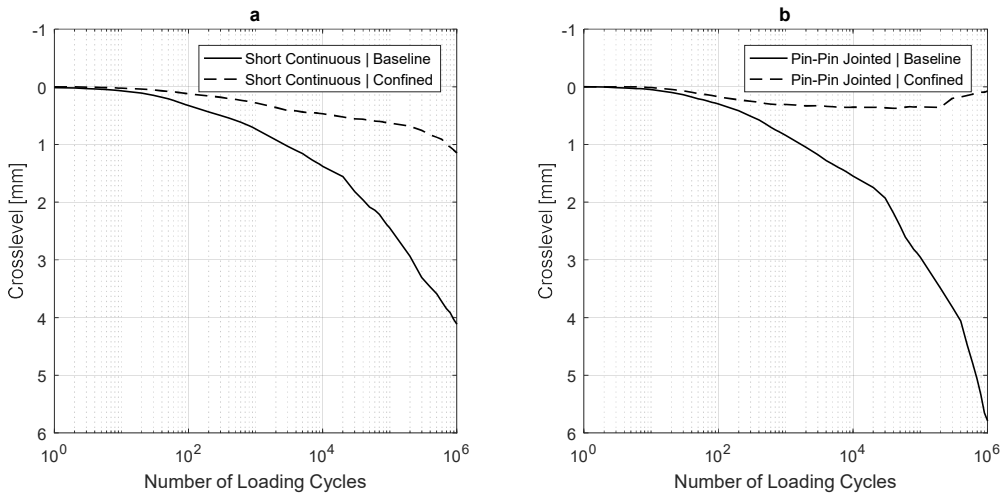

Figure 71 Crosslevel [mm] of the short continuous and short pin-pin jointed bearer with unconfined and confined ballast shoulder

Figure 72 shows the permanent settlements along the lengths of the short pin-pin jointed bearers with and without (baseline) shoulder confinement at selected numbers of loading cycles; overall, there was a significant reduction in permanent settlement of the left-hand bearer segment.

The right-hand bearer segments were little influenced by ballast shoulder confinement (Figure 72). This can be explained by its greater distance from the region affected by the confinement, together with the uncoupling effect of the pin-pin joint.

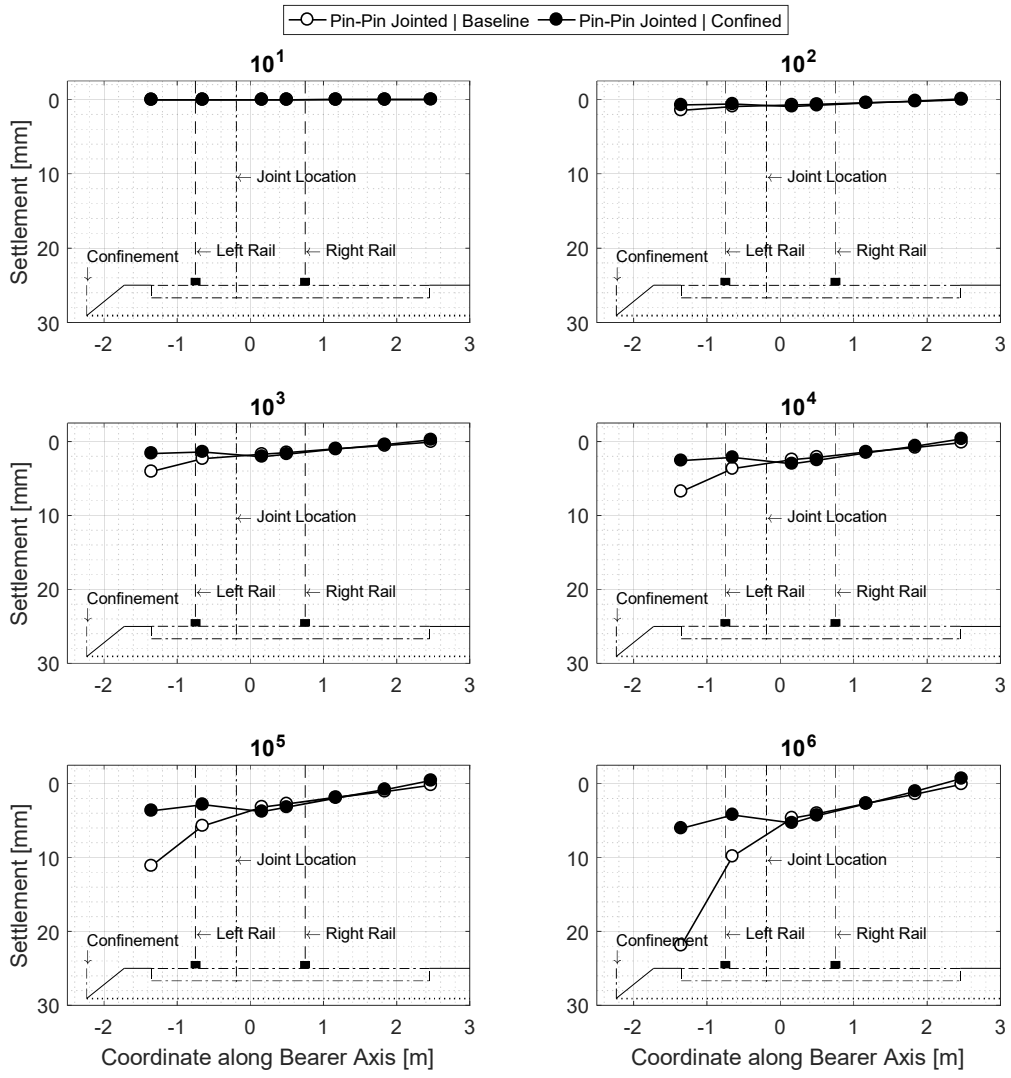

Figure 72 Settlement at key loading stages along the length of the short pin-pin jointed bearers baseline conditions and with the ballast shoulder laterally confined via a rigid wall.

5.1.4 Effect of closer confined shoulder – ballast batch 2

Further tests were carried out to assess the effect of bringing the shoulder confining wall nearer to the bearer end – a closer confined ballast shoulder. However, a different batch of ballast as described in Section 4.3.1, was used because the original ballast delivery had been exhausted. Slightly different specifications are common between deliveries, even from the same quarry (Figure 33 in Section 4.3.1). Because the new batch of ballast had a different PSD (Figure 33 in Section 4.3.1), the baseline continuous short bearer test was repeated using the different batch of ballast. This new batch of ballast showed greater settlement; Figure 73 compares the permanent vertical settlement at selected numbers of loading cycles along the lengths of the continuous bearers (with and without the confined shoulder) for both batches of ballast. Possible reasons for larger settlement from ballast batch 2 could be the larger average grain size, frictional properties of the grains and shape characteristics.

Comparison of the results of tests carried out using ballast batch 2 shows similar behaviour in terms of both the variation in settlement and the reduction in settlement on shoulder confinement (Figure 73). Permanent settlements in tests carried out using ballast batch 2 are compared for the unconfined baseline, baseline confined shoulder, closer confined shoulder tests in Figure 74. It shows that the reducing the distance of the shoulder confinement wall from the bearer end, from 875 mm (bassline confined shoulder) to 375 mm (closer confined shoulder) had no additional improvement on the long-term performance.

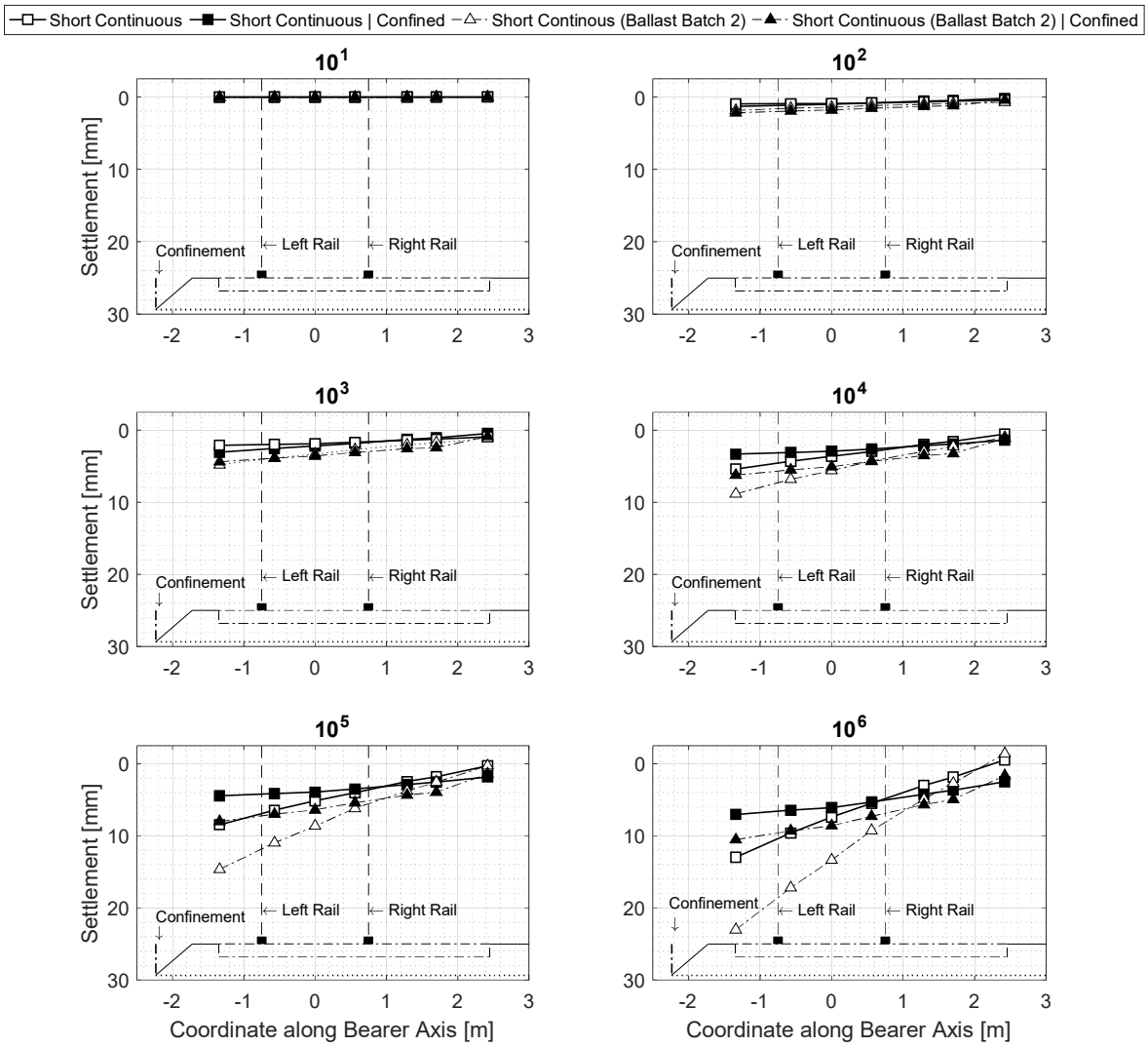

Figure 73 Comparison of the two batches of ballast in terms of the settlement along the lengths of the 3.8 m short continuous bearers with and without ballast shoulder confinement

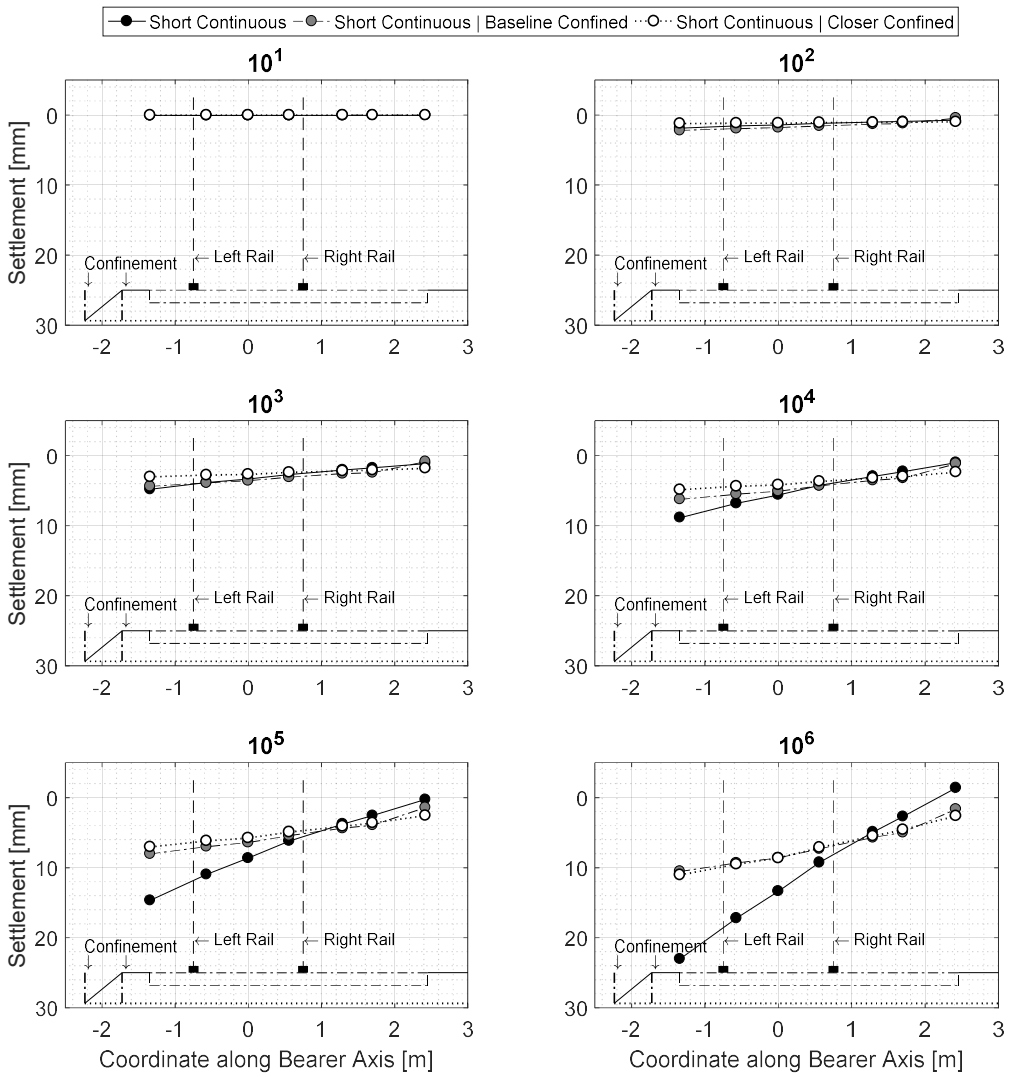

Figure 74 Settlement along the length of the continuous short bearer with and without shoulder confinement and with closer confined shoulder

5.2 Lateral movement of ballast shoulder

This section presents lateral displacements as measured using the lateral plates described in Chapter - Methodology. Ballast settlement occurs as particles rearrange by rotating or sliding relative to one another in response to changes in applied stress. Horizontally unconfined boundaries have the least resistance.

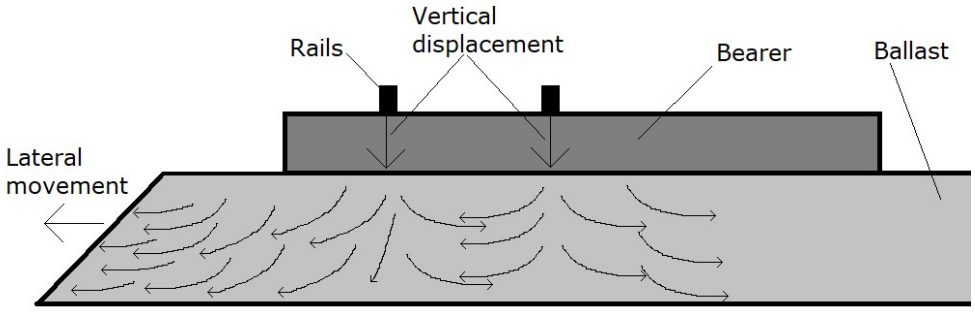

Figure 75 Schematic showing the lateral movement of the ballast shoulder and the predicted ballast migration within the ballast bed

A schematic of the ballast bed showing the direction of the lateral movement and expected paths of ballast movement is shown in Figure 75. Figure 76 plots the vertical displacement under the left-hand rail (below which ballast migrates towards the shoulder) against the lateral movement of the ballast shoulder. It shows a linear relationship between overall rail settlement and lateral movement of the ballast in all tests except for the pin-pin jointed long bearer. The higher gradient is explained by the position of the loaded rails relative to the overall length of the loaded segment – eccentric loading. Central loading of the pin-pin jointed long bearer resulted in uniform distribution of the loads and the influence of the left-hand rail on the shoulder ballast moving outward was reduced.

As shown in the Section 5.1.1, ballast under the left-hand rail undergoes relatively large permanent deformations and is linked, as shown in Figure 76, to the lateral movement of the ballast shoulder. This raised a sensible argument for the testing the effect of confinement of the ballast shoulder, which significantly reduced the variation in settlement along the lengths of the bearers.

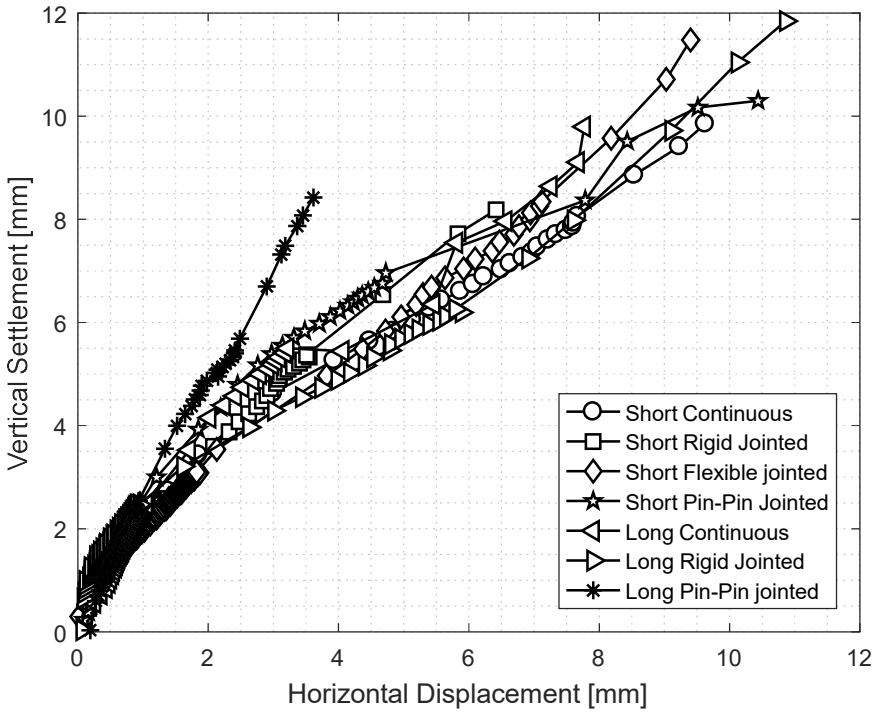

Figure 76 Vertical settlement vs horizontal movement (see Settlement - Effects of Joints, Figure 65 & Figure 66)

5.3 Resilient deflections

Resilient deflections calculated as the difference in maximum and minimum vertical deflections at key locations on the bearers are presented in this section.

5.3.1 Effect of joints

Comparison of the resilient deflections of the short continuous and short rigid jointed bearers and their repeated tests presented in Figure 77 shows that in the short term, the resilient component of continuous bearer movement may be described as sagging at both minimum and maximum loads, with the greatest deflections between the rails and towards the shoulder, with some uplift at the inward bearer end. The permanent settlement could be described as tilting in the short term. As the loading cycles accumulated, bearer movement at the shoulder end tended to be hogging, and permanent rotations about the joints - even in the case of the rigid joint - led to hogging in the long term. There was a noticeable change in peak deflection with increasing loading cycles and the behaviour was similar in the repeat test (top and middle rows in Figure 77). The rigid jointed bearer deflected in a manner similar to its continuous counterpart; however, the peak deflections in the early loading stages varied between repeat tests. This could have been a result of variations in ballast bed level or joint rigidity due to the tolerances in the joint system.

Resilient deflections along the length of the continuous bearer and its jointed counterparts are compared at key loading stages in Figure 78. Resilient deflections on the flexible and pin-pin jointed bearer were smaller but tended to increase towards the ballast shoulder. However, there was negligible change in the resilient deflections of the flexible and pin-pin jointed bearers with increasing number of loading cycles (bottom row, Figure 77).

The change in bending mode of the short continuous bearer from sagging to hogging near the shoulder region shown in Figure 77 is attributed to the loss of ballast support in that region and the development of a gap at the bearer/ballast interface. The development of the gap, together with centre-binding, causes the change in bending state of the bearers. The minimal rate of change in resilient deflection throughout the loading cycles suggest that the presence of a flexible joint prevented the development of a gap as the bearer sections remained in contact with the ballast level.

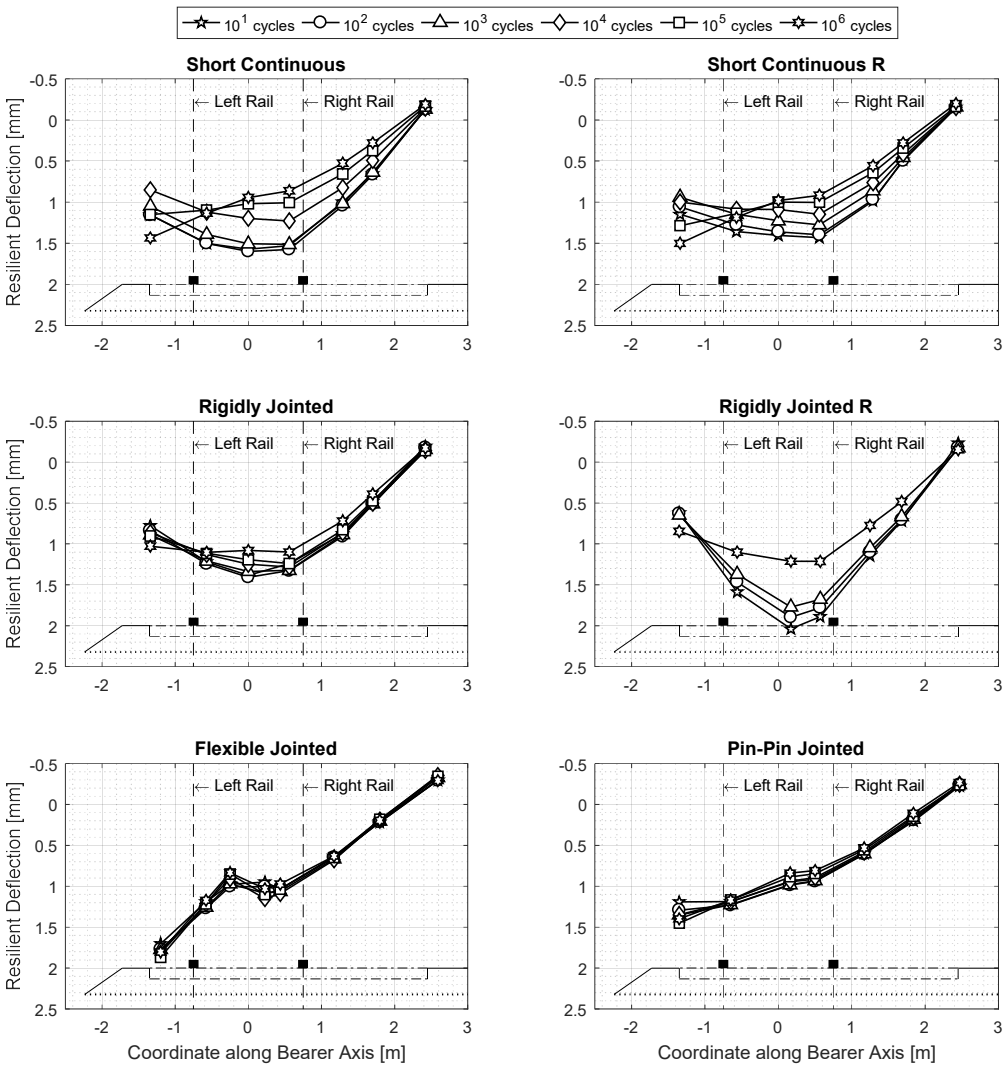

Figure 77 Graphs showing resilient deflections of continuous (and repeat test), rigidly jointed (and repeat test), flexibly jointed and pin-pin jointed bearers over the course of loading cycles

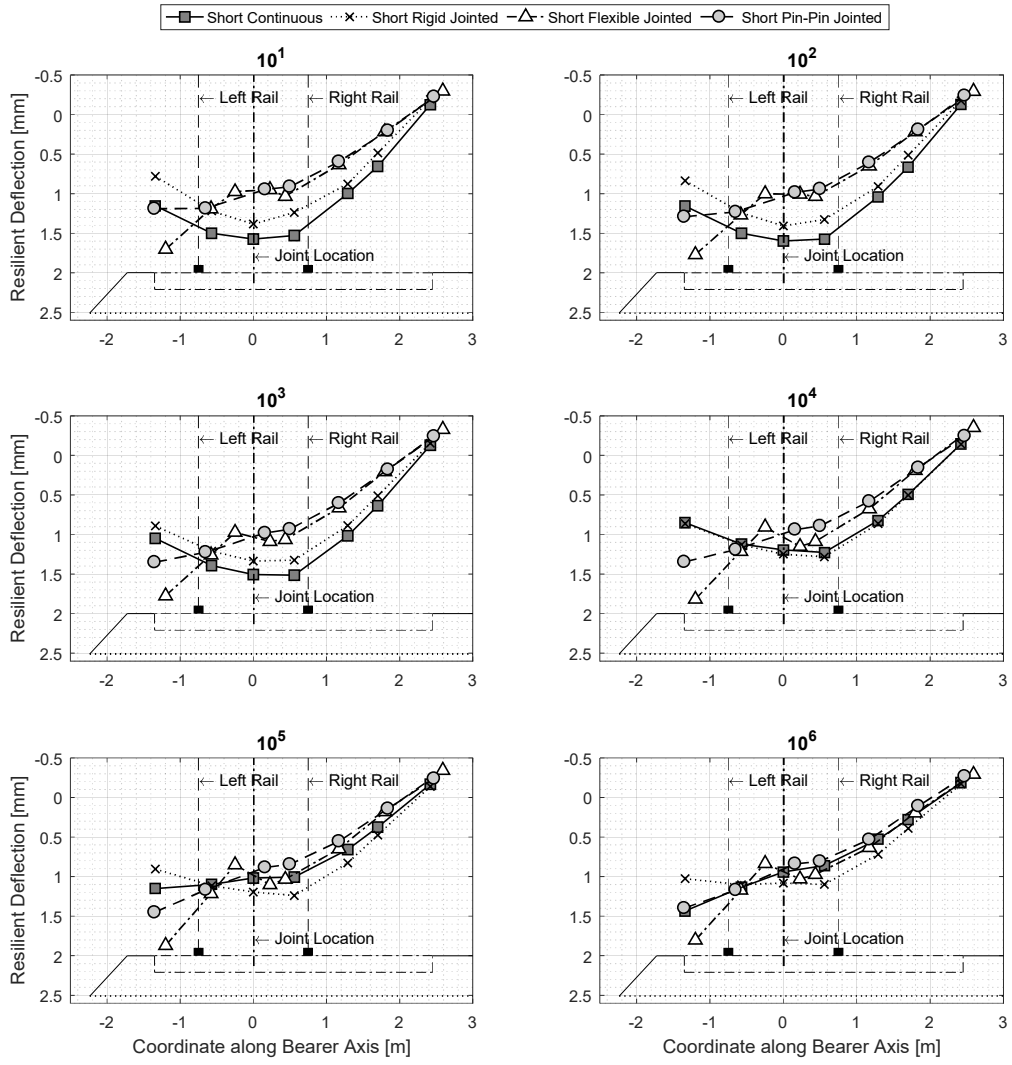

Figure 78 Graphs comparing resilient deflections along the length of 3.8 m short continuous, short rigid jointed, short flexible jointed and short pin-pin jointed bearer

Vertical resilient deflections at selected numbers of loading cycles are compared for the short and long continuous bearers with long rigid and pin-pin jointed bearers in Figure 79. The eccentric loading effect is greater on the longer continuous and rigidly jointed bearers, causing it to settle and permanently rotate more towards the left end with a significantly higher uplift, as expected. Consequently, resilient deflections in the long term tended to be greater in the region closer to the ballast shoulder as a larger gap develops at the bearer/ballast interface upon loading.

Vertical resilient deflections at selected numbers of loading stages presented by bearer type in Figure 80 show that resilient deflections were more uniform along the length of the pin-pin jointed longer bearer than for the continuous and rigidly jointed bearers, which initially

exhibited sagging but started to rotate as ballast in the region under the left shoulder rails settled permanently. Initial sagging at both ends of loaded segment was followed by hogging at both ends with the development of centre-binding. This was due to the load on the loaded segment of the pin-pinned jointed bearer being more central.

The pin-pin jointed longer bearer had the joint outside the loaded rails away from the ballast shoulder, with the loaded rails located more centrally. This central loading resulted in more uniform ballast settlement along the length of the bearer and smaller permanent rotations. Hence resilient deflections show clear signs of sagging in the short term, at both ends of the loaded bearer segment (bottom right plot in Figure 80). In the long term, the nature of bending changes to hogging at both ends.

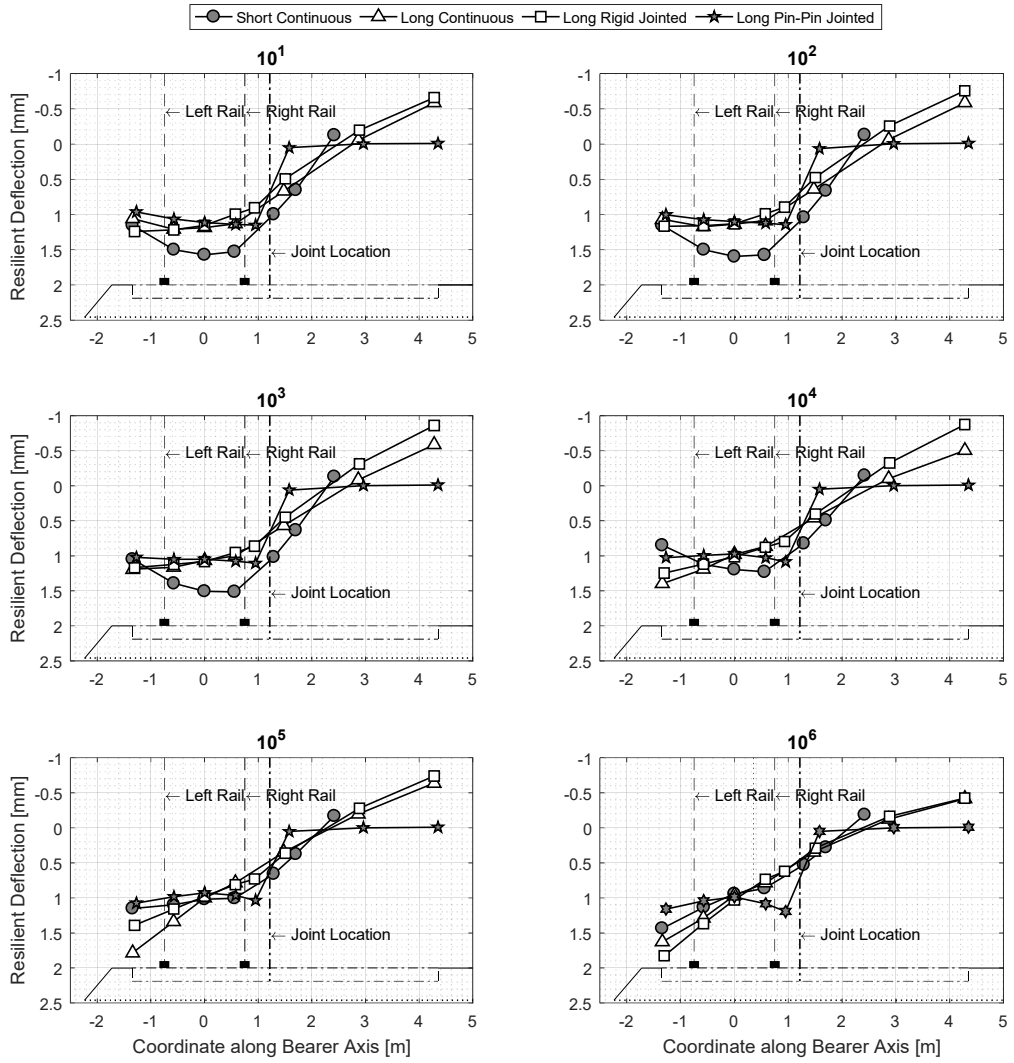

Figure 79 Graphs comparing resilient deflections along the length of long continuous, long rigid jointed and long pin-pin jointed bearers with baseline short continuous bearer

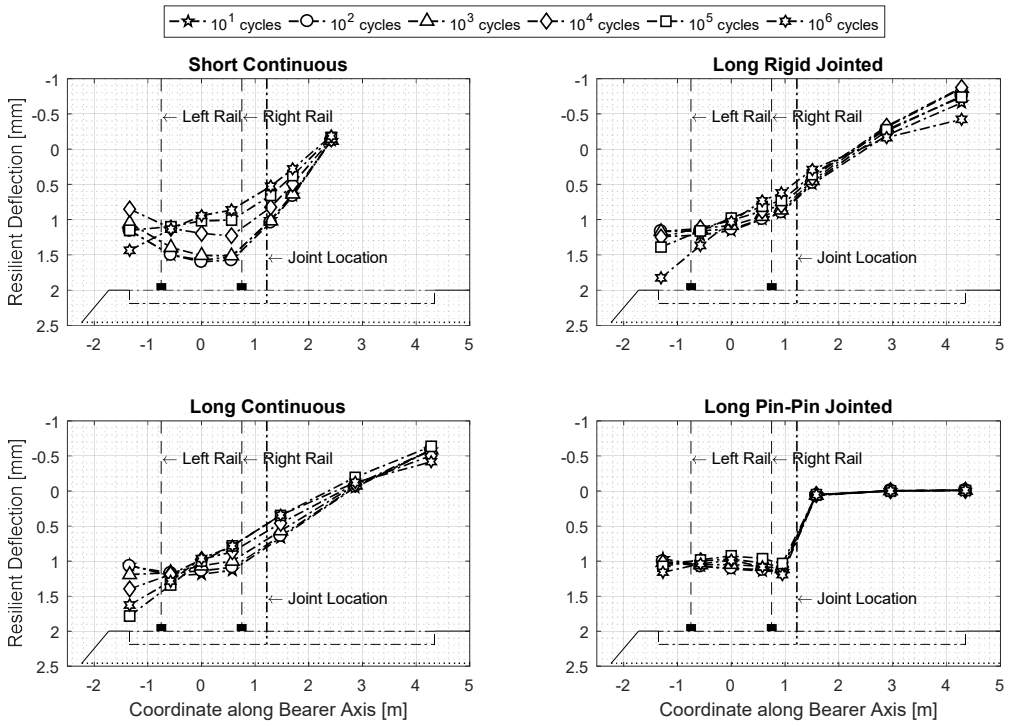

Figure 80 Graphs showing resilient deflections of short continuous, long continuous, long rigid jointed, and long pin-pin jointed bearers at selected loading cycles

5.3.2 Effect of USP

The vertical resilient deflections of the short 3.8 m continuous and pin-pin jointed bearers, with and without the use of USP, are plotted for selected numbers of loading cycles in Figure 81. The use of a USP (Figure 81) on both the continuous and pin-pin jointed bearer increased resilient deflections along the length of the bearer and also the variation in resilient deflections with increasing number of loading cycles. The location of peak deflection remained between the loaded rails on the continuous bearer but was significantly higher in the short term with the use of USP. With increasing number of loading cycles, difference in the resilient deflection between bearers with and without USP decreased.

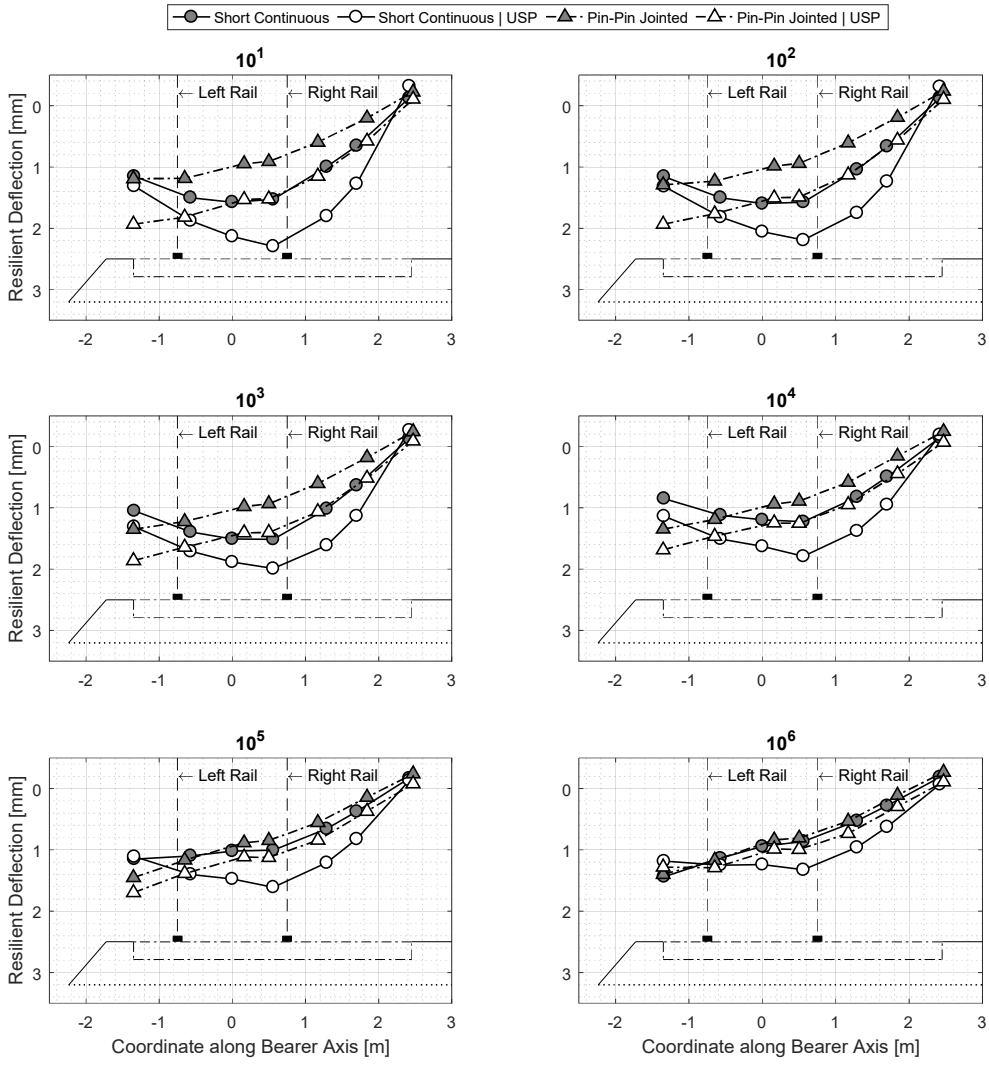

Figure 81 Graphs comparing resilient deflections along the length of the short continuous and pin-pin jointed bearer with and without the use of Under Sleeper Pads (USP)

5.3.3 Effect of shoulder ballast confinement

In Figure 82, the resilient deflections at key locations along the length of the short 3.8 m continuous and jointed bearers in both baseline conditions and with the ballast shoulder confined (using a rigid wall to offer lateral resistance) are plotted for selected numbers of loading cycles. Confinement of the ballast shoulder had a significant impact on the resilient deflections of both the continuous and pin-pin jointed bearers. By providing good ballast support in the region from the left-hand rail towards the left-hand end, the variation in resilient deflection of the continuous bearer significantly decreased with increasing number of loading cycles. There were no signs of hogging even after 1M loading cycles, and the maximum deflection remained between the rails. Likewise, the pin-pin jointed bearer performed better

with the shoulder confinement, with the variation in resilient deflections along the length of the bearer being significantly reduced.

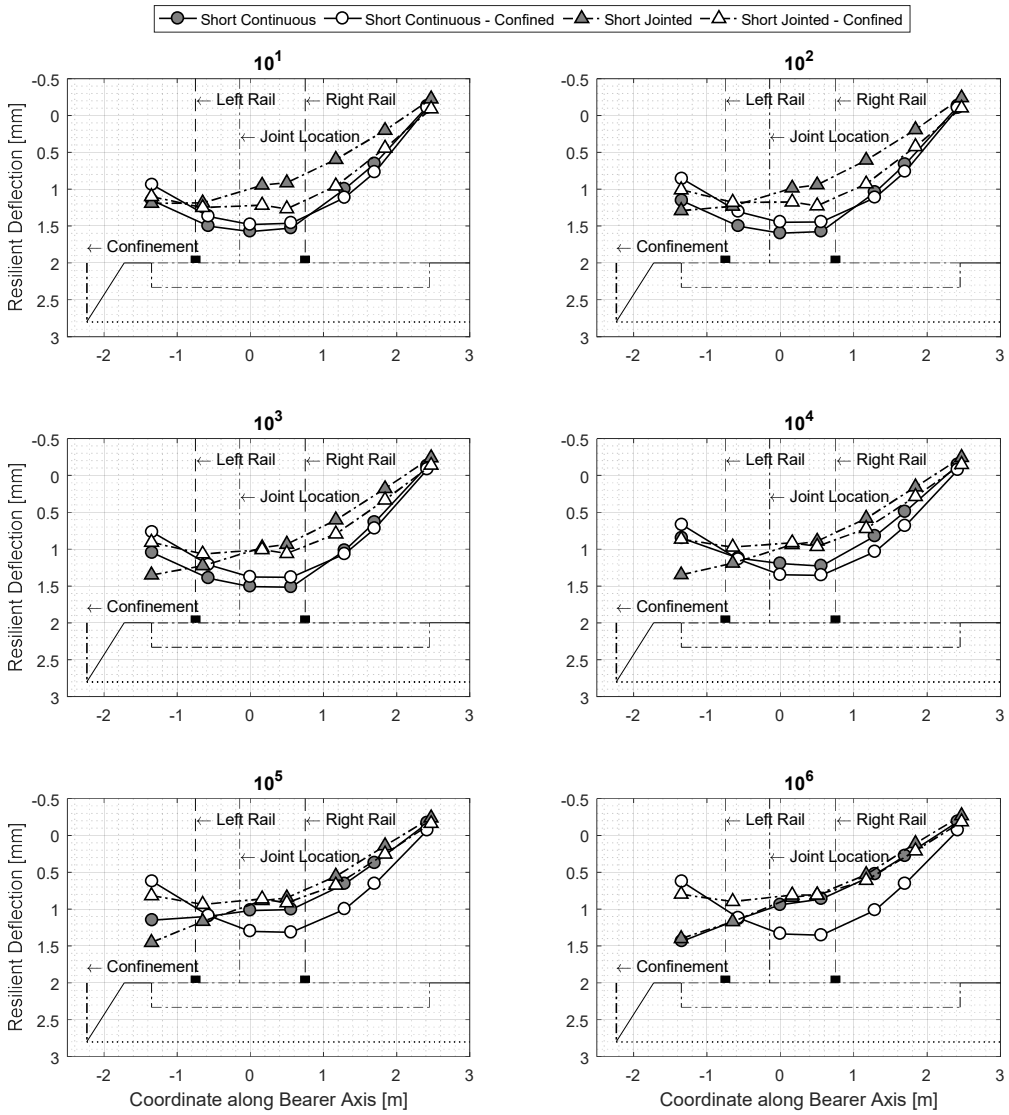

Figure 82 Graphs comparing resilient deflections along the length of short continuous and pin-pin jointed bearer with and without the ballast shoulder confinement

5.3.4 Resilient deflections and bearer voids

Figure 83 compares the resilient deflections after 1.2M loading cycles along the length of the continuous bearer for the continuous short bearer and tests including USP, confined ballast shoulder and closer ballast shoulder confinement. Deflection curves varied by test type as shown in Figure 83. With ballast shoulder confinement, there is a clear sagging deflection bowl, while the baseline and to a lesser degree the test with a USP showed minimal bending, instead rotating towards the ballast shoulder.

Differences in permanent vertical deflections of the ballast and the bearer were compared between tests to establish a link between the gap at the bearer-ballast interface near the ballast shoulder. Figure 84 shows a bar chart of the gap between the bearer end and underlying ballast, measured at 1.2M loading cycles. The highest gap was measured on the continuous bearer, followed by that utilising a USP, and negligible gap in the case of confined ballast shoulder settings. This trend strengthens the argument that the change in bending mode from sagging to hogging at the shoulder bearer end is accompanied by the formation of a gap at that region. Confinement of the ballast shoulder resulted in a consistent sagging of the bearer throughout all the loading cycles without gap formation. This links to the significantly reduced permanent settlement due to the lateral resistance offered by the confinement of the ballast shoulder.

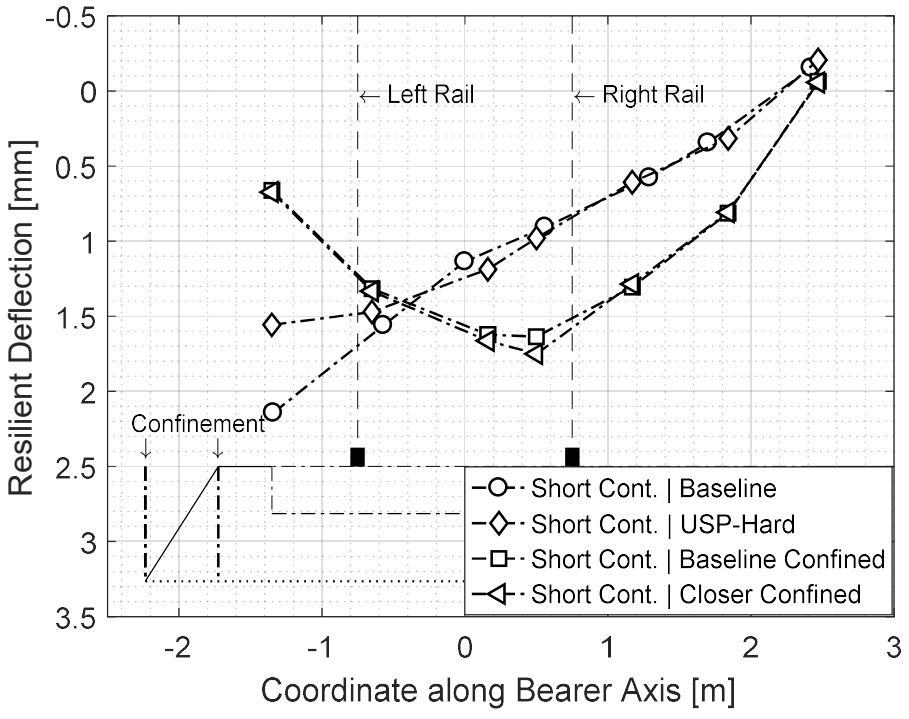

Figure 83 Resilient deflections at 1.2 million Cycles along the length of short continuous bearer in Baseline, with USP, with Ballast Shoulder Confinement and with Reduced Ballast Shoulder Confinement.

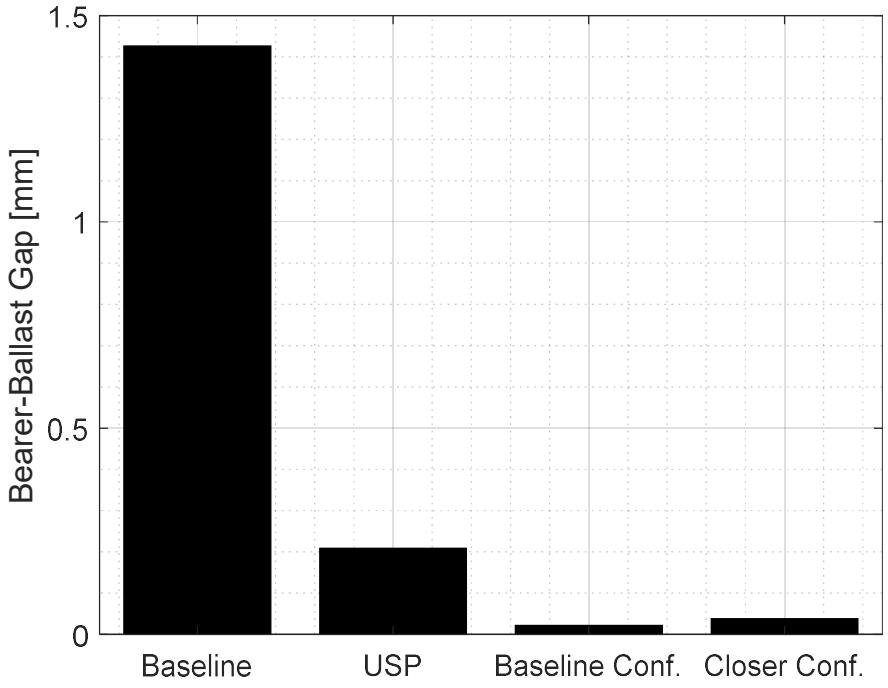

Figure 84 Bar chart showing the bearer-ballast gap measured at the left end of the bearer at the end of the test (~1.2M loading cycles)

5.3.5 Ballast breakage

Particle breakage measured in the baseline tests on the short continuous and its repeated test showed minimal breakage as shown in Table 5. Based on the initial qualitative results, visual inspection of the ballast was carried out for any damage to the ballast in further tests. There was no significant breakage observed visually in the tests.

Table 5 Average mass loss (percentage) for ballast particles sized 31.5 mm and 40 mm at locations under the loaded rails and in the middle of the loaded rails

Test	Left Rail [%]	Mid [%]	Right Rail [%]
Short Continuous (Baseline)	0.053	0.046	0.052
Short Continuous (Baseline Repeat)	0.045	0.072	0.039

5.3.6 Summary

The continuous bearer resilient deflections in the short term were concentrated at the regions under the loaded rails. Shorter bearers had a higher peak deflection in the middle of the loaded rails, while longer bearers showed a wider deflection bowl. In the long term, after the compaction and stiffening of the underlying ballast and the onset of centre-binding, the bearers tended to rotate owing to a gap that developed at the left-hand ends of the bearers. This gap or voiding is due to increased settlement in the region on the left of the bearers and stiffening of ballast elsewhere under the load, resulting in the bearers simply rotating about a fulcrum. The presence of a joint between the loaded rails significantly affected the resilient deflections both along the bearer and with the number of loading cycles. There was minimal variation in resilient deflection with increasing number of loading cycles; however, the vertical deflections were greatest towards the ballast shoulder.

The use of USP resulted in higher vertical resilient deflections with the same trend as their baseline counterparts over 1M loading cycles. Ballast shoulder confinement aided the bearers in maintaining the same bending state throughout 1.2M loading cycles with drastically reduced gaps at the ends of the bearers near the ballast shoulder. There was more uplift on the unloaded end of the longer continuous and rigidly jointed bearers than their shorter counterparts.

The locations of the loaded rails relative to the bearer ends had a significant impact on the resilient behaviour of the bearer. The long pin-pin jointed bearer with loaded rails relatively in the centre of the jointed bearer segment showed symmetrical deflection about the middle of the loaded rails, with a clear shift from sagging in the short term to hogging in the long term.

5.4 Pressures

*Pressures were measured in all tests against the sidewalls adjacent to the loaded rails (*Figure 37 *in Section 4.5). In other tests, pressures were also measured at the interface with the confined ballast shoulder. This subsection describes both sets of measurements.*

5.4.1 Sidewall pressures

Figure 85 shows graphs of sidewall pressure vs logarithm of the number of loading cycles for tests on the continuous and jointed bearers of both 3.8 m and 5.6 m length. An initial variation in pressures under both rails was observed between the tests, which may be due to variations in initial ballast compaction. The pressure adjacent to the rails when the load was a minimum indicate that on loading of freshly laid ballast, pressures from the start of the test are higher under the shoulder end than on the right inner side. This is linked to the eccentric loading of the bearers, which causes higher settlement in that region and tilting of the bearer towards the shoulder (Figure 63 in Section 5.1).

Also, in Figure 85, with increasing number of loading cycles, there was a trend for the pressure to increase adjacent to the right-hand (inner) rail and to reduce adjacent to the left-hand (shoulder) rail. Reductions in confining pressure are indicative of worsening ballast bed support, of the type observed under the rails on sleepers that are centre bound, owing to the outwards movement of the ballast shoulder. The ballast compressive stresses under the right-hand inner rail however, decreased at a lower rate with number of loading cycles because of its relatively reduced capacity to migrate in the case of continuous bearers. An exception was the longer pin-pin jointed bearer (Figure 85g). The latter showed reductions in pressures adjacent to both rails with increasing number of loading cycles. This is attributed to the relatively symmetric loading on the loaded segment of the bearer and the decrease in ballast support on the bearer ends. This is accompanied by higher resilient deflections on either side of the loaded segment relative to its middle - characteristic of centre-binding shown in Figure 79 in Section 5.3.1.

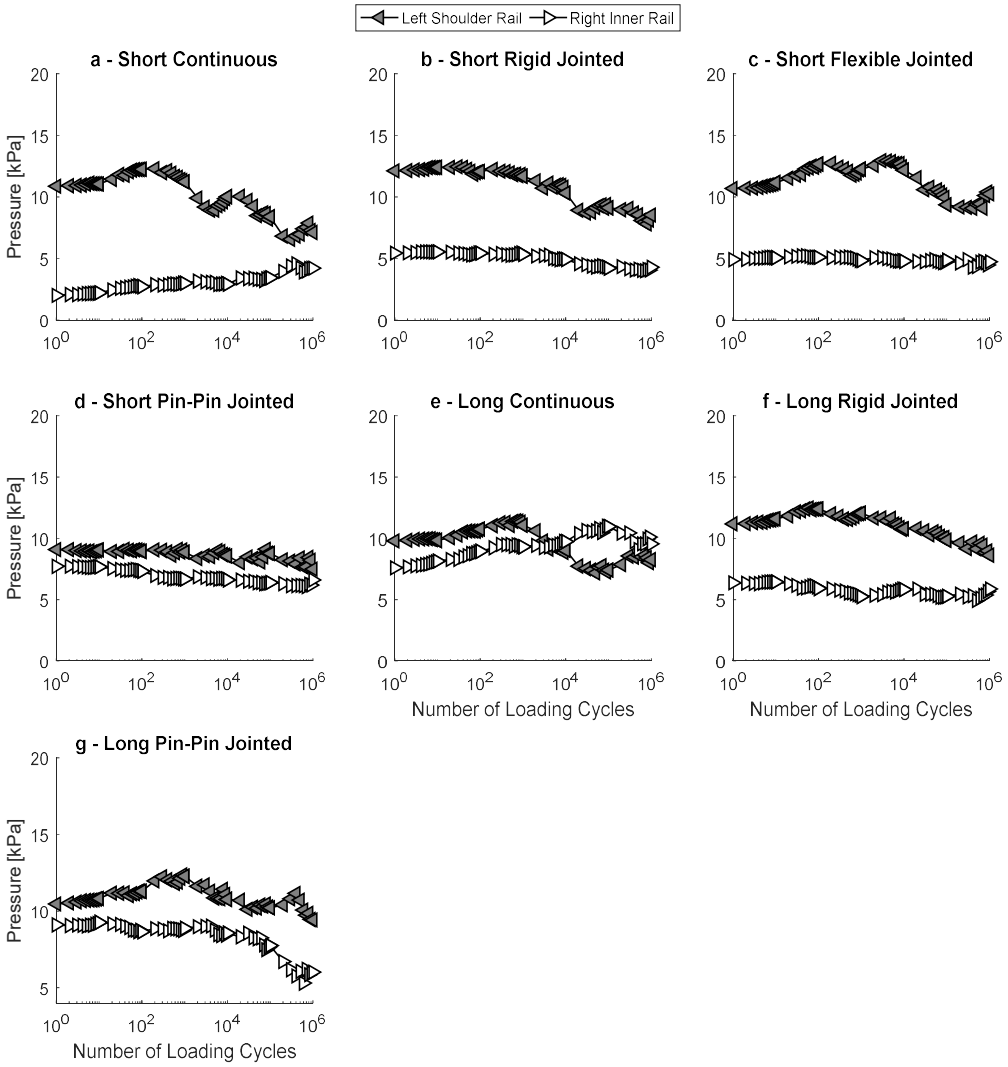

Figure 85 Accumulation of sidewall pressures (when applied load on the rails is minimum) on the left shoulder rail and right inner rail of different types of bearers: a - short continuous; b - short rigidly jointed; c - short flexible jointed; d - short pin-pin jointed; e - long continuous; f - long rigid jointed; g - long pin-pin jointed)

5.4.2 Confined shoulder wall pressures

In some tests the ballast shoulder was confined by a rigid steel wall (Table 3 in Section 4.10). Two Steel plates with load cells were used to measure pressures on the wall. This section presents the results obtained for two types of bearers (short continuous and pin-pin jointed with the joint in the middle of the loaded rails), using two different batches of ballast.

Figure 86 shows the variation in minimum cyclic stress measured on the confined shoulder wall with the logarithm of the number of loading cycles. The tests carried out using ballast batch 1 on continuous and short pin-pin jointed bearers with the ballast shoulder laterally confined, showed a small increase in lateral pressures measured on the wall. Initially (up to 10^3 loading cycles), the difference between the maximum and minimum stresses (cyclic amplitude) decreased slightly in the short term (up to 10^3 loading cycles) and remained constant in the long term. The continuous bearer with regular and closer confinement repeated using ballast batch 2 settled at a much higher rate (Figure 73 in Section 5.1.4), and there were higher stresses on the confining wall.

As the distance of the confining wall reduced from 875 mm to 375 mm in tests on the continuous bearer using ballast batch 2 (Figure 86), the minimum initial shoulder confining stresses increased with the compaction of the ballast from repeated loading. As the number of cycles of load increased there was a greater increase in shoulder confining stresses, particularly between 10^3-10^4 loading cycles (Figure 86).

The shoulder confining stress amplitude is the range of confining stress per loading cycle as shown in Figure 87. The reduction in distance of the confining wall by 43% caused the stress amplitude to triple. Stress amplitude reduced with increasing loading cycles; this is attributed to the decrease in bearer-ballast interaction in the vicinity of the bearer end (near the ballast shoulder, closer to the loaded rails), possibly due to the development of a gap.

The calculated theoretical maximum pressure against the wall as passive pressure is calculated as follows:

$$H = 0.5 \text{ m}, \varphi = 45°, \gamma = 1.665 \text{ Kg/m}^3, g = 9.81 \text{m/s}^2$$

$$K_p = (1+\text{Sin}(\varphi))/(1-\text{Sin}(\varphi)) = 5.8$$

$$\sigma_{h \text{ average}} = 0.5 \times 0.5 \times 5.8 \times 1.665 \times 9.81 = 23.7 \text{ kPa}$$

Figure 86 and Figure 87 illustrate that the compressive stresses within the ballast increase with increasing number of loading cycles. This may be explained by increasing density of the ballast as it compacted with accumulated loading cycles. On the other hand, the amplitude of shoulder confining stress decreased with increasing number of loading cycles, possibly due to the formation of a void at the bearer-ballast interface and consequently the reduced influence of maximum load transferred through the ballast on to the confining wall. The closer distance of the confining wall showed the greatest confining stress amplitude, suggesting good bearer-ballast interaction and void mitigation but with significantly higher confining stresses generated. The use of ballast batch 2, with its greater propensity to settle, gave higher ballast confining stresses than tests conducted using ballast batch 1, which also settled less.

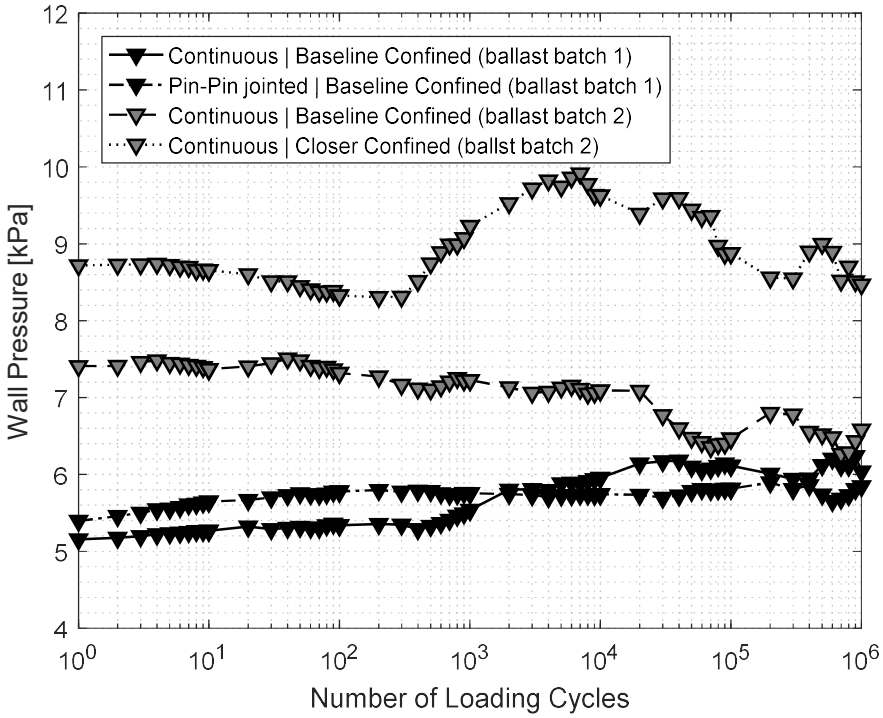

Figure 86 Minimum cyclic confining stress over the course of 10^6 loading cycles measured on tests carried out with regular confined ballast shoulder on the short continuous bearer, short pin-pin jointed bearer using ballast batch 1 and repeat test using ballast batch 2 of the short continuous bearer in both regular and closer confinement setting.

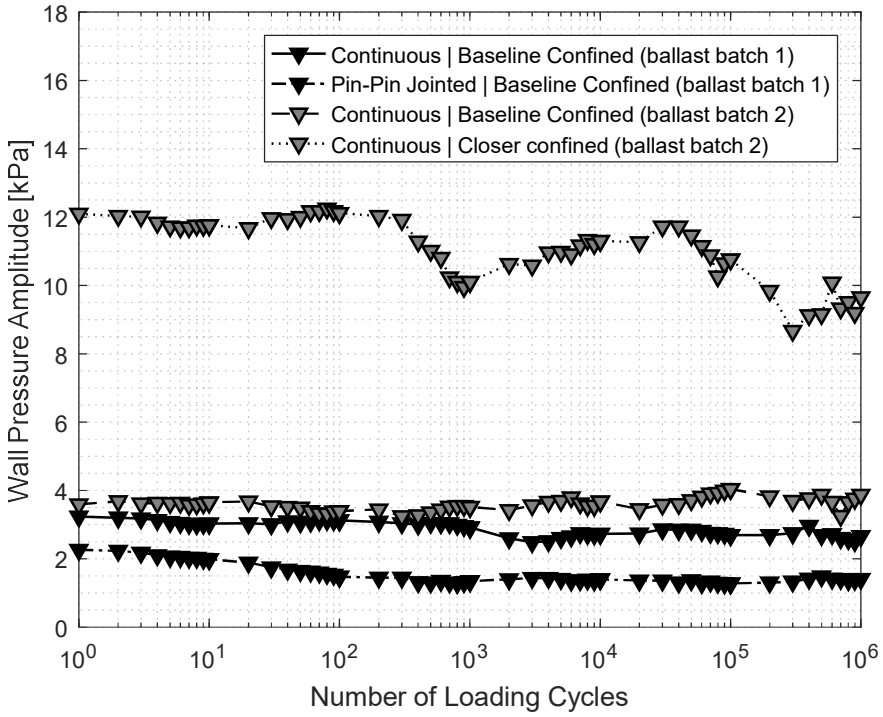

Figure 87 Variation in amplitude of pressure on the confining wall for 10^6 loading cycles

5.4.3 Vertical stress

Vertical stress under the ballast was measured adjacent to the rails and middle of the rails to give an indication of the trend in vertical stresses transferred to beneath the ballast.

Data were recorded for 6 mins at 6 hours intervals for the duration of the tests. Due to a technical issue, some tests are missing data for pressures under the middle of the loaded rails and early data points in some tests are also missing.

Figure 88 shows the distribution and evolution of maximum vertical stress under the ballast beneath both rails and the middle (see Figure 37 in Section 4.5), for the short bearers with and without the joint as well as with a USP, and with the ballast shoulder confined. It may be seen that the vertical pressures varied between tests. This is possibly due to a combination of the small soffit area of the pressure plates (which resulted in small number of contacts per plate) and limited depth of the ballast (about 8 grains at 40 mm per grain) to distribute the stress through, combined with variation in ballast stress routes and nonuniform distribution of force chains as shown by DEM work (Li & McDowell, 2020) . Albeit the pressure under the left-hand rail was mostly greater than that on the right for all the tests.

On the continuous bearer, pressures under the left-hand rail decreased with continuous loading, while those under the mid- and right-hand rails generally increased as the centre-binding took effect. With the USP, pressures were more uniformly distributed, increasing towards the left end, i.e., the highest pressures were under the left-hand rail followed by the middle then the right-hand rail. The difference in pressures was significantly reduced when the ballast shoulder was confined, and pressures remained constant with number of loading cycles. The variation in pressures under the rails of the baseline pin-pin jointed bearer was less than under its continuous counterpart. However, with the confinement of the ballast shoulder, there was an increase the variation in pressures under the loaded rails.

Maximum pressures under the long continuous bearer show less initial variation than under the short continuous bearer (Figure 89). Pressures under the left-hand rail decrease after 10^3 loading cycles while those under the middle increase significantly increase. Pressures under the right-hand rail also increase but to a lesser degree.

Pressure variation and intensity was clearly influenced by the location of both the rigid and pin-pin joints, as the difference between the pressures under the rails on the bearers with joint beside the loaded rails is significantly smaller than for those with the joint between the loaded rails. Pressures under the long pin-pin jointed bearer remained constant up to 10^5 cycles, then

decreased at both ends. This effect was particularly clear on the long pin-pin jointed bearer because the load on the loaded segment was central, and the centre-binding effect was reflected in the equal decrease in pressure under both loaded rails.

Table 6 presents the average vertical stress under the ballast for the different tests. The expected vertical stress is calculated by accounting for the weight of the loading beam, bearer and ballast, and the maximum load exerted by the loading ram. By assuming that the load is spread at a distribution angle of 45° to 60° to the floor under the bearers, the expected average vertical stress was 66 kN to 78 kN, respectively. On average the measured mean vertical stress under the ballast was closer to the expected average calculated assuming distribution angle of 60°. It can be noted that the vertical stress is higher under the left shoulder rail followed by middle of the rails and least under the right rail. This is potentially due to the non-uniform load distribution characteristic of the eccentric bearer setup.

Table 6 Average vertical stress under the ballast

Bearer Type	Left Shoulder Rail Average [kN]	Right Inner Rail Average [kN]	Rails Mid Average [kN]	Total Average [kN]
Short Continuous	99.82	64.69	42.47	68.99
Short Pin-Pin jointed	99.74	47.04	-	73.39
Short Continuous USP	113.30	40.62	61.57	71.83
Short Pin-Pin USP	103.6	67.16	88.27	86.34
Short Continuous Confined	61.50	53.29	71.48	62.09
Short Pin-Pin Confined	103.90	41.26	107.60	84.25
Long Continuous	99.62	68.01	98.23	88.62
Long Rigid Jointed	70.98	57.62	42.61	57.07
Long Pin-Pin Jointed	77.24	72.35	-	74.80
Short Rigid Joined	124.60	55.64	-	90.12
Total Average	95.43	56.77	73.18	**75.12**
Calculated Average (45°)	-	-	-	**66**
Calculated Average (60°)	-	-	-	**78**

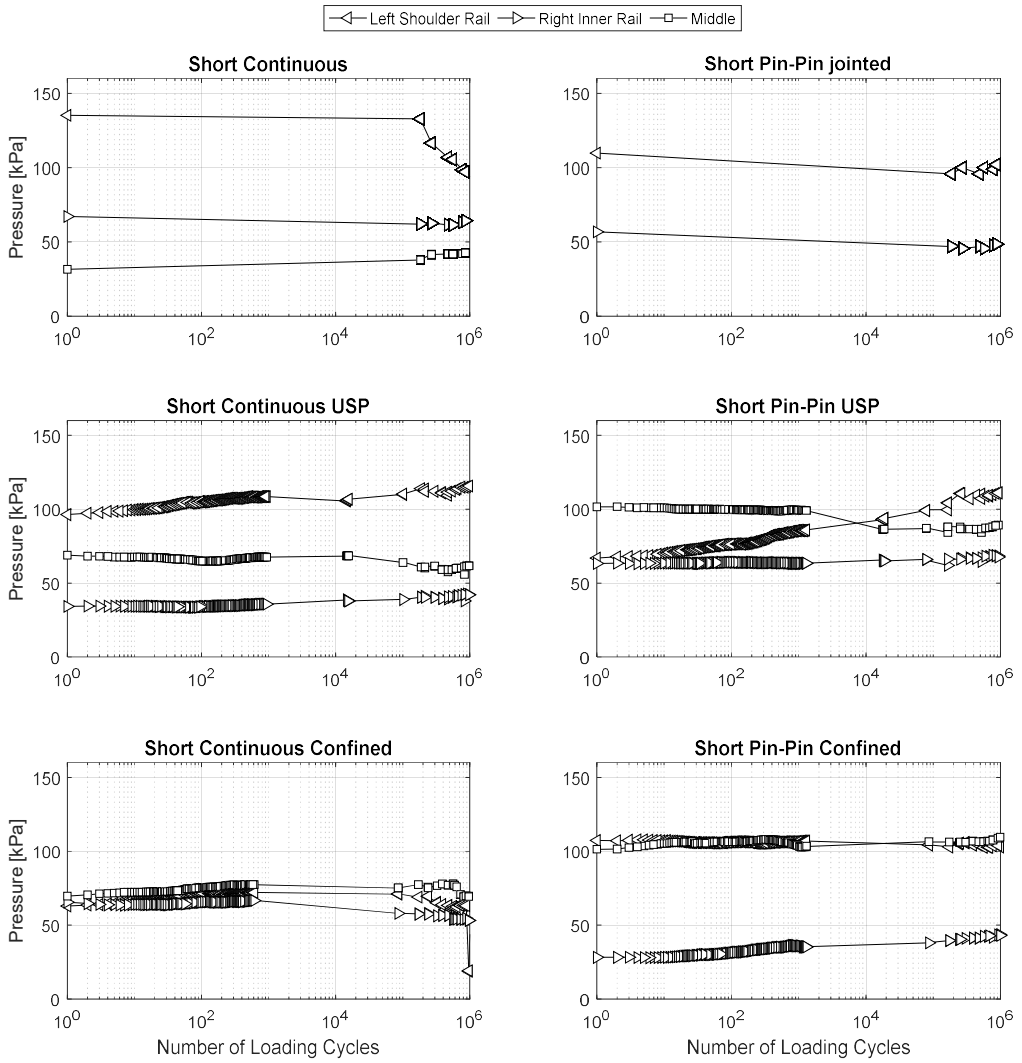

Figure 88 Maximum vertical pressures under the ballast at key locations for the baseline short continuous and pin-pin jointed bearer and with USP and under confined shoulder setting.

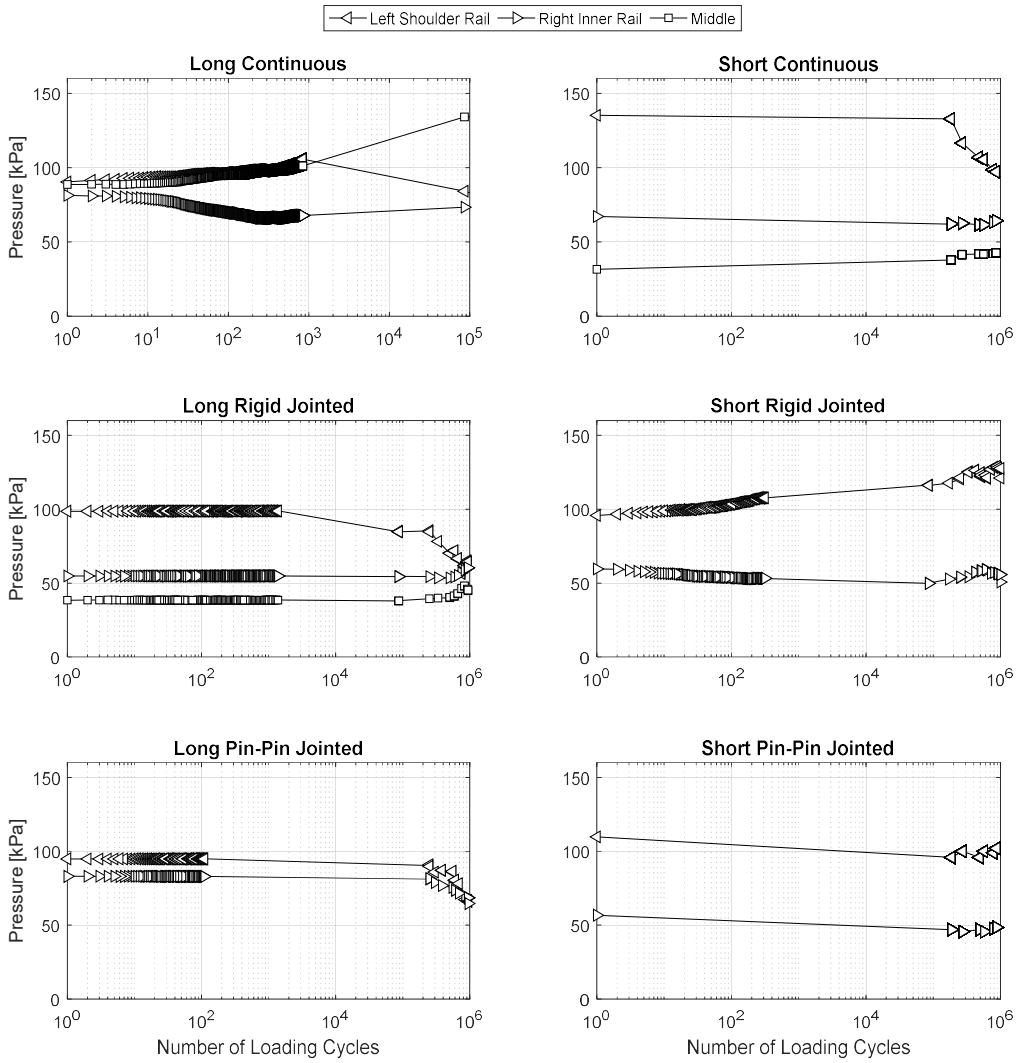

Figure 89 Maximum vertical pressures under the ballast at key locations comparing the long and short continuous bearer and the effect of joint location on the distribution and evolution of vertical pressures – the long bearers have the joint aside the running rails whilst the short bearers have it between the running rails.

5.5 Bearer-ballast contact area

The cumulative bearer/ballast contact areas at key locations i.e., below, and middle of the rails and the bearer ends were measured using pressure sensitive paper. Two types of pressure sensitive paper were used, sensitive to pressures greater than 2.5 MPa and 10 MPa. Scanned images of the bearer/ballast contact areas are presented, and the percentage of contact area is quantified.

A summary of the contact areas at key locations and their average, for all of the tests carried out, is presented in Table 7. It shows that contact area increases towards the bearer shoulder end in all cases.

Bar charts showing the distribution of contact area at key locations on the bearers are presented in Figure 90 - 92. These are organised so that:

- the short continuous bearer test and its repeat are presented in Figure 90.
- the short continuous bearer with USP and short continuous bearer with the ballast shoulder laterally confined is shown in Figure 91.
- the short continuous bearer with bearers utilising various types of joints in the middle of the loaded rails is presented in Figure 92.

Figure 90 for the continuous short bearer shows that the contact area was the highest under the left-hand rail towards the ballast shoulder and lowest at the right-hand end, furthest from the loaded rails. The loaded rails were associated with a larger contact area than at the middle of the rails.

Figure 91 shows that the variation in contact areas along the length of the bearer reduced with the confinement of ballast shoulder and there was also an increase in the contact area compared with continuous bearer baseline tests. The use of a USP significantly increased the contact area. The inclusion of a joint in the middle of the rails also increased the contact area as shown in Figure 92.

*Table 7 Percentage (%) of ballast in contact with the bearer at key locations on the bearer-ballast interface accumulated over 10^6 loading cycles, measured using medium [10 MPa] pressure paper, * Tests conducted using ballast batch 2*

Category	Test Name	Average Area [%]	Right End [%]	Right Rail [%]	Joint Right [%]	Rail Mid [%]	Joint Left [%]	Left Rail [%]	Left End [%]
USP	Continuous	14.5	2.82	7.15		16.28		23.29	22.86
	Jointed	14.2	1.16	9.88	17.23		11.53	19.46	25.78
Baseline Continuous	Short (Repeat)	0.7	0.17	0.97		0.47		1.34	
	Short*	4.4	0.96	1.77		1.47		4.64	13.28
	Long (Repeat)	1.9	0.26	1.04		1.81		1.89	4.26
Shoulder Confinement	Continuous	1.7	0.92	2.42		1.40		2.26	1.68
	Continuous*	1.3	1.31	0.83		0.50		2.33	1.76
	Continuous (closer confinement)	2.7	3.15	0.96		2.56		2.30	4.32
	Short Jointed	0.8	0.23	1.13	0.94		0.81	0.02	1.93
Short Jointed	Rigid (Repeat)	1.2	0.23	0.63	1.74		0.89	1.74	2.08
	Pinned	2.3	1.05	2.12		1.31		2.07	4.79
	Flexible	0.9	0.09	0.61		0.46		2.51	
Long Jointed	Continuous	1.7	0.15	0.78		0.96		2.25	4.26
	Rigid	2.3	0.26	1.18		1.31		3.31	5.57
	Pinned	2.6	0.52	2.06		1.53		2.50	6.39

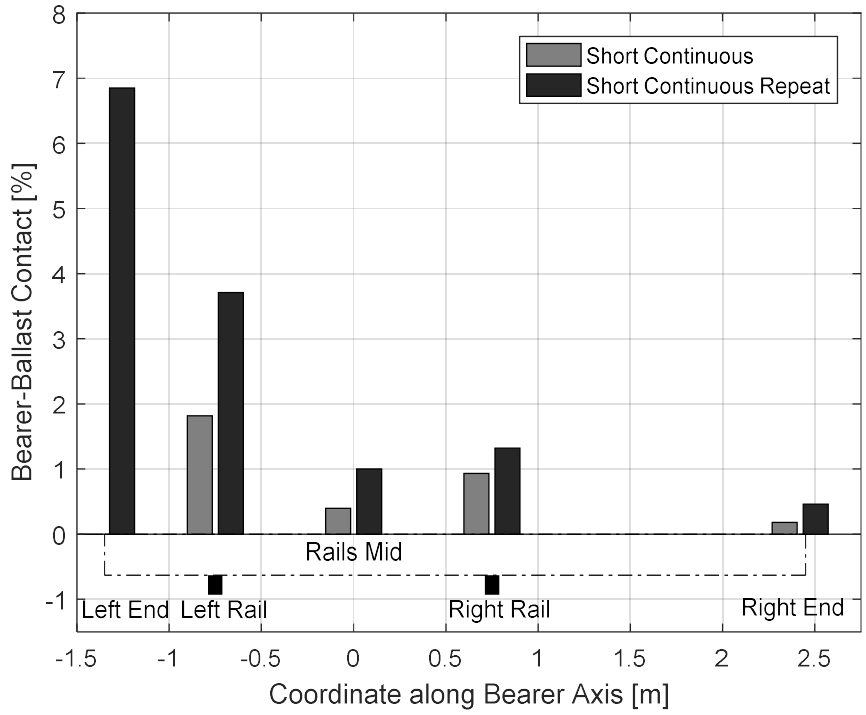

Figure 90 Bar chart showing the distribution of accumulated contact area (as fraction of overall area in the region) over the short bearers with both ranges of ballast.

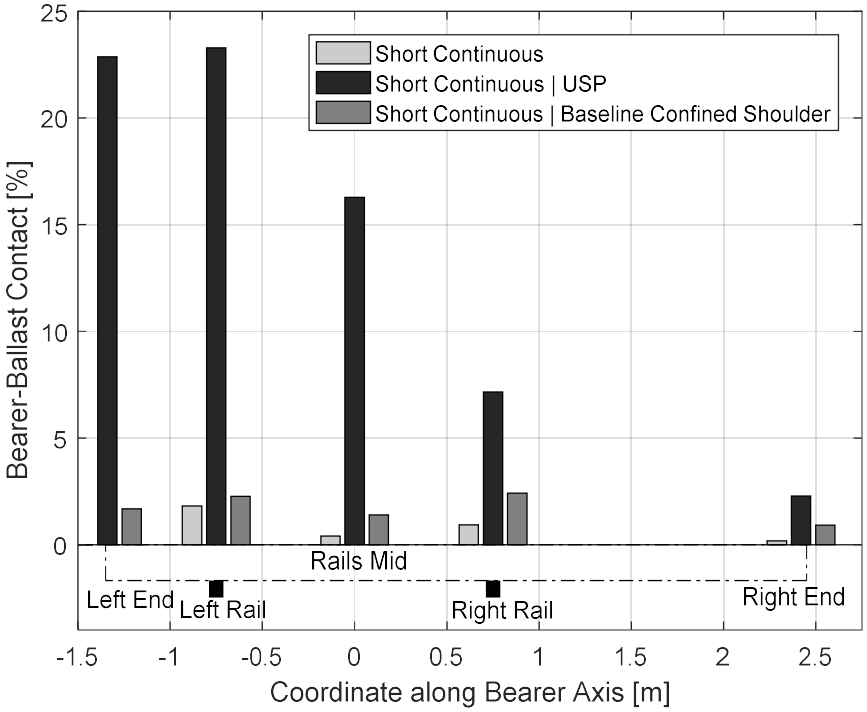

Figure 91 Bar chart comparing the distribution of contact area (as fraction of overall area in the region) over the short bearers with USP and Confined Shoulder.

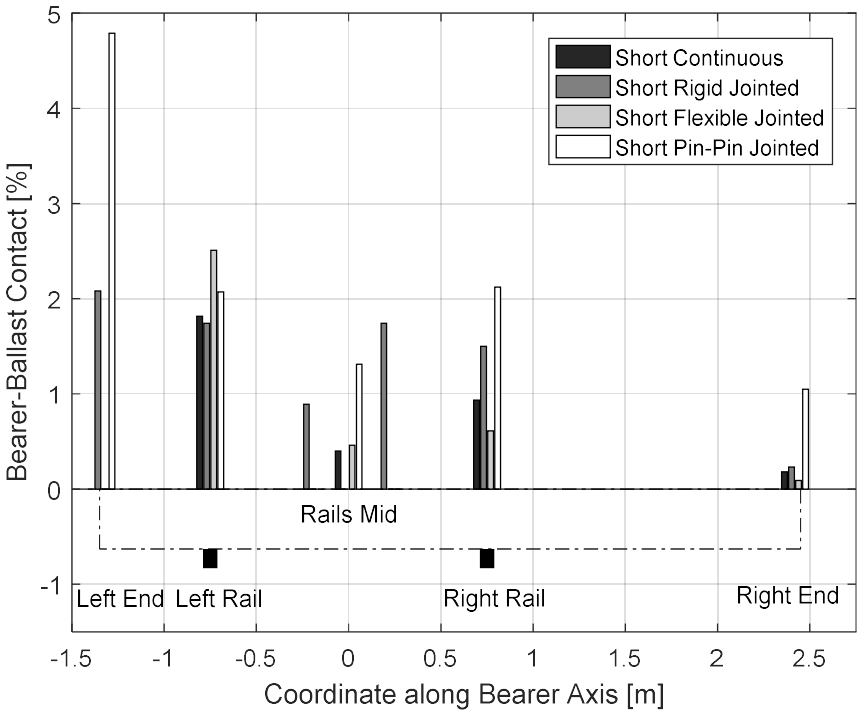

Figure 92 Bar chart comparing the distribution of contact area (as fraction of overall area in the region) over the short continuous bearer with jointed bearers of varying rigidity.

The use of USP significantly increased the ballast/bearer contact area. However, there was little difference in the permanent settlement response and a significantly higher resilient deflection along the length of the bearers utilising USP. The presence of a joint within the bearer resulted in increased contact area and higher permanent settlements. Confinement of the ballast shoulder resulted in increased contact area compared with the baseline test, with the highest contact area under the loaded rails owing to improved ballast support.

While an increase in contact area could improve the load distribution and reduce permanent settlement, in the case of long bearers that are subjected to eccentric loading the ballast contact area had little effect on the permanent settlement. This was because settlement of those bearers was due to the movement of the unconfined ballast shoulder.

6 Ballast Support Interventions

This chapter presents results from tests that included the modification of the ballast support conditions towards the end of the tests, to replicate differential ballast support and investigate its impact on the permanent and resilient deflections of the underlying ballast, the resulting strains developed in the bearer joint and the sidewall pressures.

6.1 Introduction

Intervention tests were carried out to assess the performance of the jointed bearers on (a) the failure of one or more of the bolts on the metal shroud joining the two bearer segments together; (b) where the ballast under the shorter segment is looser than under the right-hand (inner) joining segment; and (c) where the ballast under the joint is looser than under the rail. A list of these tests is presented in in Table 8.

Table 8 List of intervention tests carried out on the short rigid jointed bearer

Test	Loading cycles	Notes
s0	1.2M	Rigid joint in optimal conditions
s1	50000	Inner left bolt pair removed
s2	250000	Inner left and right bolt pair removed
s3	250000	Shorter bearer unbolted- joint attached to longer bearer part
s4	350000	Joint completely unbolted
s5	130000	Loose ballast under the shorter bearer part
s6	300000	Loose ballast under the joint in the middle of the rails

The failure of bolts was replicated simply by sequential loosening/removal of the bolts on the metal shroud joint (s1 to s4). Differential ballast support along the length of the bearer was replicated by lifting the bearer to restore the crosslevel and packing fresh ballast under the shorter segment of the jointed bearer (s5) and under the joint between the rails (s6).

These tests were continued after the completion of 1.2M loading cycles in baseline conditions (i.e., with the bolts in their optimum condition, torqued to 340 Nm as per NR specification). After 2.1M loading cycles, the ballast under the shorter segment of the jointed bearer towards the ballast shoulder was re-laid and the bearer returned to its original vertical position, whilst ballast under the loaded rails remained compacted from prior loading. This was done to replicate conditions where the track has become compacted (e.g., due to traffic on partially installed modular S&C) on one side of the joint only, or where only the region under the shorter bearer segment (close to the ballast shoulder, susceptible to higher settlement) has been tamped.

The case of replacement of a broken joint and repacking of ballast around the new joint was replicated in Test s6.

6.2 Sequential loosening of bolts

Figure 94 and Figure 95 present the settlement and resilient deflections along the length of the rigidly jointed bearer at the key stages (s1 to s4), respectively, as described in Table 8 and shown schematically in Figure 93. Figure 96 shows the corresponding longitudinal pressures under the rails.

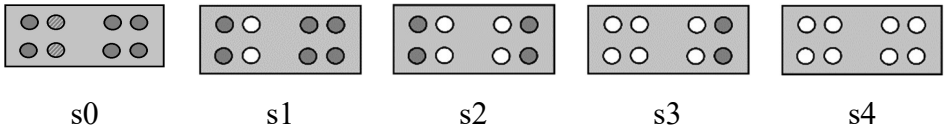

Figure 93 Illustration of sequential bolt removal, white circles representing bolts that were removed

Stages s1 to s4 totalled 900,000 loading cycles in addition to the 1.2M loading cycles initially carried out at the point when the bolts were loosened. The rate of settlement was expected to reduce with increasing number of loading cycles; however, on sequential loosening of the bolts, the additional 900,000 loading cycles gave a similar rate of settlement to that when the bearer was initially loaded with freshly laid ballast. It is thought that the decreased joint stiffness due to the loosened/removed bolts caused the higher rate of settlement apparent in Figure 94.

The resilient deflection shown in Figure 95 is also significantly affected by the various stages of the bolt removal process. The hogging state in s0 changes to sagging in s2. In s3 and s4 the two segments of the bearer are effectively separated and the joint acts like the pin-pin jointed bearer.

Longitudinal pressures in Figure 96 shows that the general trend remains constant under the right-hand rail and decreasing under the left-hand rail which reduced abruptly at each bolt removal stage. This is possibly due to the changing pressure distribution characteristics of the jointed bearer segments with the removal of bolts.

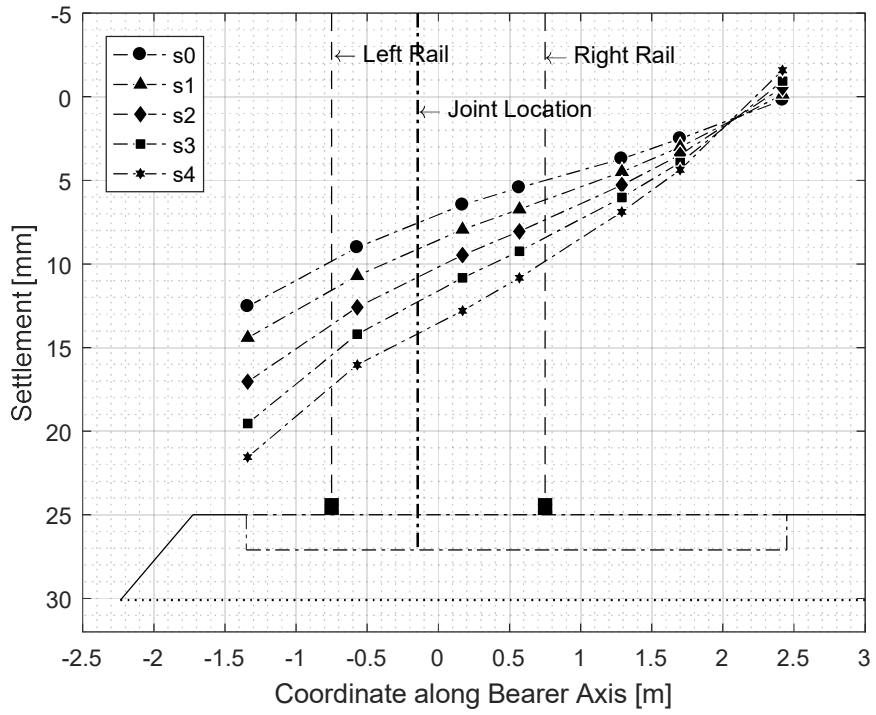

Figure 94 Evolution of settlement along the length of the rigid jointed bearer subjected to sequential removal of bolts on the metal shroud joint (s1 - 4)

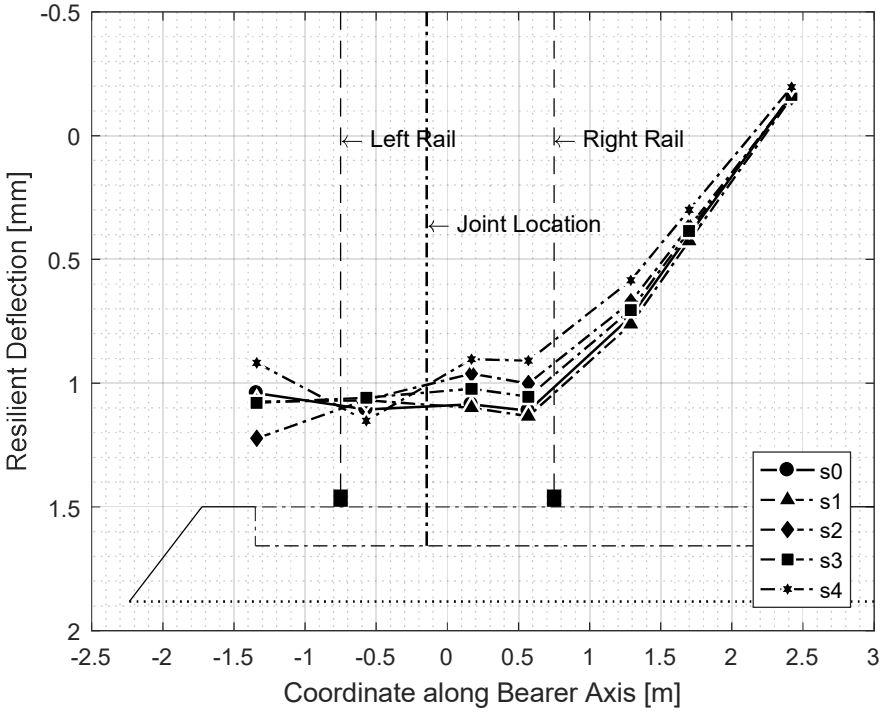

Figure 95 Evolution of resilient deflections along the length of the rigid jointed bearer subjected to sequential removal of bolts on the metal shroud joint (s1 - 4)

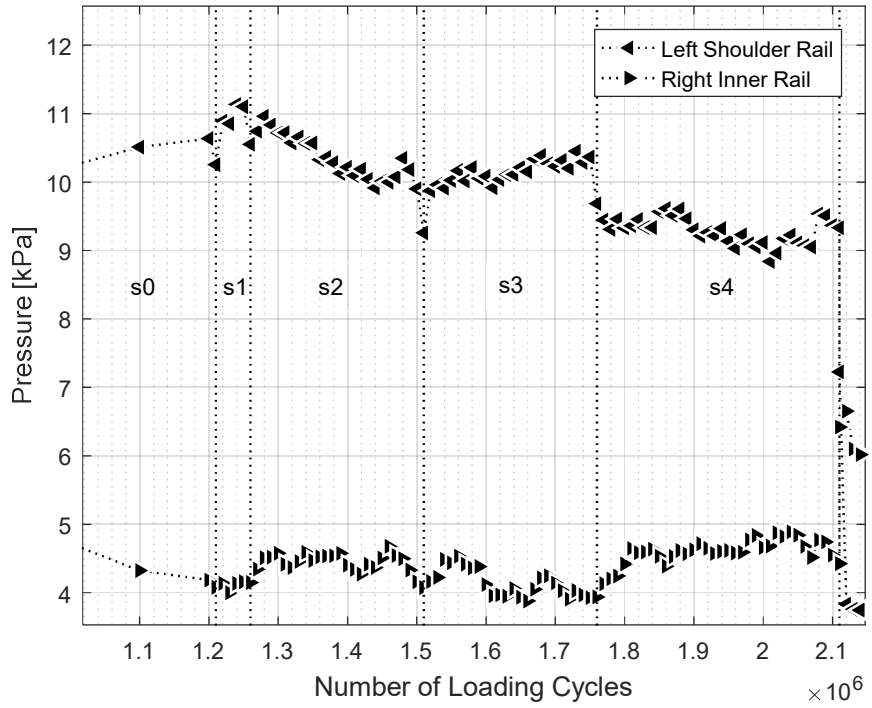

Figure 96 Longitudinal pressures measured over sequential bolt removal off the rigid jointed bearer

6.3 Differential ballast support

Figure 98 presents the permanent settlement under the length of the short rigid jointed bearer in s5 and Test s6 shown schematically in Figure 97. Ballast settlement under the left-hand rail on the shorter segment of the bearer is significantly greater than under the right-hand rail on the longer segment of the bearer away from the ballast shoulder (Figure 98). Overall, the fresh ballast under the left-hand (shorter) bearer segment settled approximately four times the amount in the baseline test.

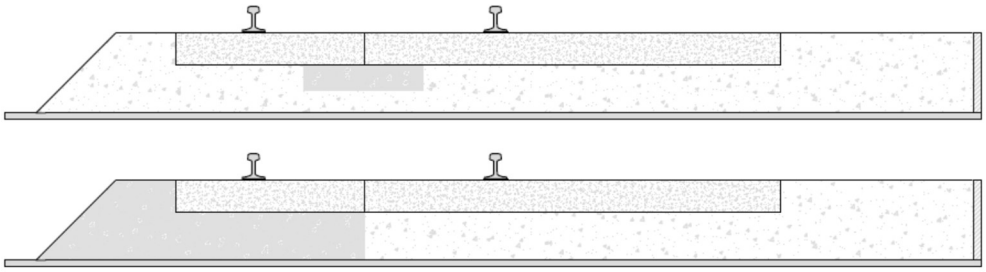

Figure 97 Illustration of differential support under the Joint (Top) and under the short bearer part (Bottom), where the shaded area represents refreshed ballast

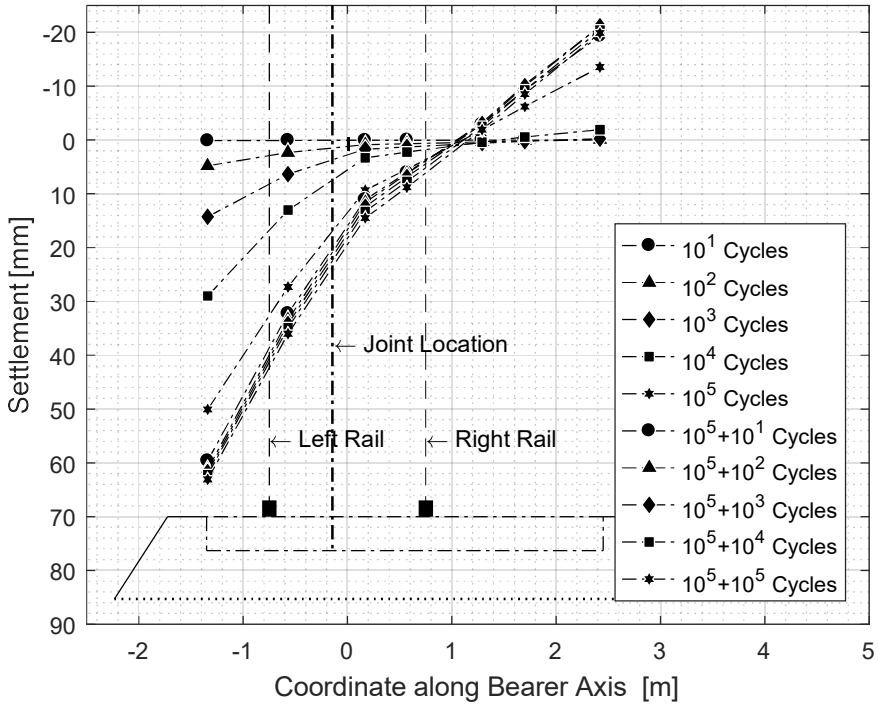

Figure 98 Evolution of settlement along the length of the rigid jointed bearer subjected to differential ballast support (first five lines represent s5 and subsequent five lines represent s6)

Figure 99 and Figure 100 present the resilient deflection along the length of the short rigid jointed bearer at selected numbers of loading cycles in s5 and s6, respectively. The resilient deflections were more pronounced, with peak deflections greater than the baseline, Also, the onset of the change in bending state from sagging to hogging was much earlier owing to the higher settlement seen in Figure 98, particularly under the shorter bearer segment. In the case of fresh ballast under the joint in s6, resilient deflections were significantly increased at both ends of the bearer, and the bending state remained hogging throughout the loading cycles. However, the resilient deflections decreased with increasing number of loading cycles as the freshly laid ballast under the joint settled.

Figure 101 and Figure 102 show the variation in longitudinal pressure under both rails as a function of the number of loading cycles in s5 and s6, respectively. In Figure 101, the ballast compressive stresses increase up to 10^3 loading cycles; there is then a sharp fall in pressure under the left-hand rail. This is synonymous with the change resilient deflection at the same loading cycle in Figure 99, when the bearer began to bend in a sagging state. As pointed out earlier, this was related to the formation of a gap at the ballast-bearer interface, which could also be the cause the reduced ballast compressive stresses observed in Figure 101.

Figure 102 shows that the ballast compressive stresses in s6 tend to increase under both rails with increasing number of loading cycles. This can be linked to the resilient deflections seen Figure 100, which decreased on both sides of the joint (under the rails). Ballast support improved with decreasing resilient deflections, as also reflected in the increasing longitudinal pressures.

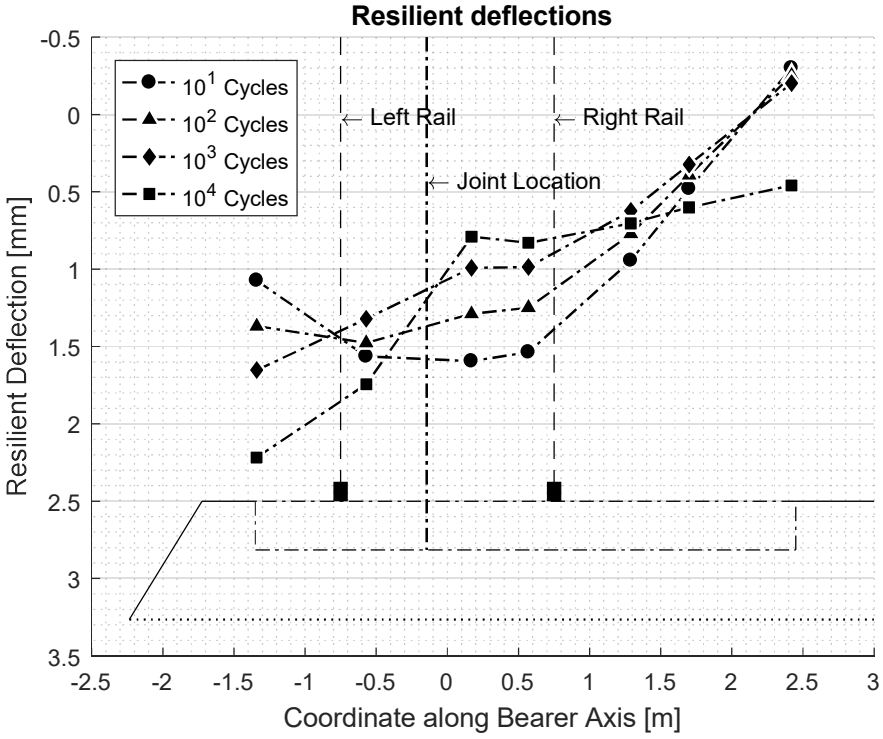

Figure 99 Evolution of resilient deflections along the length of the rigid jointed bearer subjected to differential ballast support under shorter segment of the bearer (s5)

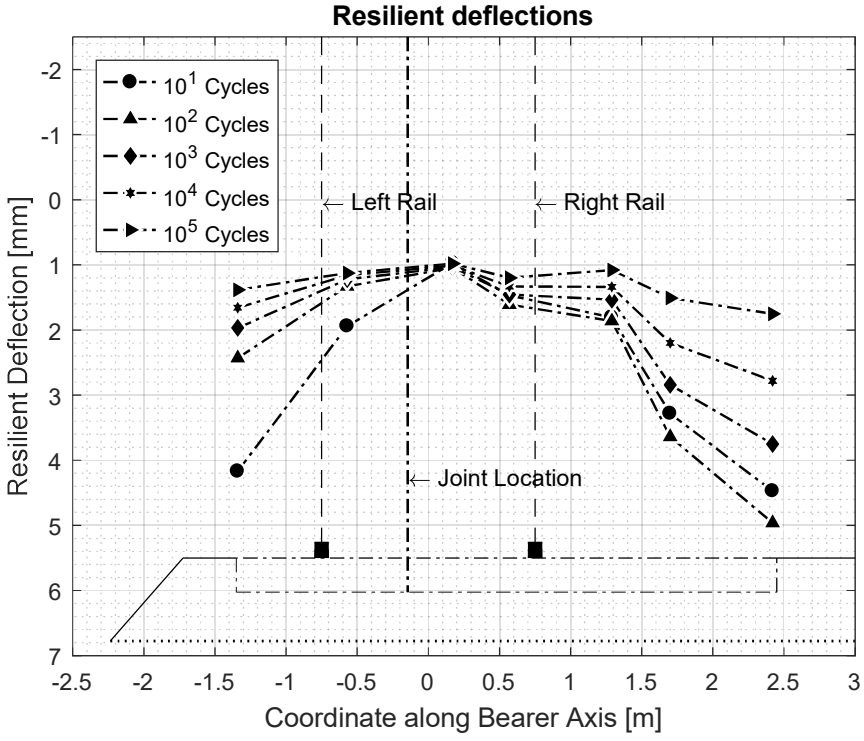

Figure 100 Evolution of resilient deflections along the length of the rigid jointed bearer subjected differential ballast support under the joint (s6)

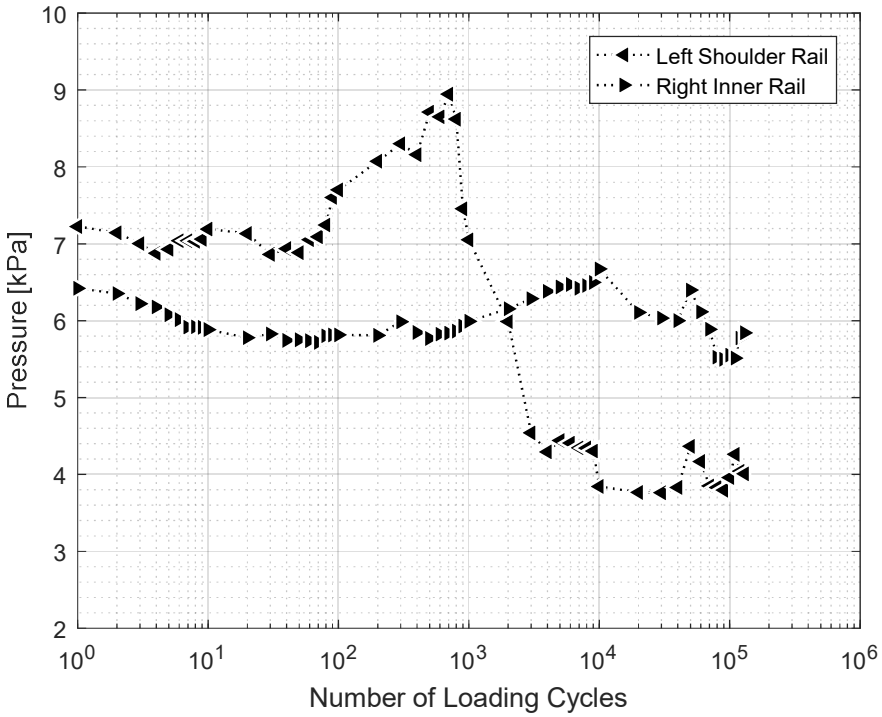

Figure 101 Longitudinal pressures measured during test s5

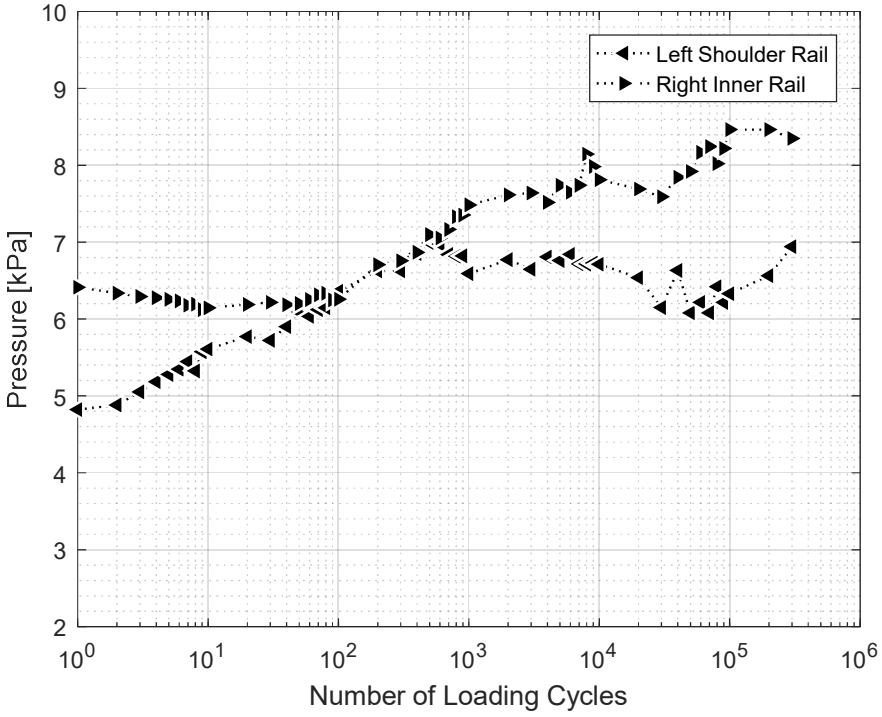

Figure 102 Longitudinal pressures measured during test s6

6.4 Strains on the metal shroud joint

Results from strain gauges installed at selected locations on the metal shroud joint ('rigid joint') were analysed to assess the impact of the interventions listed in Table 8. Figure 103 shows the recorded microstrains at the key locations during the first applied load cycle, shown in the schematic included within the figure. Positive values indicate extension and negative values indicate compression. The microstrains recorded in s5 were larger, and those in s6 significantly larger, than in the baseline test s0. In s6 the locations that were in compression in the other tests had changed to extension and vice versa. This was due to the bearer bending in sagging initially in s5 (Figure 99), but in hogging in s6 (Figure 100).

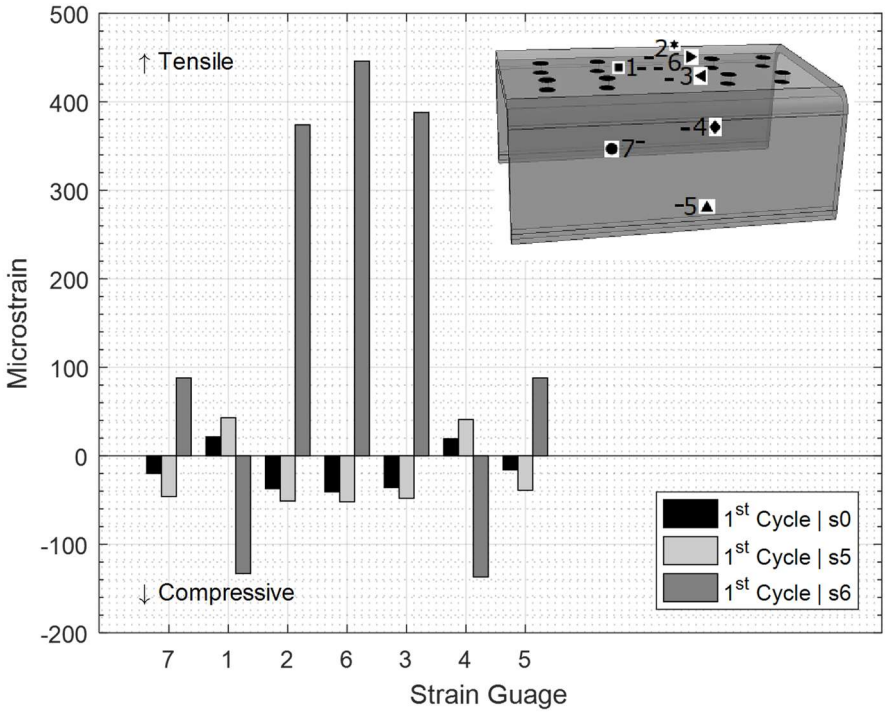

Figure 103 Bar chart showing microstrains measured over the first loading cycle on s0 (baseline conditions), s5 (ballast under the jointed segment closer to the ballast shoulder fresh and relatively loose), s6 (ballast under the joint fresh and relatively loose)

Figure 104, Figure 105 and Figure 106 present the strains at key locations on the rigid joint over the course of the baseline test s0, differential support test s5 and differential support test s6, respectively.

Strains on the joint on the bearer subjected to differential support (Figure 105) remained like the case of the baseline test (Figure 104) which was uniform in the short term (10^2 loading cycles). These strains changed from compressive to tensile and vice versa, in the long term due to the change of bearer bending state from sagging to hogging. Such changes were more evident in the case of the bearer subjected to differential support with a clear shift in the from compression to extension and vice versa. The trend in strains agree with the change in bending state apparent on the resilient deflections of the bearer. The higher magnitude of strains in the long-term correlate with the large peak deflection of the bearer (see Figure 99). This is explained by the significantly large permanent settlement of the bearer segment towards the ballast shoulder where the ballast was less compacted owing to re-laid ballast in the region (Figure 98).

In the case of re-laid ballast under the joint, resilient deflections of the bearer showed significantly large degree of hogging (Figure 100) which was reflected in the strains on the joint within the bearer (Figure 106). Large magnitude of strains in the early stages of loading cycles steadily decreased in the long term. This happened as the peak deflection of the bearer decreased with continuing loading cycles. The re-laying of ballast under the joint replicated an exaggerated case of centre-binding, where the level of ballast under the joint was higher than surrounding regions such as under either loaded rails. Ballast under the joint compacted with accumulating loading cycles causing a decrease in ballast level variations hence a decrease in peak deflections and hence decrease in magnitude of strains on the joint.

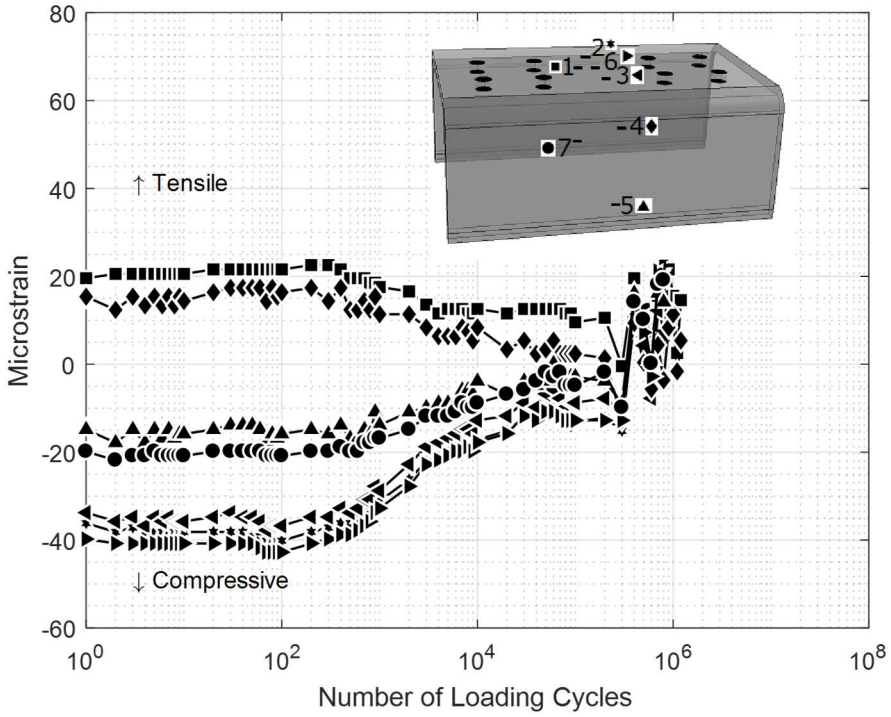

Figure 104 Strains (Microstrains) measured over the loading cycle on s0 (joint and ballast in baseline conditions) when the load is maximum (98 kN)

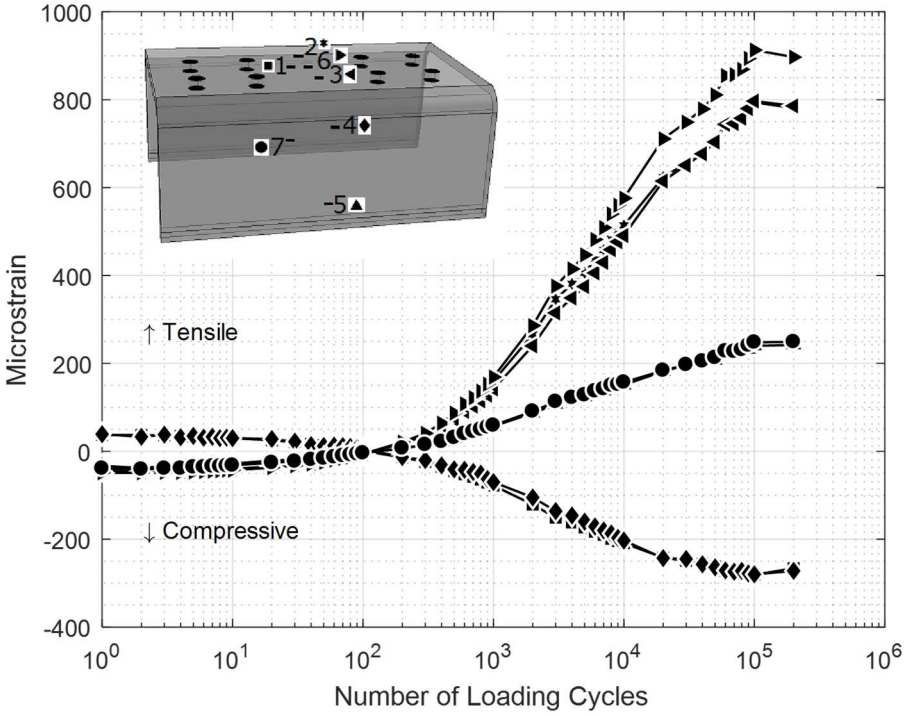

Figure 105 Strains (Microstrains) measured over the loading cycle on s5 (ballast under the jointed segment closer to the ballast shoulder loosened) when the load is maximum (98 kN)

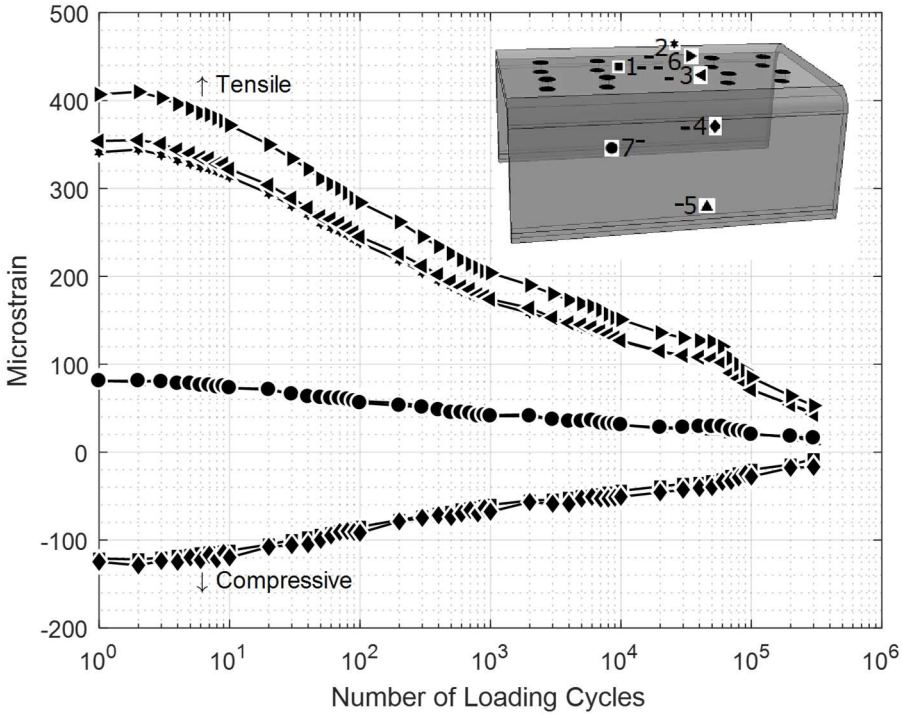

Figure 106 Strains (Microstrains) measured over the loading cycle on s6 (ballast under the joint loosened) when the load is maximum (98 kN)

6.5 Summary

This chapter summarised tests replicating differential ballast support scenarios, in which the ballast under one part of the joined bearer was re-laid and looser than under the other; ballast under the joint was re-laid; and bolts on the joints were degraded sequentially.

Looser ballast under the jointed segment of the bearer closer to the ballast shoulder resulted in significantly larger ballast settlement compared with its baseline counterpart. This was accompanied by a change in bending state of the bearer which shifted from sagging to hogging beyond 10^3 loading cycles. The decrease in sidewall pressures under the left-hand rail at 10^3 loading cycles corresponded with the change in bending state of the bearer which was likely due to the poor ballast support. This behaviour is explained by the changing ballast support, as the ballast under the length of the bearer closer to the ballast shoulder permanently settled, the bearer-ballast contact shifted away from the bearer end. This caused the bearer to bend in a hogging state with compacted ballast in the region between the loaded rails offering reaction force. The change in bending state of the bearer was accompanied by shift in strains on the joint from compressive to tensile.

Loose ballast under the joint did not affect the permanent settlement, but resilient deflections were clearly affected. Vertical resilient deflections were sagging in the short term and remained

so in the long term, with a decrease in peak deflection owing to compaction of the mass of ballast under the joint. Compaction under the joint reduced the variation in ballast level between that under the joint (located between the loaded rails) and the loaded rails. This resulted in the strains in the joint to decrease in magnitude with increasing number of loading cycles as the peak deflection also decreased.

Results suggest that joint between the loaded rails experiences large strains depending on the nature of ballast support at a given stage of the loading cycles. Centre-binding of the bearer was worsened by permanent settlement under the bearer end. Centre-binding was indicated by hogging of the bearer with large peak deflections in the middle of the loaded rails. These induced large strains in the joint which could be detrimental to the integrity of the joint itself. This highlights the importance of minimising both the variations in resilient deflections along the length of the bearer and with increasing loading cycles.

7 Three-point Bending Tests and FE Modelling of the Jointed Metal Shroud Bearer – Results and Discussion

This chapter presents results obtained from comparative three-point bending tests performed on a continuous and a jointed bearer in both sagging and hogging states. A finite element model of the jointed bearer in three-point bending conditions was created to study the stresses within the bolts and the influence of spring stiffness, bolt load and rubber pad stiffness on maximum deflection of the bearer.

7.1 Flexural rigidity of jointed bearers

Figure 107 presents deflection curves obtained via LVDTs in contact with the bearer jointed via the bolted metal shrouded joint torqued to two different levels, i.e., 320 Nm and 340 Nm, subjected to three-point bending in the sagging state (+ve bending). It reveals the maximum deflection of the jointed bearer in both cases and presents a comparison with the bearer without a joint. Increasing bolt torque from 320 Nm to 340 Nm (6.25% increase) yielded 10% decrease in the maximum deflection. The jointed bearer showed significantly reduced flexural rigidity as the maximum deflection was dramatically higher than its unjointed counterpart.

Figure 108 presents a comparison of the deflection curve obtained for the continuous bearer with that of the jointed bearer, both in hogging state (-ve bending) subjected to three-point bending. It is clear from the results that the flexural rigidity of the jointed bearer is higher in hogging than in sagging (9 mm in sagging vs 4.7 mm in hogging).

When two bearer segments having an Elastic Modulus, E and Second Moment of Area, I are tied via a mechanical joint of stiffness, k_θ and simply supported with a spanning distance of length, L, are centrally loaded by P, we arrive at Equation 1 for its maximum deflection, Δ_{max}. Rearranging this equation for k_θ is presented in Equation 2. Full detail is given in Appendix 1.

$$y = \Delta_{max} = -\frac{PL^3}{48EI} + \frac{PL^2}{8k_\theta} \qquad \text{Equation 1}$$

$$k_\theta = \frac{PL^2}{8y + \frac{PL^3}{6EI}} \qquad \text{Equation 2}$$

$$E = \frac{PL^3}{48\Delta_{max}I} \qquad \text{Equation 3}$$

Table 9 Values used to obtain Young's Modulus of the continuous reinforced concrete bearer using equation for a simply supported beam to be used in FE model

Parameter [Unit]	Value
W [kN]	32.75
L [m]	1.5
Δ_{max} [m]	0.00028
I [m^4]	1.64E-04

Using Equation *3* and parameters in Table 9, the Elastic Modulus, E of the concrete bearer was calculated to be 50.1 GPa for use within the ABQUS model. Using Equation 2, the rotational stiffness k_θ of the joint is 1.e^6 Nm/rad.

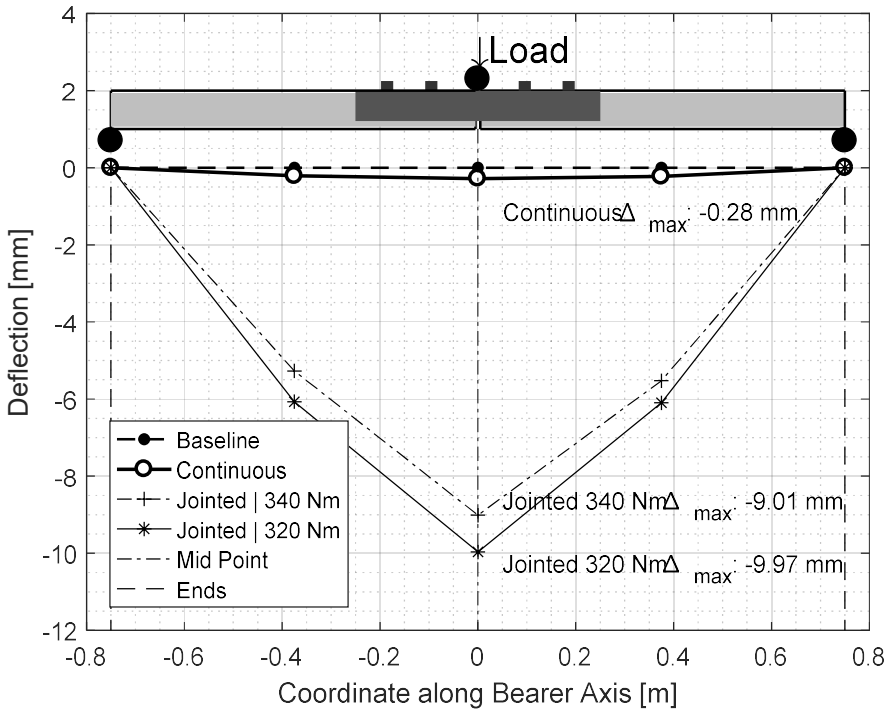

Figure 107 Deflection graph for jointed bearer bend via three points (Load = 35 kN) in a sagging state with the rigid joint bolted to 320 Nm and 340 Nm, and continuous bearer showing the maximum deflections at the applied load, showing the effect of torque on maximum deflection

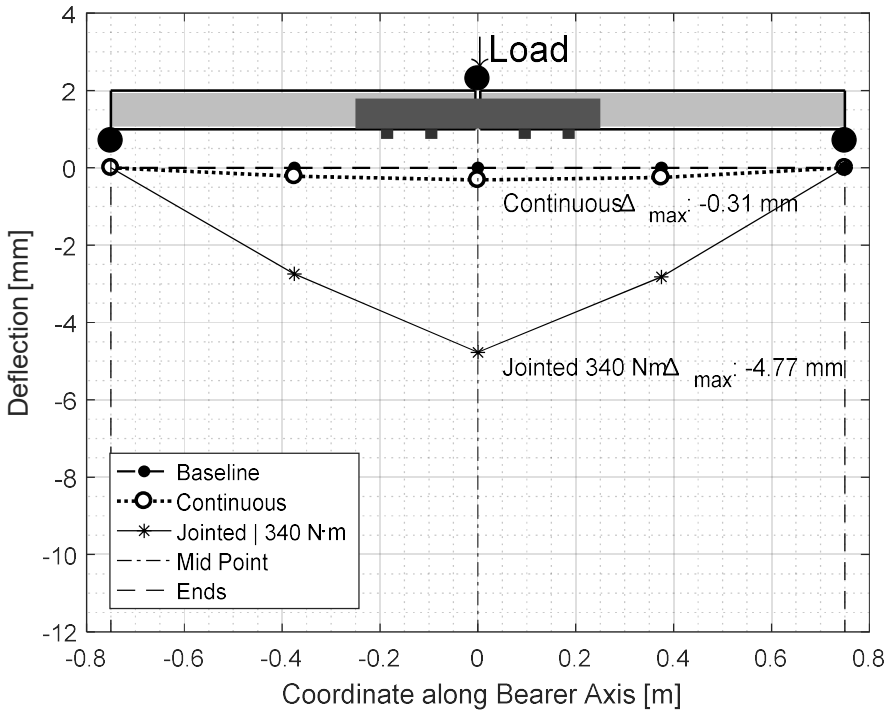

Figure 108 Deflection graph for jointed bearer bend via three points (Load = 35 kN) in a hogging state with the rigid joint bolted to 340 Nm, and continuous bearer showing the maximum deflection at the applied load

Previous chapters have shown that bearer resilient deflections change significantly with increasing loading cycles. The dependence of the jointed bearer bending stiffness on its bending state (i.e., sagging or hogging) implies that the system stiffness of the S&C will vary with increased loading cycles as bearer deflections change from sagging to hogging.

The previous chapter showed how spatial variations in ballast support under the bearer impact bending strains in the joint. A hogging state induced by centre-binding will exacerbate such strains and could compromise the bolt fasteners.

The significant decrease in bending stiffness of the jointed bearer relative to the continuous bearer suggests that, in the case of combined usage on an S&C, it is important to consider the influence of bearer bending stiffness on system stiffness.

7.2 Results (FEA) and analysis/discussion

7.2.1 Continuous bearer

Static analysis is carried out in ABAQUS. The continuous bearer was modelled with the geometry described earlier and material properties of the assembly parts are presented in Table 10. The element type was Linear Hexahedron, type C3D8R. The applied load was 35 kN at the centre via a thin strip of thickness 1 mm to mimic the contact made by the primary roller in the experimental setup. Boundary conditions were applied at the bottom rollers (y = 0) and at the primary roller (z = 0), to ensure the load was applied only in the vertical, y axis.

Table 10 Material properties used withing the finite element model of the bolted metal shrouded jointed bearer and continuous bearer assembly in three-point bending conditions

Material	Stiffness [GPa]	Poisson's Ratio
Concrete (bearer)	50.1	0.2
Steel-1 (bolts, shrouded joint)	200	0.3
Steel-2 (double coil spring washer)	1	0.3
Nylon 66 (dowel)	3	0.4
Rubber bonded cork (pads)	0.1	0.45

Figure 109 presents a comparison of the deflection curve for the continuous bearer under three-point bending obtained from both the laboratory test and the ABAQUS model. Figure 110 shows the vertical displacement as a contour plot. The deflection curves are in good agreement with a difference of about 4.5% between the maximum deflection of the beam in laboratory setting to the that obtained from the FEA.

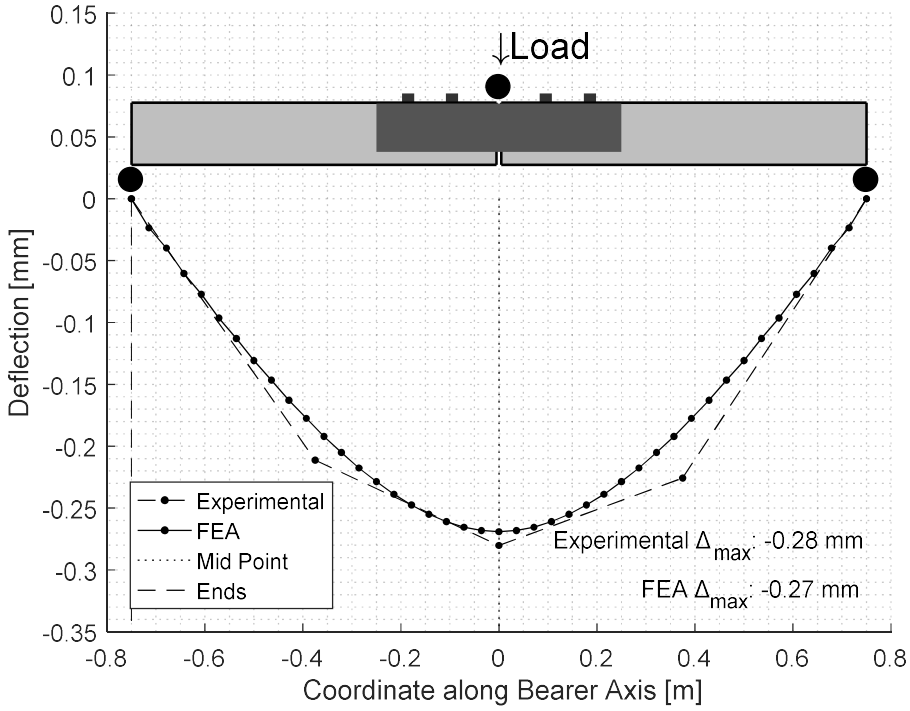

Figure 109 Graph showing the displacement curve for the continuous bearer under three-point bending conditions with a load of 35kN. Solid line: Experimental results; Dashed line: FEA results

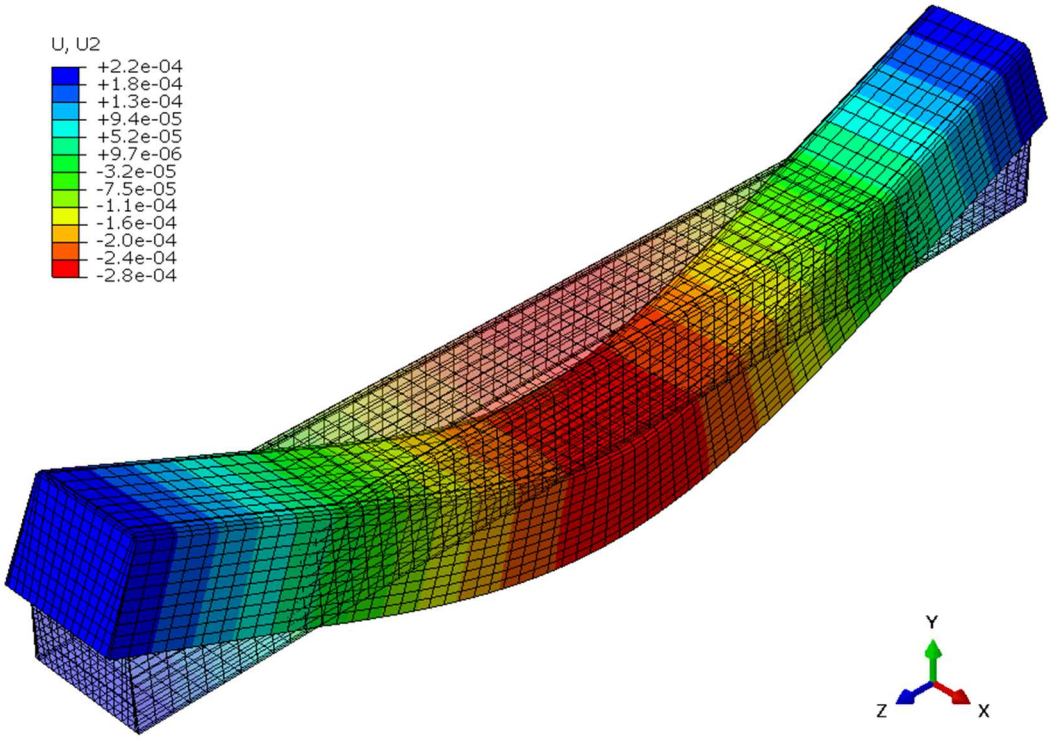

Figure 110 Contour plot showing vertical displacement [m] of the continuous bearer under three-point bending conditions in ABAQUS

7.2.2 Jointed bearer

A quarter model of the jointed bearer was implemented in ABAQUS/Standard. Figure 111 displays the 3D solid model of the assembled parts. Figure 112 presents an exploded view of the model for the jointed bearer assembly where the contact surfaces are annotated with the corresponding numbering for the pairing contacts within the model and a tie or frictional contact indicator as "{T}" or "{F}" respectively. Figure 113 shows the boundary conditions and loads on the quarter model showing the x and z symmetry, bolt loads, actuator loads and rollers.

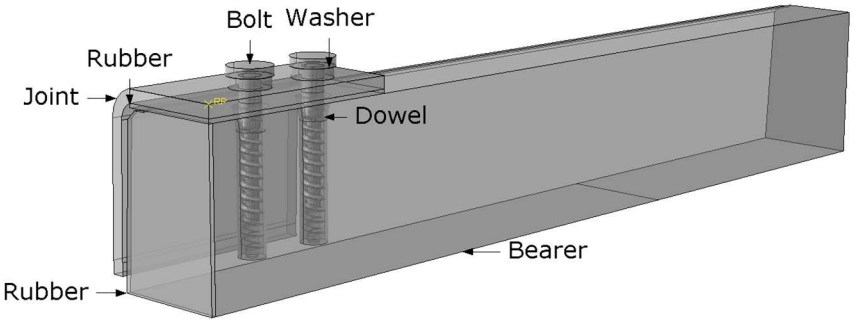

Figure 111 Bearer assembly used within ABAQUS

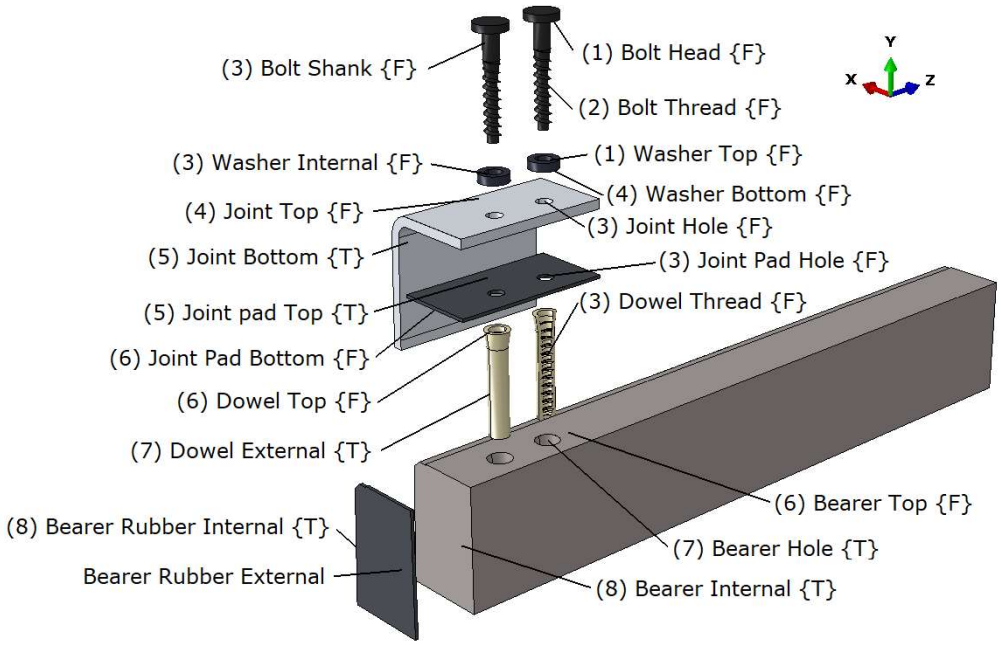

Figure 112 Exploded view annotating the surfaces on parts that are in contact

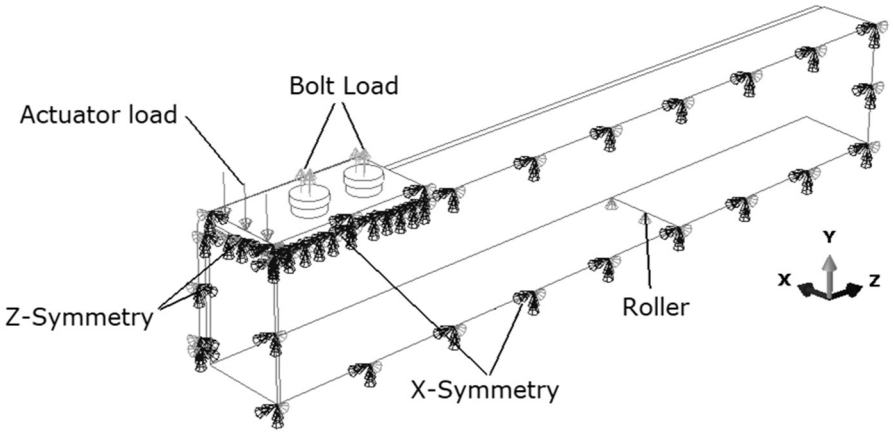

Figure 113 Annotated schematic showing the Loads and Boundary conditions

Justification for the selection of the rubber stiffness properties is based on compression tests carried out on the cork filled rubber pads. The stress distribution on the rubber between the joint and bearer was evaluated through FEA. The maximum compressive stress on the rubber was ~19 MPa which equates to 12 kN force on the rubber specimen tested in the laboratory under compression. The laboratory-obtained force-compression data, shown in Figure 114, was converted into true stress-strain and the elastic modulus was obtained, as shown in Figure 115 the tangent modulus of the rubber at the stress which corresponds with the peak stress on the rubber obtained from FEA was used in the main model.

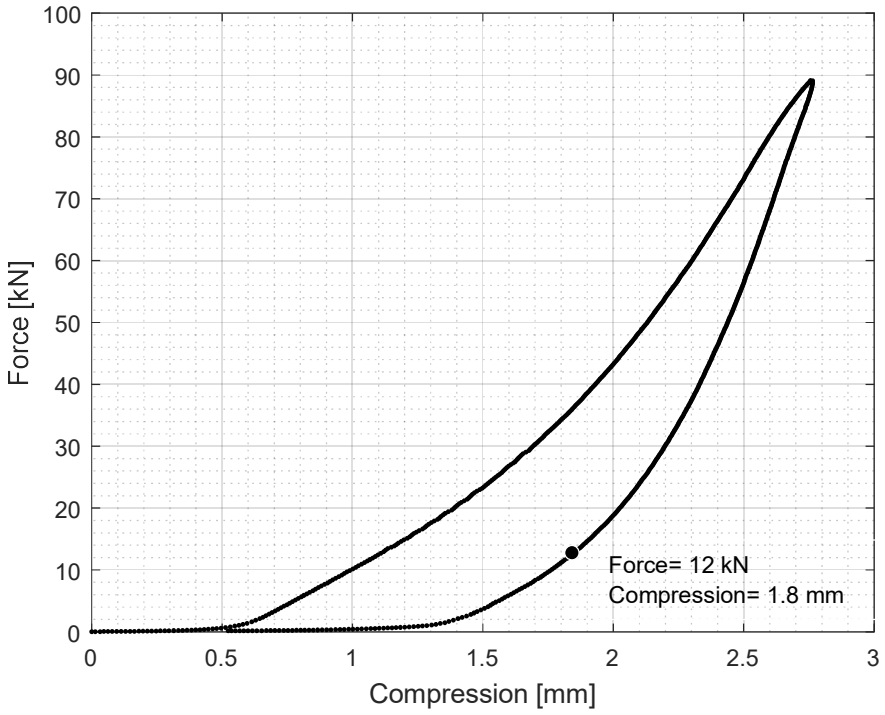

Figure 114 Force vs compression graph of the cork filled rubber pads used within the jointed bearer assembly. The rate of compression is 10 mm/min

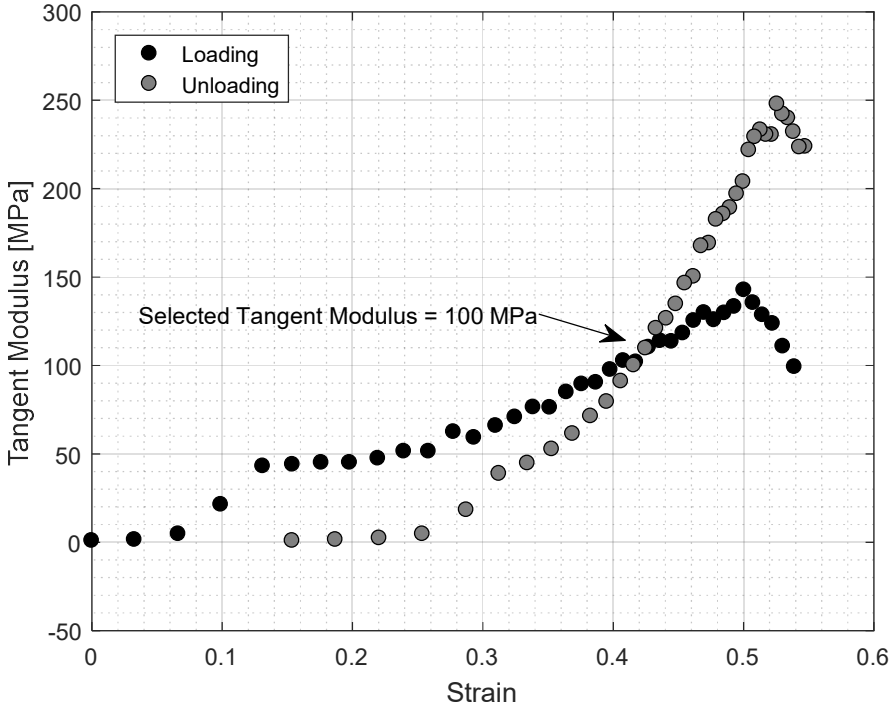

Figure 115 Tangent elastic modulus vs applied strain for the cork filled rubber pad used within the jointed bearer assembly

Bolt load is achieved by the torquing of a bolt, and it ensures that the joint members are clamped. The difficulty in measuring the bolt loads on the jointed bearers that were subjected to three-point bending tests was addressed by subjecting the double coil spring washers to compression tests in the laboratory. The obtained force-compression data on the spring washers provided the load required to compress the springs with a 1mm gap remaining between the coils as specified by NR. The specification states that the bolt tightness should be 340 N.m with 1 mm gap between the coils. This gap was determined by measuring the difference between the spring thickness and the coil thickness.

Figure 116 shows the force vs compression graph of the double coil spring washer in compression. The spring compression test and its repeat tests showed that the load required to reach the required gap was 40 kN (±5 kN). This variation may be due to the inherent variations in physical dimensions (within the tolerances) of the samples. Compression tests were carried out using Instron hydraulic testing machine. Data from the compression tests on the springs were converted to true stress-strain and the elastic modulus was selected when the spring had 1mm gap, this is shown in Figure 117.

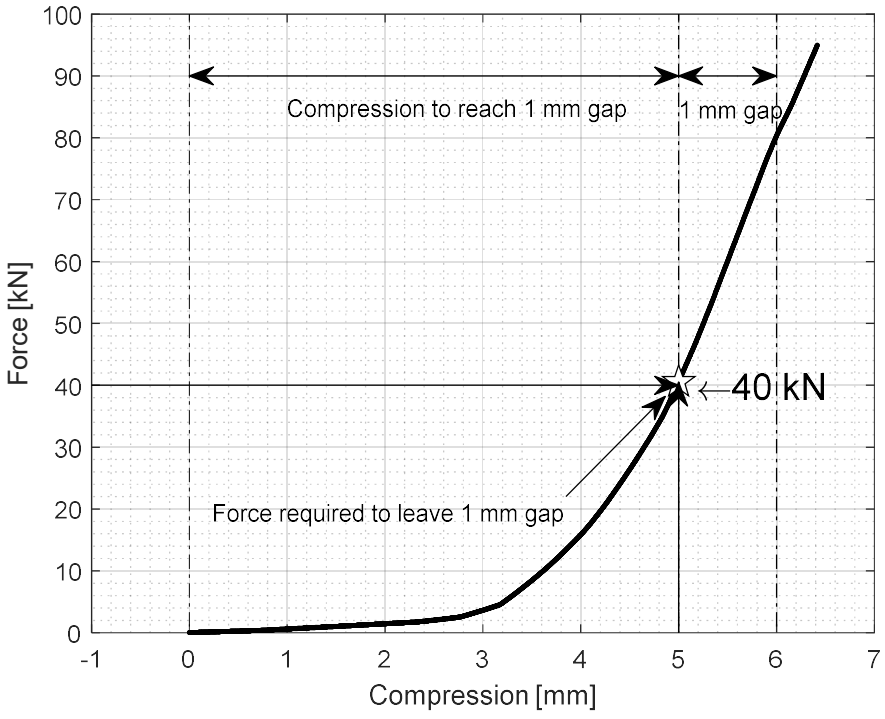

Figure 116 Force-compression graph of the double coil spring washer in compression showing the extent of compression to various stages, i.e., compression to reach the prescribed 1 mm gap between the spring coils, filling of this gap and the bolt load used within the FE model to calibrate the model with laboratory data from the three-point bending test where the bolts were tightened to 340 N.m torque.

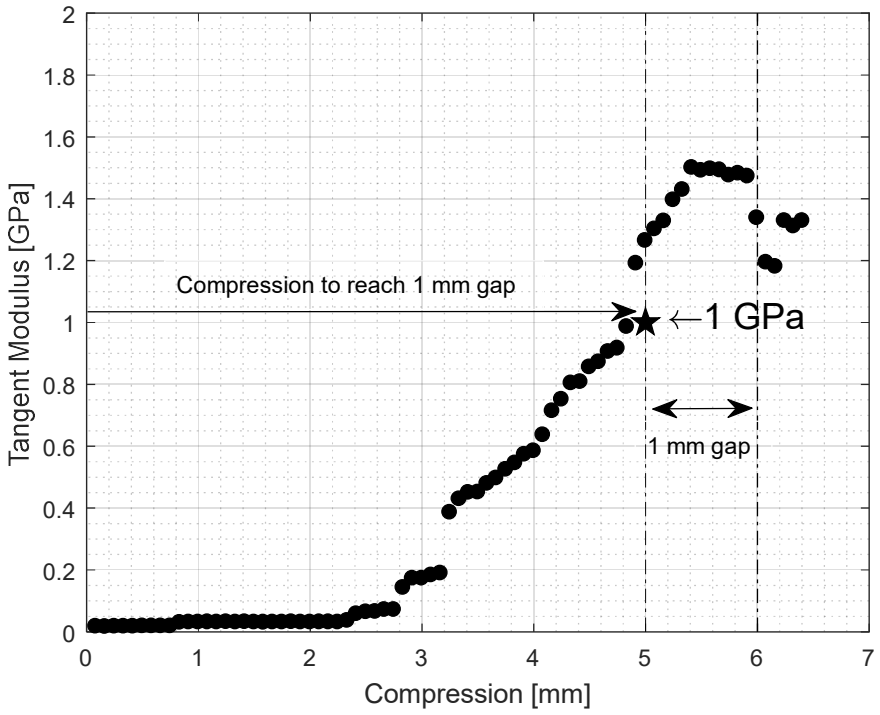

Figure 117 Tangent elastic modulus vs applied strain for the double coil spring washer used within the jointed bearer assembly

The stiffness of the concrete bearer was obtained by performing a three-point bending test on the unjointed, continuous bearer and the Elastic stiffness was calculated using Equation *3*. The Young's modulus of the dowel is assumed to be 3000 MPa (Nylon 66) and that of steel in both the joint and bolts to be 200,000 MPa.

Figure 118 presents the force vs deflection data from the experimental and the FEA model of the jointed bearer in three-point bending conditions. Using the experimentally determined material values, the FEA model yielded the maximum displacement with 1.2% difference to the experimental data shown in Figure 118.

Figure 119 shows the results from the parametric study performed to assess the impact of bolt preloads, rubber pad and spring washer stiffness on the maximum deflection of the jointed bearer in three-point bending. It was observed that changing the spring washer stiffness from 500MPa to 1500MPa produced very little decrease in maximum deflection compared to the greater reduction achieved by increasing the bolt load and rubber pad stiffness.

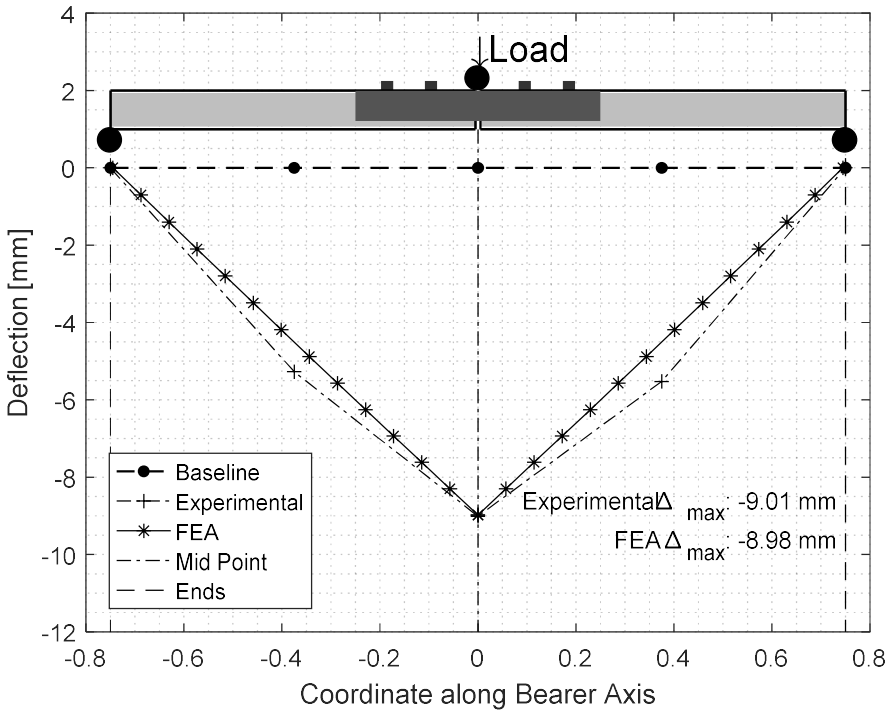

Figure 118 Figure comparing the experimental and FEA results of the jointed bearer deflection under three-point bending conditions with a load of 35 kN

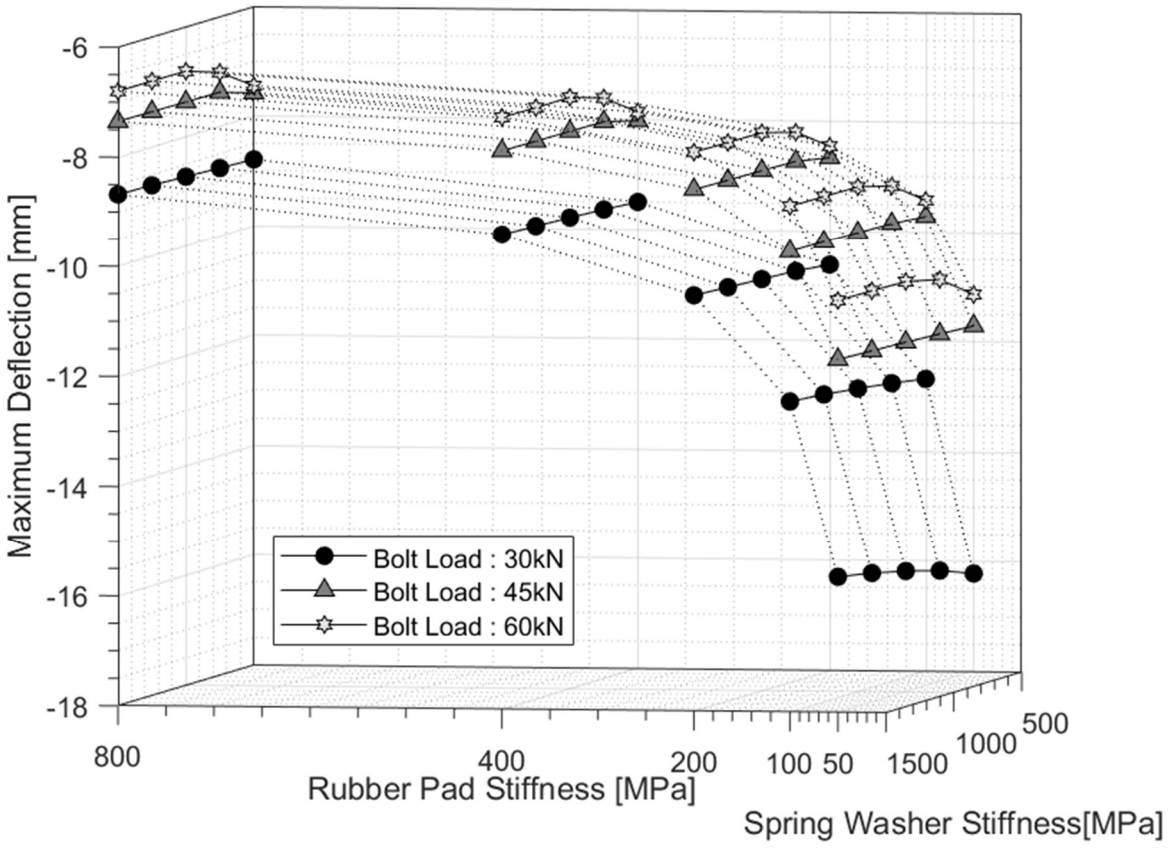

Figure 119 FE model-based relationship between the bolt load, Rubber Pad Stiffness and Spring Washer Stiffness

Figure 120 presents a contour plot of the vertical displacements of the jointed bearer assembly. Figure 121 presents the contour plot of vertical stresses on the bolts with the arrow indicating moments on the bolts. The direction of the moment vector indicates that the bolts are bending. A maximum tension of 450 MPa on the bolt is seen to be at the location on the bolts where they are observed to break from site inspections (see Figure 122).

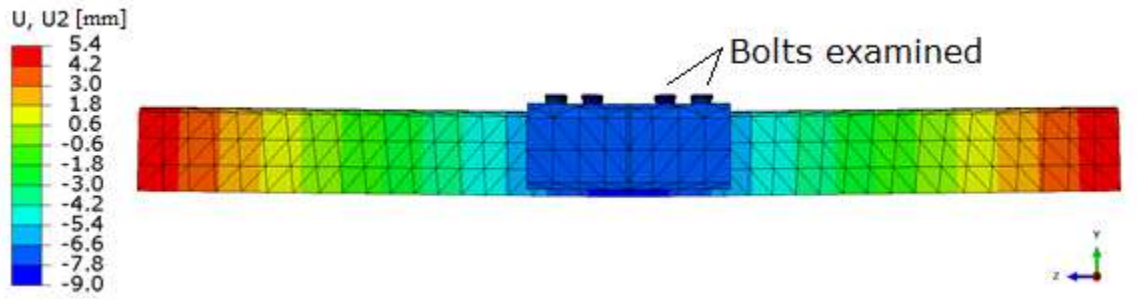

Figure 120 Displacement [mm] contour plot of the Jointed bearer

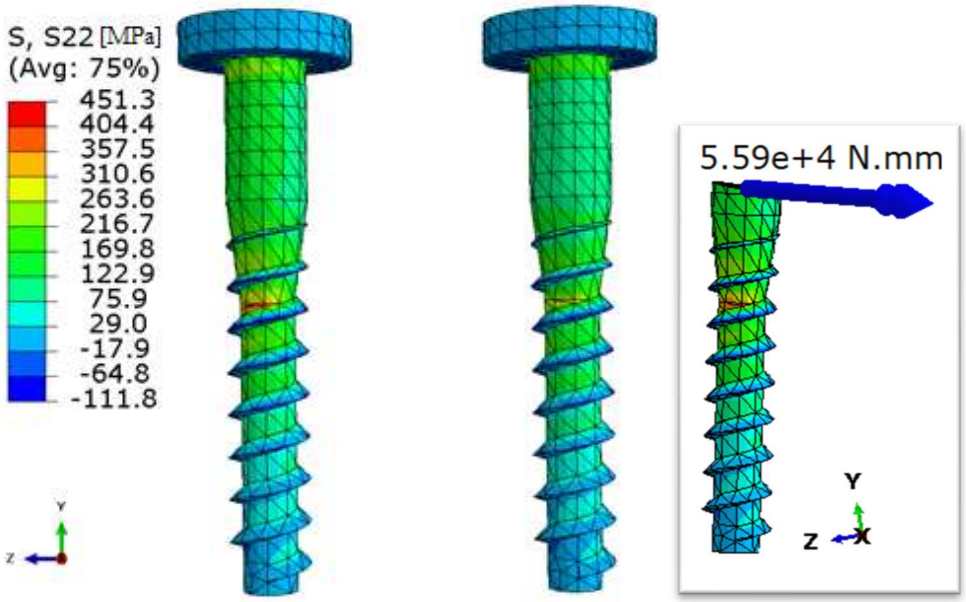

Figure 121 Contour plot showing vertical (y-axis) stresses [MPa] and torque [N.mm] on the bolts

Figure 122 Photograph showing screws broken at approximately where the neck of the bolt narrows (Sinsin Hsu NR)

7.3 Summary

In summary, an equation to determine the spring stiffness of the jointed bearer was obtained and presented. The elastic stiffness of the reinforced concrete bearer used within the modular jointed bearer assembly was determined via three-point bending tests in the laboratory. This obtained E value was used within the spring rotational stiffness equation and within the subsequent FEA of the jointed bearer in three-point bending conditions.

Detailed 3D model of the jointed bearer was created in SolidWorks and analysed in finite element software ABAQUS FEA. Material properties used within the model such as the cork filled rubber pads and the double coil spring washer were determined through laboratory compression tests. Elastic stiffness values obtained were used in the model with the bolt loads also evaluated thorough compression tests on the springs.

It is understood that the criterion for tightening the bolts (to 340Nm with 1mm gap between the spring coils) is difficult to understand on site and practically implement. Moreover, to arrive at a reasonable value for the bolt loads, compression tests on the springs were carried out to leave a millimetre gap between the coils. These values varied between the samples (40-45 kN). The bolt load used within the model was 40 kN.

The three variables that affected the joint stiffness and therefore the flexural rigidity of the jointed assembly were the stiffness of the rubber pads, stiffness of the spring coil and the bolt load. The latter is verified in the lab as a decrease from 340Nm to 320Nm resulted in ~1 mm increase (10%) in the maximum deflection of the rigidly jointed bearer.

Stress concentrations were observed on the bolts on the FE model of the jointed bearer at locations where these bolts have been observed to fail in the field. This suggests that the current design that utilises generic spike screw bolts may need re-evaluating and that a different type of bolt may be more appropriate.

The laboratory three-point bending tests showed a significantly lower flexural rigidity of the jointed bearer in contrast to its continuous counterpart. The use of a joint within an S&C may significantly decrease the flexural rigidity of the joined bearers therefore affecting the bearer-ballast interaction. This could also influence dynamic forces and damage the underlying ballast and the joint itself.

Flexural rigidity of the jointed bearer system was affected by the bending state (maximum deflection was 9 mm in sagging vs 4.7 mm in hogging). Based on results from tests carried out

on the bearers in the SRTF, the initial bending state of the bearers was positive (sagging); this becomes negative (hogging) in the long term upon centre-binding taking effect. This implies that system stiffness of the modular S&C will change depending on the bending state of the jointed bearers. It could also be deduced that the joint would be subject to a range of stresses over its lifetime.

The parametric study conducted showed that for a given bolt stiffness and bolt load, the rubber pad stiffness was a significant factor in changing the flexural rigidity of the jointed bearer assembly. Furthermore, with increasing fatigue cycles on the system, the rubber pads could permanently deform, leading to a loss of bolt loads. The reduction in bold loads is seen to contribute to the decrease in flexural rigidity of the system as reflected in the higher maximum deflections of the jointed bearer. The increase in permanent strains on the rubber pads and the resulting reduction in bolt loads could lead to an increased likelihood of shearing of the bolts.

8 Conclusion

8.1 General conclusions

The aim of this research was to contribute to the understanding of the mechanics of S&C bearer performance. This involved investigating the performance of different types of jointed bearers under general conditions, in terms of long-term permanent settlement and resilient deflections up to 1M loading cycles. The effectiveness of mitigation measures such as USPs and confining the ballast shoulder was also assessed. The work involved full-scale laboratory experimentation on S&C long bearers (both standard continuous and modular jointed bearers) and finite element modelling of the jointed bearer, aided by three-point bending tests and compression tests of the individual parts of the assembly. Figure 123 provides a definition sketch of the various terms/orientations used.

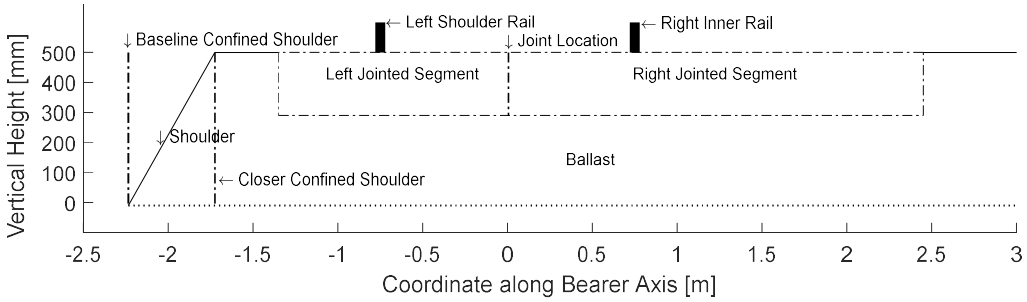

Figure 123 Definition diagram

The full-scale ballast fatigue tests carried out on S&C bearers in the modified SRTF apparatus showed the following:

- Eccentric loading
  - In its current form, S&C designs feature rail configurations that lead to eccentric loading on the bearers, which causes an uplift on the unloaded bearer ends. To evaluate the effect of such loading on the bearers, baseline tests on the continuous bearers were carried out. These showed that off-centre loading of the bearers results in an increased vertical settlement towards the loaded end of the bearers (and uplift on unloaded end, that increased with bearer length).
  - The presence of the ballast shoulder, which provides the least lateral resistance and is prone to permanent lateral deflections, resulted in an exacerbation of the vertical settlement towards the shoulder end. Vertical pressures transmitted through the ballast were measured to increase towards the loaded side of the bearers and the

longitudinal (in the direction of the rails) compressive stresses in the ballast were always higher under the loaded rail where ballast settlement was the highest, closest to the ballast shoulder. Variations in permanent settlement along the bearer lengths could mean increased difference in crosslevel, which could have detrimental impact on the safe running of trains.

- The variation in settlement along the length of continuous or rigidly jointed bearers also affected the resilient response of the bearers, i.e., the bending state of these bearers changed from sagging to tilting (or with minimal hogging). This is because of deteriorated ballast support under the rail owing to the ballast shoulder displacements. There was also a decrease in the longitudinal compressive stresses with increasing loading cycles, suggesting weakened bearer-ballast interaction in that region. The reduced ballast support was accompanied by a gap at the bearer-ballast interface in the problem region (bearer end near the ballast shoulder), which will have adverse effect on ballast life and will increase maintenance frequency.
- Ballast contact areas on the short continuous bearer were greatest under the left-hand rail towards the ballast shoulder and lowest at the right-hand end, furthest from the ballast shoulder. Bearer-ballast contact area generally increased towards the loaded end of the bearers. The loaded rails were associated with a larger contact area than at the middle of the rails.

- Joint location
  - Stiffness variations along the length of the S&C can have detrimental impact on its performance. When a bearer with a joint located between the loaded rails is followed by a bearer with a joint away from the loaded rails, the bearer-ballast interaction may vary and cause differential settlement. It was found that the location of a rotational bearer joint relative to the loaded rails significantly affected the permanent settlement, resilient deflections, and crosslevel. Rotational joints effectively decoupled joining bearer segments, so when positioned such that the bearer segment is symmetrically loaded, the vertical permanent ballast settlement along its length became more uniform, with improved crosslevel and drastically reduced uplift on the unloaded bearer end. This helps to achieve more symmetric resilient deflections about the middle of the loaded rails. The advantage of uniformly distributed loads on the underlying ballast will prolong time between maintenance cycles.
- Joint type
  - The inclusion of flexible joints in the middle of the loaded rails led to increased vertical permanent ballast settlement under the jointed segment of the bearer near the ballast shoulder. This also increased the crosslevel on the jointed bearers. This is because the flexible joints allow the jointed bearer segments to respond and transfer rail loads to the ballast more independently than a continuous bearer of the same dimensions. The change in pressure distribution due to the inclusion of the joint in the middle of the rails increased the bearer-ballast contact area compared to the baseline tests.
  - Differential ballast support under the bearers resulted in large permanent vertical deflections of the bearer and large strains on the bearer joint located between the loaded rails.
  - The presence of a flexible joint between the loaded rails decreased the rate of change in resilient deflections with accumulating loading cycles due to its ability to conform to the ballast bed. Thus, it decreased any bending (and change in bending states) that a continuous bearer experienced due to evolving ballast support along its length.
- Use of USP
  - The use of USP on continuous and jointed bearers did not make a noticeable difference to the weighted area average of permanent settlement on the bearers,

however, the crosslevel was reduced by 21.8% on the continuous bearer and 6.3% on the jointed bearer. As expected, the magnitude of resilient deflections was increased using USPs. The gap between the bearer and ballast at the bearer end (near the ballast shoulder) reduced significantly with the use of USPs. The reduced gap at the bearer-ballast interface suggests that there is adequate ballast support, which will reduce damage to the ballast and prolong its life.

- Ballast shoulder interventions
  - The confinement of the ballast shoulder delivered the most significant improvement to the crosslevel between the loaded rails, vertical permanent settlement, and resilient deflections on both the continuous bearer and the fully rotational (pin-pin) jointed bearer. The confinement of the ballast shoulder, by providing adequate lateral support to the ballast, helped maintain good bearer-ballast interaction over the length of the bearer. This significantly decreased the gap at the bearer-ballast interface near the left shoulder end of the bearer. This was reflected in the lower magnitude sagging of the bearer, sustained up to 1M loading cycles. Variation in contact areas along the length of the bearer reduced with the ballast shoulder confinement and there was also an increase in the contact area compared with continuous bearer tests.
  - It is ideal to achieve consistent bearer-ballast interaction, but in reality, this varies with accumulating loading cycles. Three-point bending tests on the continuous and jointed bearers showed that the 'rigid' joint used on S&C in the UK is 30 and 16 times more flexible than its continuous counterpart in the sagging and hogging state, respectively. This implies that modular bearer flexibility depends on its bending state. Over the course of its lifetime, as its underlying ballast support changes, so will the stiffness characteristics of the bearers and the flexibility of the S&C.
  - The confinement of the ballast shoulder by maintaining, in the long term, a consistent bending state of the bearer could in turn help with maintaining more consistent stiffness of the bearers in the long term. However, it is equally important to consider the design of the joint used on bearers. This is because FE analysis highlighted locations of significant stress concentrations on bolts used within the joints where they have already been reported to break on various sites. The parametric study of the rigid jointed bearer suggested that the flexural rigidity of the mechanism was influenced the most by the rubber layers used within the joint assembly, followed by the bolt load and spring washer stiffness.

8.2 Further research

This research provided input for further investigations:

- Fatigue testing of bearer joint bolts - analysis of the fatigue properties through laboratory testing of the bolts used on the joints in the rigid jointed bearers and proposal of improvements to the joint design. This will aid the design of the joints used in the modular S&Cs to prolong their service life.
- Practicality of ballast shoulder confinement - while ballast shoulder confinement has been shown to have a significant advantage in terms of reducing permanent ballast settlement and crosslevel between the loaded rails, field trials need to be conducted to assess its performance and cost benefits. This will help justify its use in practice.
- Understanding differences in ballast batch settlements – Tests conducted on both the continuous and jointed bearers consistently showed larger settlements for a particular batch of ballast. Slight variations are not uncommon between deliveries from the same quarry but whilst the use of a single batch may be adequate for a comparative study, it is important to quantify the relative merits of different batches of ballast from the same quarry.
- Multi actuator testing - this research has included a comparative study of the different bearer types in specific ballast support settings. However, more realistic conditions can be achieved by applying loads (to mimic traffic) on both the through and diverging rails, and with consecutively placed bearers with changing joint location. This will help gain a more realistic understanding of how bearers behave when joint location changes abruptly.
- Vehicle Track Interaction (VTI) model - the measured rotational stiffness of the jointed bearer could be used in a vehicle track interaction model that incorporates multiple bearers of varying lengths and joint locations to forecast and give further insights into the overall behaviour of the modular S&C.

9 References

Abadi, T., 2015. *Effect of sleeper and ballast interventions on rail track performance,* s.l.: University of Southampton, Engineering and the Environment, Doctoral Thesis, 302pp.

Abadi, T., Le Pen, L., Zervos, A. & Powrie, W., 2015. Measuring the area and number of ballast particle contacts at sleeper/ballast and ballast/subgrade interfaces. *The International Journal of Railway Technology,* 4(2), pp. 45-72.

Abadi, T., Le Pen, L., Zervos, A. & Powrie, W., 2015. Measuring the Area and Number of Ballast Particle Contacts at Sleeper-Ballast and Ballast-Subgrade Interfaces. *International Journal of Railway Technology,* 4(2), pp. 45-72.

Abadi, T., Le Pen, L., Zervos, A. & Powrie, W., 2016. A Review and Evaluation of Ballast Settlement Models using Results from the Southampton Railway Testing Facility (SRTF). *Procedia Engineering,* Volume 143, pp. 999-1006.

Abadi, T., Le Pen, L., Zervos, A. & Powrie, W., 2018. Improving the performance of railway tracks through ballast interventions. *Proceedings of the Institution of Mechanical Engineers, Part F: Journal of Rail and Rapid Transit,* 232(2), pp. 337-355.

Alabbasi, Y. & Hussein, M., 2021. Geomechanical Modelling of Railroad Ballast: A Review. *Arch Computat Methods Eng,* Volume 28, pp. 815-839.

Alfi, S. & Bruno, S., 2009. Mathematical modelling of train-turnout interaction. *Veh. Syst. Dyn.,* 47(5), pp. 51-574.

Anderson, C. & Zeitlinger, B. V., 2000. *Load Impacts at Railway Turnout Crossing.* Lisse, Netherlands, THE DYNAMICS OF VEHICLES ON ROADS AND ON TRACKS - SUPPLEMENT TO VEHICLE SYSTEM DYNAMICS, VOLUME 33. PROCEEDINGS OF THE 16TH IAVSD SYMPOSIUM HELD IN PRETORIA, SOUTH AFRICA.

Anderson, W. & Key, A., 2000. Model testing of two-layer railway track ballast. *J Geotech Geoenviron Eng,* 126(4), pp. 317-323.

Andersson, C. & Dahlberg, T., 1998. Wheel/rail Impacts at a railway turnout crossing.. *Institute of mechanical Engineers, Part F: Journal of Rail and Rapid transit,* 212(2), pp. 123-134.

Askarinejad, H., Dhanasekar, M. & Cole, C., 2012. Field Measurement of Wheel–Rail Impact Force at Insulated Rail Joint. *Experimental Techniques,* 39(5), pp. 61-69.

Brown, S., Thom, N. & Kwan, J., 2006. Optimising the geogrid reinforcement of rail track ballast. *Railfound Conference*.

CEC, 2002. *Permanent Way Institute.* [Online] Available at: https://www.thepwi.org/technical_hub/technical_hub_files/track_maintenance_general_guides/twist_faults_guide_2002
[Accessed 30 06 2018].

Coleman, I., 2014. *The development of modelling tools for railway switches and crossings. PhD thesis.* London, Imperial College, London.

Coleman, I. & Cornish, A., 2010. *Global Railway Review.* [Online] Available at: https://www.globalrailwayreview.com/article/6772/predicting-the-future-for-switches-and-crossings/
[Accessed 23 04 2019].

Cui, X.-H., Xiao, H. & Ling, X., 2021. Analysis of ballast breakage in ballast bed when using under sleeper pads. *Geomechanics and Geoengineering.*

Dahlberg, T., 2003. *Railway track settlements – a literature review,* s.l.: Division of Solid Mechanics, IKP, Linköping University. Report for the EU project SUPERTRACK..

Diesel Locomotives, 2019. *Diesel Locomotives.* [Online] Available at: http://www.eng.dieselloc.ru/railway-engineering/crossing.html
[Accessed 23 05 2019].

Ferro, E., 2018. *The mechanical behaviour of fibre reinforced railway ballast,* s.l.: University of Southampton, Doctoral Thesis, 230pp.

Grassie, S. L. & Cox, S. J., 1984. The Dynamic Response of Railway Track With Flexible Sleepers to High Frequency Vertical Excitation. *Proceedings of the Institution of Mechanical Engineers, Part D: Journal of Automobile Engineering ,* 198(2), pp. 117-124.

Grassie, S. L. & Cox, S. J., 1985. The Dynamic Response of Railway Track With Unsupported Sleepers. *Proceedings of the Institution of Mechanical Engineers, Part D: Journal of Automobile Engineering,* 199(2), pp. 123 - 136.

Grossoni, I. et al., 2020. The role of stiffness variation in switches and crossings: Comparison of vehicle–track interaction models with field measurements. *Proceedings of the Institution of Mechanical Engineers, Part F: Journal of Rail and Rapid Transit,* 234(10), pp. 1184-1197.

Grossoni, I. et al., 2021. Modelling railway ballasted track settlement in vehicle-track interaction analysis. *Transportation Geotechnics,* 26(100433), pp. 1-14.

Guo, Y., Markine, V. & Jing, G., 2021. Review of ballast track tamping: Mechanism, challenges and solutions. *Construction and Building Materials,* 300(123940).

Han, X. & Selig, E., 1996. *Investigation of the effects of fouling material and degree of fouling on the settlement of ballast bed by ballast box. box. Project Report No. AAR95-426R for Association of American Railroads,* Amherst: University of Massachusetts.

In2Rail, 2017. *Deliverable D3.3: Evaluation of optimised track systems,* s.l.: s.n.

IN2TRACK, 2020. *Research into enhanced tracks, switches and structures,* s.l.: IN2TRACK.

Indraratna, B., Biabani, M. & Nimbalkar, S., 2015. Behavior of geocell-reinforced subballast subjected to cyclic loading in planestrain condition. *J Geotech Geoenviron Eng,* 141(1).

Indraratna, B. & Ionescu, D., 2000. *State of the art large scale testing of ballast,* s.l.: s.n.

Indraratna, B. & Nimbalkar, S., 2013. Stress-strain degradation response of railway ballast stabilized with geosynthetics. *J Geotech Geoenviron Eng,* 139(5), pp. 684-700.

Johansson, A. et al., 2011. Simulation of wheel–rail contact and damage in switches & crossings. *Wear,* 271(1-2), pp. 472-481.

Jorge, P., Bezin, Y., Grossoni, I. & Neves, S., 2020. Modelling Track Flexibility in Turnouts Using MBS Approach. *Klomp, M., Bruzelius, F., Nielsen, J., Hillemyr, A. (eds) Advances in Dynamics of Vehicles on Roads and Tracks. IAVSD 2019. Lecture Notes in Mechanical Engineering. Springer, Cham*, pp. 359-366.

Kaewunruen, S., Ngamkhanong, C., Goto, K. & Janeliukstis, R., 2018. Asymmetrical effects on railway turnout bearers due to wheelset impact over a crossing nose. *The 5th International Conference on Road and Rail Infrastructure*, 19 May, pp. 623-629.

Kalker, J., 1991. Wheel-rail rolling contact theory. *Wear,* Volume 144, pp. 243-261.

Kassa, E., Andersson, C. & Nielsen, J. C., 2006. Simulation of dynamic interaction between train and railway turnout. *Vehicle System Dynamics,* 44(3), pp. 247-258.

Kennedy, J., Woodward, P., Banimahd, M. & Medero, G., 2012. Railway track performance study using a new testing facility. *ICE Proceedings Geotechnical Engineering,* 165(5), pp. 309-319.

Kwan, C. C. J., 2006. *Geogrid Reinforcement of Railway Ballast - PhD Thesis,* s.l.: University of Nottingham.

Lagos, R., San Emeterio, A., Vinolas, J. & Alonso, A., 2014. The Influence of Track Elasticity when travelling on a Railway Turnout. *J. Pombo, (Editor), "Proceedings of the Second International Conference on Railway Technology: Research, Development and Maintenance", Civil-Comp Press, Stirlingshire, UK, Paper 208*.

Lau, A. & Hoff, I., 2018. Simulation of Train-Turnout Coupled Dynamics Using a Multibody Simulation Software. *Modelling and Simulation in Engineering,* pp. 1-10.

Le Pen, L., 2008. *Track behaviour: the importance of the sleeper to ballast interface,* s.l.: University of Southampton, School of Civil Engineering and the Environment, Doctoral Thesis, 292pp..

Le Pen, L., Milne, D., Thompson, D. & Powrie, W., 2016. Evaluating railway track support stiffness from trackside measurements in the absence of wheel load data. *Can Geotech J,* Volume 53, pp. 1156-1166.

Le Pen, L., Watson, G., Hudson, A. & Powrie, W., 2017. Behaviour of under sleeper pads at switches and crossings - Field measurements. *Proceedings of the Institution of Mechanical Engineers, Part F: Journal of Rail and Rapid Transit ,* 232(4), pp. 1049-1063.

Li, H. & McDowell, G., 2020. Discrete element modelling of two-layered ballast in a box test. *Granular Matter,* 22(76).

Li, X., Nielsen, J. C. & Palsson, B. A., 2014. Simulation of track settlement in railway turnouts. *Vehicle System Dynamics,* 52(1), pp. 421-439.

Loughran, J., 2021. *Institution of Engineering and Technology.* [Online] Available at: https://eandt.theiet.org/content/articles/2021/09/latest-figures-show-the-uk-rail-sector-was-booming-before-pandemic-losses/
[Accessed 09 12 2021].

Loy, H., 2009. Under Sleeper Pads in Turnouts. *Railway Technical Review,* pp. 35-38.

MAINLINE, 2014. *Rail Switches and Crossings. Development of new technologies for replacement,* s.l.: MAINLINE.

Mandal, N. K., Dhanasekar, M. & Sun, Q. Y., 2016. Impact forces at dipped rail joints. *Journal of Rail and Rapid Transit,* 230(1), pp. 271-282.

Markine, V. L., Steenbergen, M. J. M. M. & Shevtsov, I. Y., 2011. Combatting RCF on switch points by tuning elastic track properties. *Wear,* 271(1-2), pp. 158-167.

MI-NE SEISAKUSHO CO., L., 2014. *MI-NE SEISAKUSHO CO., LTD.*. [Online] Available at: http://www.mine-s.co.jp/english/business/products_rail.html [Accessed 09 05 2019].

Neidhart, T. & Shultz, G., 2011. Dynamic Stability of Railway Tracks – DyStaFiT, and Inoovation in Testing. *Proceedings from Georail.*

Network Rail, 2009. *Network Rail.* [Online] Available at: https://www.networkrailmediacentre.co.uk/resources/4-ready-to-be-lowered-3 [Accessed 26 11 2022].

Network Rail, 2012. *networkrailmediacentre.* [Online] Available at: https://www.networkrailmediacentre.co.uk/news/network-rail-breaks-track-records
[Accessed 23 04 2019].

Network Rail, 2012. *networkrailmediacentre.* [Online] Available at: https://www.networkrailmediacentre.co.uk/news/network-rail-breaks-track-records
[Accessed 29 06 2018].

Network Rail, 2021. *Network Rail expenditure in 2019/20,* s.l.: Network Rail.

Ngamkhanong, C. & Kaewunruen, S., 2020. Effects of under sleeper pads on dynamic responses of railway prestressed concrete sleepers subjected to high intensity impact loads. *Engineering Structures,* 214(110604).

Nicklisch, D., Nielsen, J., Ekh, M. & Iwnicki, S., 2010. Geometry and stiffness optimization for switches and crossings, and simulation of material degradation. *Proceedings of the Institution of Mechanical Engineers, Part F: Journal of Rail and Rapid Transit,* 224(4), pp. 279-292.

ORR, 2020. *Cost benchmarking of Network Rail, Annual report: year 1 of control period 6,* s.l.: Office of Rail and Road.

ORR, 2021. *Rail industry finance (UK) 2020-21,* s.l.: Office of Rail and Road.

ORR, n.d. *Office of Rail and Road.* [Online] Available at: http://orr.gov.uk/glossary [Accessed 30 06 2018].

Pålsson, B. A. & Nielsen, J. C., 2012. Wheel–rail interaction and damage in switches and crossings. *Vehicle System Dynamics,* 50(1), pp. 43-58.

Parsons Brinckerhoff, 2012. *Track Design Handbook for Light Rail Transit,* Washington: Transportation Research Board.

Plasek, O. & Hruzikova, M., 2017. *Under sleeper pads in switches & crossings.* s.l., IOP Conf. Ser.: Mater. Sci. Eng. 236 012045.

Priest, J. et al., 2013. The effect of enhanced curving forces on the behaviour of canted ballasted track. *Proceedings of the Institution of Mechanical Engineers, Part F: Journal of Rail and Rapid Transit,* 227(3), pp. 229-244.

RAIB, 2017. *Rail Accident Report,* s.l.: RAIB.

RAIB, 2018. *Freight train derailment at Lewisham,* s.l.: Rail Accident Investigation Branch.

RailEngineer, 2021. *RailEngineer.* [Online] Available at: https://www.railengineer.co.uk/longer-life-crossings/ [Accessed 03 02 2022].

railone, n.d. *railone.* [Online] Available at: https://www.railone.com/products-solutions/long-distance-and-freight-transport/ballasted-track-systems/turnout-sleepers [Accessed 23 04 2019].

Remennikov, A. M. & Kaewunruen, S., 2007. A review of loading conditions for railway track structures due to train and track vertical interaction. *STRUCTURAL CONTROL AND HEALTH MONITORING,* Volume 15, pp. 207-234.

RSSB, 2011. *GCRT5021 Iss 5 Track System Requirements,* s.l.: RSSB.

Salim, W., 2004. *Deformation and degradation aspects of ballast and constitutive modelling under cyclic loading,* s.l.: s.n.

Selig, E. & Waters, J., 1994. *Track geotechnology and substructure management.* London: Thomas Telford.

Shi, S. et al., 2020. Effect of tamping operation on mechanical qualities of ballast bed based on DEM-MBD coupling method. *Computers and Geotechnics,* Volume 124.

Siew, J. S., Mirza, O. & Kaewunruen, S., 2017. Torsional Effect on Track-Support Structures of Railway Turnouts Crossing Impact. *Journal of Transportation Engineering, Part A: Systems,* 143(2).

Six, K. et al., 2021. A whole system model framework to predict damage in turnouts. *Vehicle System Dynamics.*

Stewart, H., Selig, E. & Norman-Gregory, G., 1985. Failure criteria and lateral stresses in track foundations.

Sun, Y. Q., Cole, C. & McClanachan, M., 2010. The calculation of wheel impact force due to interaction between vehicle and a turnout. *Proceedings of the Institution of Mechanical Engineers, Part F: Journal of Rail and Rapid Transit,* 224(5), pp. 391-403.

Sun, Y. Q., Cole, Colin & Spiryagin, M., 2015. Monitoring vertical wheel–rail contact forces based on freight wagon inverse modelling. *Advances in Mechanical Engineering,* 7(5), pp. 1-11.

Tennakoon, N., Indraratna, B. & Nimbalkar, S., 2014. *Impact of ballast fouling on rail tracks. Second International Conference on Railway Technology: Research, Development and Maintenance (pp. 1-11).* Scotland, Civil-Comp Press, pp. 1-11.

Torstensson, P. et al., 2019. Wheel–rail impact loads and noise generated at railway crossings – Influence of vehicle speed and crossing dip angle. *Journal of Sound and Vibration,* Volume 456, pp. 119-136.

Voestalpine, 2020. *Voestalpine.com.* [Online] Available at: https://www.voestalpine.com/turnout-technology-germany/static/sites/turnout-technology-germany/.downloads/en/products/Swt_Flyer_ENG.pdf [Accessed 03 02 2022].

Wang, P. et al., 2017. Optimization of Rail Profiles to Improve Vehicle Running Stability in Switch Panel of High-Speed Railway Turnouts. *Mathematical Problems in Engineering,* 2017(Article ID 2856030), pp. 1-13.

Zhang, S., Xiao, X., Wen, Z. & Jin, X., 2009. Effect of unsupported sleepers on wheel/rail normal load. *Soil Dyn Earthq Eng,* 28(8), pp. 662-673.

Zhu, J. Y., 2006. On the effect of varying stiffness under the switch rail on the wheel–rail dynamic characteristics of a high-speed turnout. *Proceedings of the Institution of Mechanical Engineers, Part F: Journal of Rail and Rapid Transit,* 220(1), pp. 69-75.

Zhu, J. Y. & Luo, Y. Y., 2004. Comparison investigation on dynamic characteristics by applying elastic baseplate under switch rail. *J. China Railw. Soc.,* 26(1), pp. 77-81.

Zhu, J. Y. & Thompson, D. J., 2009. Characterization of forces, dynamic response, and sound radiation from an articulated switch sleeper in a turnout system. *Proceedings of the Institution of Mechanical Engineers Part F: Journal of Rail and Rapid Transit,* 224(1), pp. 53-60.

Appendix 1

Derivation of equation for spring stiffness

The below equation (with derivation) is used to obtain the rotational stiffness of the jointed bearer.

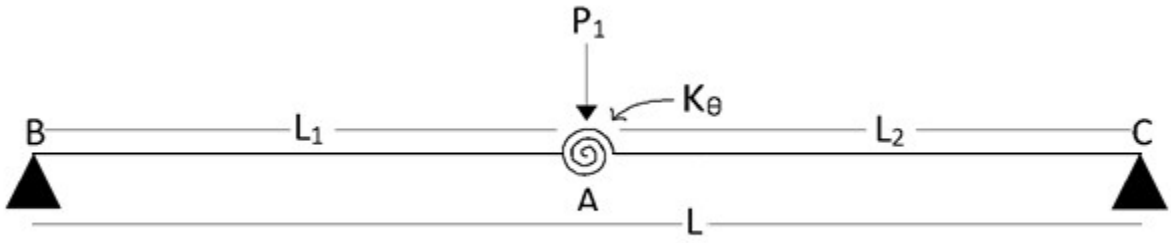

Figure 124 Three-point bending diagram for the test carried out in the laboratory and ABAQUS, showing the lengths of bearer segments (L_1 & L_2) on either side of the joint A with stiffness K_Θ which is subjected downwards load P_1, the bearer ends are supported simply at points B and C.

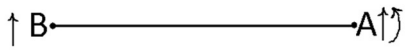

Figure 125 Free body diagram of bearer segment B-A, showing reaction force on B, and moment and shear arrows on A

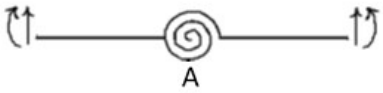

Figure 126 FBD cut of joint A showing shear and movements arrows on either side

$$Reaction_B = \frac{P_1 L_2}{L_1 + L_2}$$

$$Shear\ force_A = \frac{P_1 L_2}{L_1 + L_2}$$

$$Moment_A = \frac{P_1 L_2 L_1}{L_{1+} L_2} = k_\theta \times \theta$$

$$\sum M_a = 0$$

Also, $M = EI\frac{d^2y}{dx^2}$ $\theta = y'$ $y_{disp} = f(x)$ $v = \frac{d^3y}{dx^3}.EI$

At B:

$y_b = 0$ when $y(x = 0) = 0$

$$M_B = 0 \rightarrow EIy''_{(x=0)} = 0$$

$$V_B = \frac{P_1 L_1}{L_1 + L_2} \rightarrow EIy'''_{(x=0)} = \frac{P_1 L_2}{L_1 + L_2}$$

At A:

$$y_A = unknown$$

$$M_A = EIy''_{(x=L_1)} = \frac{P_1 L_1 L_2}{L_1 + L_2}$$

$$v_A = EIy'''_{(x=L_1)} = \frac{P_1 L_2}{L_1 + L_2}$$

$$M(x) = \frac{P_1 L_2}{L_1 + L_2} \times x = EIy''$$

$$\frac{P_1 L_2}{L_1 + L_2} \times \frac{x^2}{2} + c = EIy'$$

$$\frac{P_1 L_2}{L_1 + L_2} \times \frac{x^3}{6} + cx + d = EIy$$

$$y = \frac{P_1 L_2}{EI(L_1 + L_2)} \times \frac{x^3}{6} + \frac{cx}{EI} + \frac{d}{EI}$$

Due to (2) x=0, y=0 so d=0

$$y' = \theta = \frac{d_y}{d_x}$$

$$\mathrm{EI} \times \theta = \frac{P_1 L_2}{L_1 + L_2} \times \frac{x^2}{2} + c = EIy'$$

$$\theta = \frac{P_1 L_2}{\mathrm{EI}(L_1 + L_2)} \times \frac{x^2}{2} + \frac{c}{EI}$$

$$\mathrm{M} = k_\theta \times \theta = P_1 \frac{L_1 L_2}{L_1 + L_2}$$

$$\theta = P_1 \frac{L_1 L_2}{(L_1 + L_2) k_\theta}$$

$$\frac{P_1 L_1 L_2}{(L_1 + L_2) k_\theta} = \frac{P_1 L_2}{\mathrm{EI}(L_1 + L_2)} \times \frac{x^2}{2} + \frac{c}{EI}$$

To find c when x = L_1:

$$\frac{c}{EI} = \frac{P_1 L_1 L_2}{(L_1 + L_2)k_\theta} - \frac{P_1 L_2}{\mathrm{EI}(L_1 + L_2)} \times \frac{{L_1}^2}{2}$$

$$c = \frac{P_1 L_1 L_2 EI}{(L_1 + L_2)k_\theta} - \frac{P_1 L_2}{(L_1 + L_2)} \times \frac{{L_1}^2}{2}$$

$$c = \left(\frac{P_1 L_2}{(L_1 + L_2)}\right)\left(\frac{L_1}{k_\theta} - \frac{{L_1}^2}{2EI}\right)(EI)$$

And

$$y = \frac{P_1 L_2}{EI(L_1 + L_2)} \times \frac{x^3}{6} + \frac{cx}{EI}$$

Displacement at x=L_1

$$y = \frac{P_1 L_2}{(L_1 + L_2)EI} \times \frac{x^3}{6} + c\frac{x}{EI}$$

$$c = P_1 \frac{L_2}{(L_1 + L_2)}\left(\frac{L_1}{k_\theta} - \frac{{L_1}^2}{2EI}\right)EI$$

$$y = \frac{P_1 L_2}{(L_1 + L_2)EI}\frac{{L_1}^3}{6EI} + \left[\frac{P_1 L_2}{L_1 + L_2}\left(\frac{L_1}{k_\theta} - \frac{{L_1}^2}{2EI}\right)\right]L_1$$

$$y = \frac{P_1 L_2 {L_1}^3}{6EI(L_1 + L_2)} + \frac{P_1 L_1 L_2}{L_1 + L_2}\left(\frac{L_1}{k_\theta} - \frac{{L_1}^2}{2EI}\right)$$

$$y = \frac{P_1 L_2 {L_1}^3}{6EI(L_1 + L_2)} + \frac{P_1 {L_1}^2 L_2}{(L_1 + L_2)k_\theta} - \frac{P_1 {L_1}^3 L_2}{2(L_1 + L_2)EI}$$

$$y = -\frac{1}{3}\frac{P_1 L_2 {L_1}^3}{EI(L_1 + L_2)} + \frac{P_1 {L_1}^2 L_2}{(L_1 + L_2)k_\theta}$$

If $L_1 = L_2 = L/2$

$$y = \Delta_{max} = -\frac{P_1 L^3}{48EI} + \frac{P_1 L^2}{8k_\theta}$$

$$k_\theta = \frac{P_1 L^2}{8y + \frac{PL^3}{6EI}}$$